POLITECNICO DI TORINO

Department of Mechanical and Aerospace Engineering

Monitor and control system of the dynamic stability on a telescopic handler with telemetry and experimental data

Acedemic tutor:

Prof. Aurelio Somà

Company tutor:

Ing. Federico Fraccarollo

Student:

Gianmarco Priora

October 2019

Contents

Summary

Nowadays the governments of all over the world are increasingly sensitive to the safety in the workplace. Even if the number of accidents has decreased during last years the standards regulating all the safety related aspects of the workplace are becoming more stringent. Some of those regulations concern the risks derived from the operations of the industrial machines. Most of them impose some tests simulating dangerous operating conditions of those machines. The possibility to sell a specific machine in a certain part of the world depends on the outcome of those tests. The producers of industrial machines adopt two main strategies to satisfy those standards: reduce the risk of accident by installing some systems making dangerous operations impossible to perform, record the temporal evolution of some key parameters of the machine that can be analysed in case of accident to understand its causes.
This Master thesis deals with both those two strategies applied on a telescopic handler. This document is the result of a collaboration with Movimatica: a company that is part of Merlo group, one of the world's leader in the production and sale of telescopic handlers. In particular it has been developed a stand-alone GUI (Graphic User Interface) able to read the file recorded by a data-logger installed on a telescopic handler. The data-logger is integrated in the CAN network of the machine and records the temporal evolution of some safety related parameters of the machine. This GUI returns a 3D animated representation of the telescopic handler showing the operations that the machine has done during the recorded period of time. This application is useful in case of overturning of the machine in order to investigate the causes that have led to the accident. On the other hand the risk of accident can be reduced with a control system of the machine's dynamic stability. In this document it is described a detailed study on the dynamic behaviour of the machine during the test prescribed by ISO EN 15000:2008. After the execution of some tests on a real machine, the data coming from the on-board sensors have been compared with those of some external IMUs (Inertial Measurement Unit) installed on the chassis and the boom of the machine. A simplified analytic model of the machine and a numerical one have been created to simulate the dynamic behaviour of the machine also for configurations different from those of the test. The results of the test on the machine have been useful to tune those models and increase their reliability. The results of this study will be used to improve the control law of an innovative control system of the telescopic handler' s dynamic stability.

Chapter 1

Introduction to CAN bus

1.1 Overview

Controller Area Network (CAN) is a serial network technology that was originally designed for the automotive industry, but has recently gained popularity in industrial automation as well as many other applications [10]. CAN is a two wire network system, that is far superior to other serial technologies such as RS232 in regards to functionality and reliability and yet CAN implementation is cheaper. The diffusion of CAN sales in many different high volume markets, such as automotive, domestic appliances and industrial control, guarantee the availability for the future. The following description of CAN does not want to be exhaustive from the electronic point of view but it aims to easily explain the basic principles of how the communication via CAN bus works and how it is possible to read and analyse CAN messages.

1.2 History of CAN bus

The development of the CAN bus started in 1983 at Robert Bosch GmbH. They investigated the market for a suitable field-bus technology for the automotive market that would enable them to add further functionality to the on board electronic devices. The main focus was a system allowing the communication between the ECUs (electronic control units) in cars produced by Mercedes-Benz. None of the existing communication protocols satisfied the specific requirements for communication speed and this led to the development of their own standard.
The protocol was firstly released in 1986 at the Society of Automotive Engineers (SAE)

conference in Detroit, Michigan. The first CAN controller chips produced by Intel (Intel 82526) and Philips (Philips 82C200), were introduced in 1987. Since then many other semiconductor manufacturers made a decision to produce stand-alone CAN controllers implementing them into their single-chip designs. The main steps in the development of CAN are summarized in the Table 1.1.

The CAN protocol is protected by patents granted to Robert Bosch GmbH. Bosch will grant licenses to manufacturers and universities.

By now, the automotive and vehicle industries still represent the biggest part of the market of CAN controllers and single-chip controllers with integrated CAN controller buying the 80% of the entire production . The 20% portion represents many applications in various non-automotive markets. The fast success that CAN has had since

1983	Start of the Bosch internal projet to develop an in-vehicle network
1986	Official introduction of the CAN protocol
1987	First CAN controller chips available from Intel and Philips
1991	Bosch publishes CAN specification 2.0
1992	CAN in Automation (CiA) established as international users and manufacturers group
1992	CAN Application Layer (CAL) protocol published by CiA
1992	Fisrt cars by Mercedes Benz are being equipped with CAN
1993	ISO 11898 standard published
1994	First International CAN conference (iCC) organized by CiA
1994	DeviceNet protocol introduced by Allen-Bradley
1995	ISO 11898 amendment (extended frame format) published
1995	CANopen protocol published by CiA

Table 1.1: Main steps in CAN evolution

its introduction is certified by the increasing number of nodes, ECUs able to send and receive CAN messages, that have been installed in the first years of its distribution as shown in Fig. 1.1.

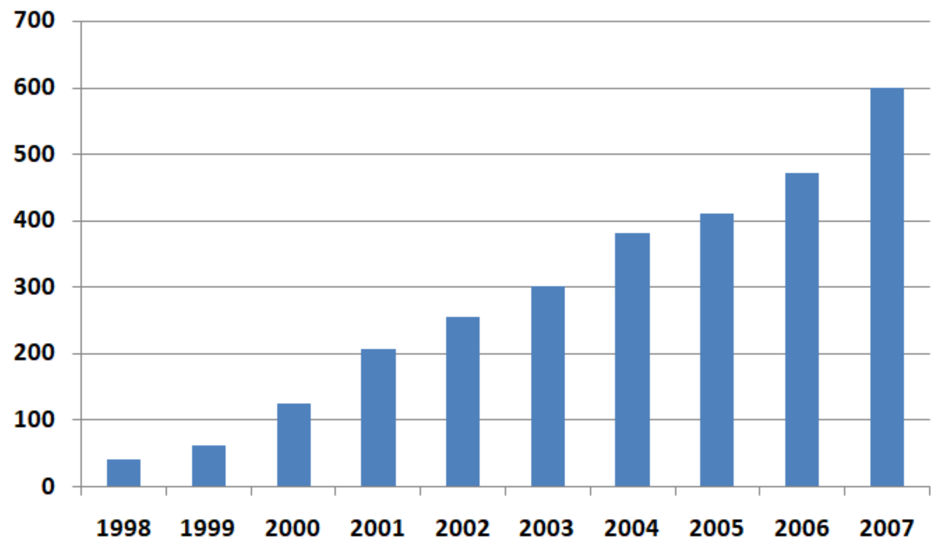

Figure 1.1: Number of millions CAN nodes used over time

1.3 CAN application

The modern car may have as many as 70 electronic control units (ECU) for various subsystems (fig. 1.2). Typically the biggest processor is the engine control unit but other ones are used in subsystems like for transmission, airbags, electric power steering, audio systems, power windows, doors, mirror adjustment, battery and recharging systems for hybrid/electric cars, etc. The communication among these subsystems is essential. A subsystem may need to control actuators or receive feedback from sensors of other subsystems. The CAN standard was developed to fill this need. One key advantage is that interconnection between different vehicle systems can grant a wide range of safety, economy features to be implemented using software alone - functionality which would add cost and complexity if such features were "hard wired" using traditional automotive electronic connections. Even if CAN finds its best field of application in the automotive sector, it is successfully used also in many other fields. The main advantage of fieldbus system like CAN lies in the reduction of expensive and maintenance intensive wiring and in the increased performance of a multi-processor system and this aspect can be useful also outside of the automotive field.
The main applications for CAN are in the fields of:

- Passenger cars
- Trucks and buses

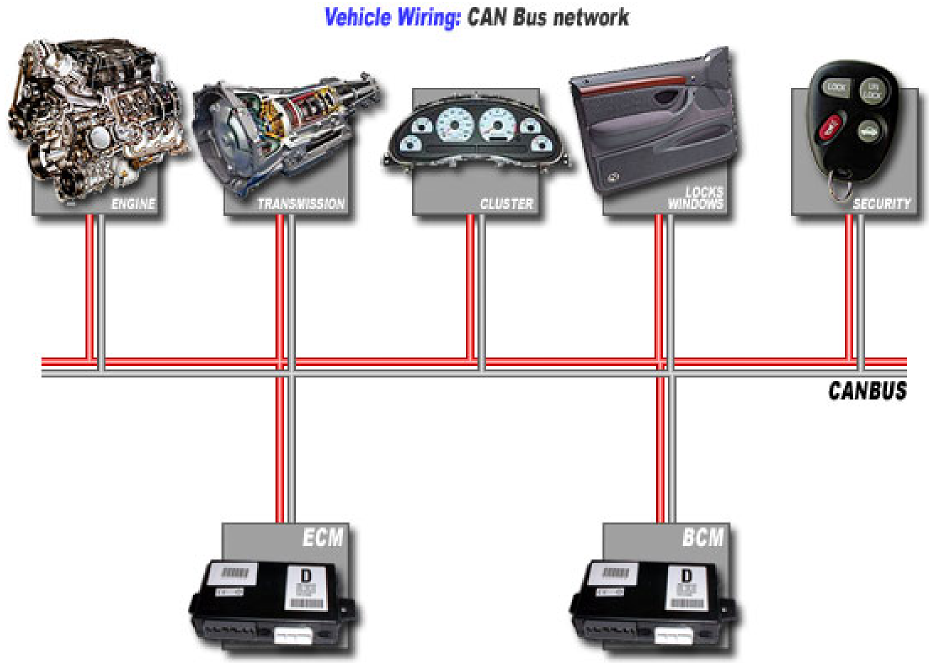

Figure 1.2: Simplified scheme of a passenger car CAN

- Off-road vehicles
- Passengers and cargo trains
- Maritime Electronics
- Aircraft and Aerospace Electronics
- Factory Automation
- Industrial Machine Control
- Building Automation
- Lifts and Escalators
- Medical Equipment and Devices

Cisco Systems, a networking company, uses a CAN sub-network to implement system initialization and hot-swapping on the large PC boards that implement routers. With a number between 500,000 and 1 million of installed CAN nodes, makes this one of the largest applications out of the automotive sector.

The CAN bus protocol has been used on the Shimano DI2 electronic gear shift system for road bicycles, and is also used by the Ansmann and BionX systems in their direct drive motor applications.

1.4 Frames

CAN is a multi-master serial bus standard for connecting Electronic Control Units [ECUs] also known as nodes. Two or more nodes are required on the CAN network to communicate and each node can transmit a message, referred to as frames, as soon as the bus is idle and read the ones sent by the other ones.
CAN provides four different types of message frames:

- **Data frame**: Data transfer from one sending node to one or more receiving nodes
- **Remote frame**: Any node may request data from another node. A remote frame is consequently followed by a data frame containing the requested data sent by the node addressee of the request
- **Error frame**: Any bus node may signal an error condition at any time during the transmission of a data or remote frame
- **Overload frame**: A node can request a delay between the transmission of two data or remote frames, meaning the overload frame can only occur between data or remote frame

In this description we will focus only on data and remote frame since they are the only one that will be object of further analysis.
It is possible to have standard (Figure 1.3) CAN frames and extended ones (Figure 1.4).
Per definition a standard CAN data or remote frame has the following components:

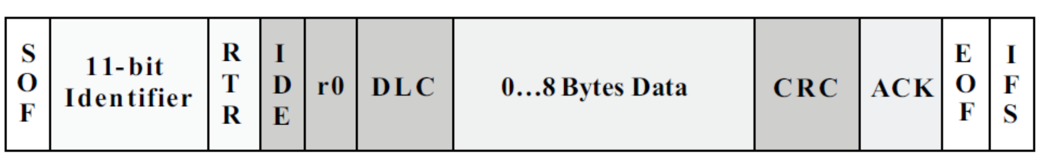

Figure 1.3: Standard CAN frame: 11 bit identifier [3]

- **SOF**(Start Of Frame): signals the beginning of data and remote frames

- **Arbitration field**: includes the message ID and RTR (Remote Transmission Request) bit, which distinguishes data and remote frames

- **Control Field**: used to determine data size and message ID length. It is composed of an IDE (identifier extension) bit that distinguishes standard and extended frame format, r0 bit which is reserved for future applications and DLC (Data Length Code) containing the number of bytes of data being transmitted (between 0 and 8)

- **Data field**: the actual data up to 64 bits (only in data frame, not in a remote frame)

- **CRC** (Cyclic Redundancy Check): contains the number of bits transmitted, called checksum

- **ACK** (Acknowledgement): marks the integrity of the frame or the presence of errors in the transmission

- **EOF**(End Of Frame): signals the end of data and remote frames

- **IFS** (Inter Frame Space): contains the time required by the controller of the node to place a correctly received frame to its proper position in a message buffer area

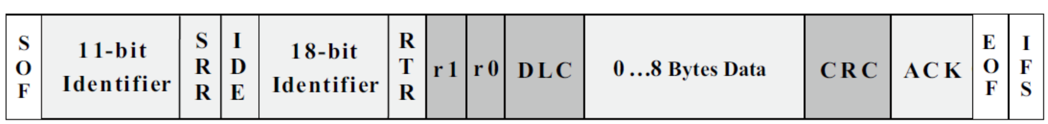

Figure 1.4: Extended CAN frame: 29 bit identifier

The extended CAN frame is the same as the Standard message with the addition of:

- **SRR** (Subatitute remote request): replaces the standard message location as a place-holder in the extended format

- **r1**: an additional reserved bit has been included ahead of the DLC

An 11 bit identifier(standard format) allows a total of 2^{11}(= 2048) different messages. A 29 bit identifier(extended format) allows a total of 2^{29}(= 536.870.912) messages. Both format may co-exist in the same CAN bus network.

A Data frame broadcasts a message to the CAN bus, either due to change of an event (for example the change of an input signal, a timer event, etc.) or as a response to a message request by another node. The Data frame, identified by its ID, may be accepted by any number of nodes in the network according to the application needs, but can be transmitted by the only node associated with the data message. On the other hand, a Remote frame requests the transmission of a message by another node. The data requested by the Remote frame can be sent by the only node associated with the requested message.

1.5 Bus topology

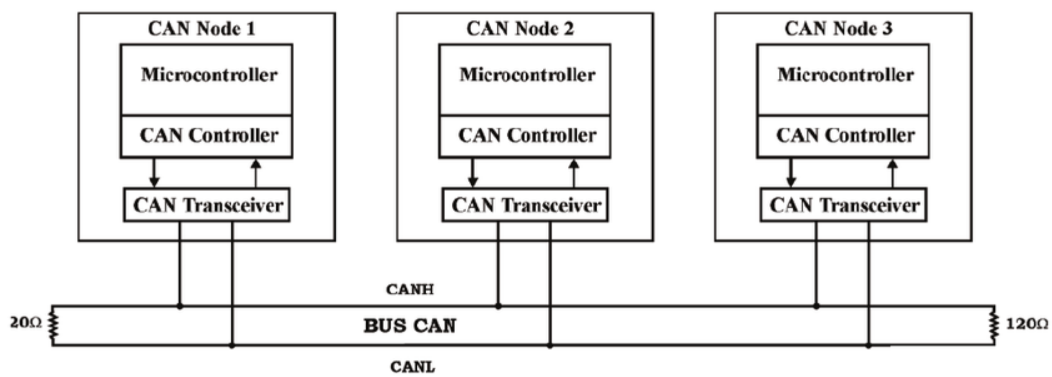

Figure 1.5: Bus topology

Figure 1.5 shows a simple CAN network. All nodes are connected by two wires, `CAN_H` (CAN High) and `CAN_L` (CAN low). The bus is terminated by two resistors, which are typically 120 Ω and are necessary to suppress any electrical reflections. According to specification the CAN bus medium must support two logical states: recessive (bit value=1) and dominant (bit value=0). As shown if Figure 1.6 the CAN bus voltage level ranges normally between 1.25 V (`CAN_L` during dominant bit) and 3.75 V (`CAN_H` during dominant bit). However, the actual signal status, recessive or dominant, depends on the differential voltage V_{diff} between `CAN_H` and `CAN_L`.

$$V_{diff} = V_{\texttt{CAN\_H}} - V_{\texttt{CAN\_L}}$$

V_{diff} is equal to 2.5 V during a dominant bit and 0 V during recessive bit. The use of a differential voltage between `CAN_H` and `CAN_L` makes the bus resistant to electromagnetic interferences (EMI). Any EMI affects both wires in the same way, but the differential voltage level keeps constant.

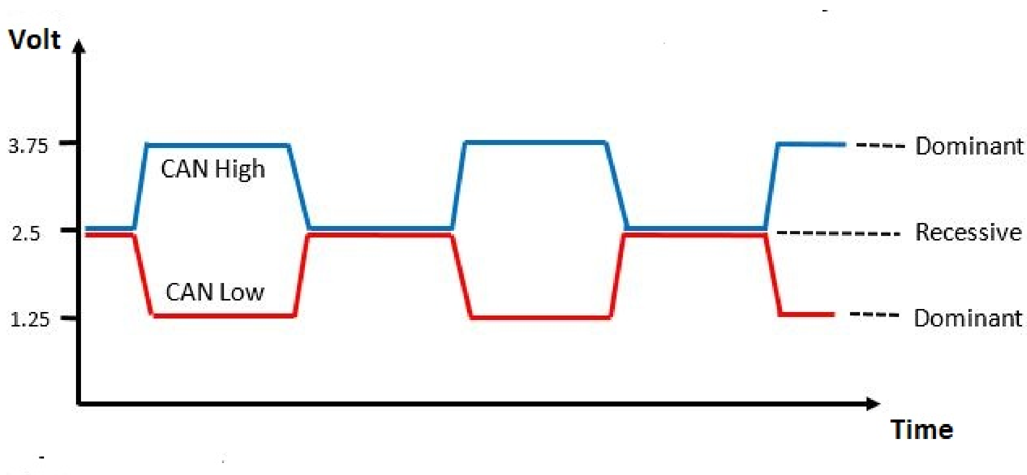

Figure 1.6: CAN bus voltage level

Figure 1.7 shows an example of the voltage signal referred to a single CAN frame.

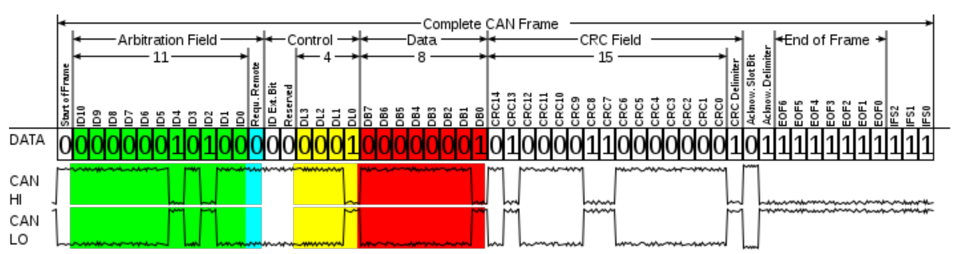

Figure 1.7: Complete CAN frame

1.6 Connector

In order to connect a CAN network to external devices the CiA DS-102 document suggests the use of a 9 pin D-sub connector according to DIN 42652.

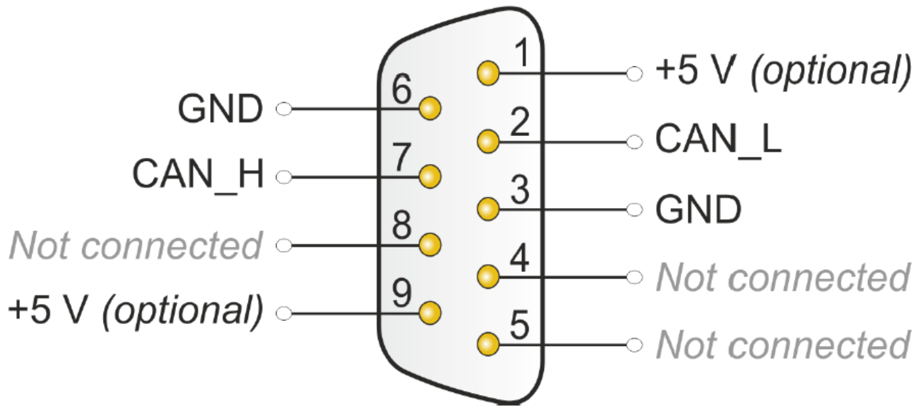

Figure 1.8: D-sub 9 pin connector

1.7 SAE J1939

The CAN standard defines the hardware and the communication on a basic level. The CAN protocol itself just specifies how to transport small packets of data using a shared communications medium. It contains nothing on topics such as flow control, transportation of data larger than 8-byte message, node addresses, establishment of communication, etc. In order to manage the communication within a system, a higher layer protocol is required. The higher layer protocol typically specifies things like how to distribute message identifiers among the different nodes in a system or how to translate the contents of the data frames. There are many higher layer protocols for the CAN bus for different field of application (automation, off-highway vehicle, embedded application etc.).
J1939 is an higher layer protocol released by the Society of Automotive Engineers (SAE) and explicitly designed for communication among ECUs on off-highway machines in applications like construction, material handling and forestry machines (Figure 1.9). The messages exchanged between these units can be data such as engine speed, engine torque, inlet air temperature and many more. Since its introduction, J1939 has quickly become the accepted industry standard for off-highway machines [11]. However some organizations in the agricultural, military and marine industries developed their own protocols slightly modifying the original version of J1939 in order to satisfy their specific needs.
These derived protocols are:

- **ISO 11783**: also known as ISOBUS and adopted in agriculture and forestry machinery, it was originally designed to link the CAN of the tractor with the one of the different attachment and grant an easy communication between the two parts

- **MilCAN**: used in military vehicles
- **NMEA2000**: it's the preferred protocol for marine navigation systems

(a) Boat

(b) Autobus

(c) Military vehicle

(d) Truck-trailer connection

(e) Construction machinery

(f) Agriculture machinery

Figure 1.9: Example of j1939 applications

As reported at the beginning of this chapter the goal of this introduction to CAN is to give to the reader a short explanation on how the CAN works and how the data transmitted on the bus can be interpreted. For this reason in this section i am going to describe the key aspects of J1939 focusing on the structure of the Data frames written according to J1939 neglecting all the other aspects that this standard covers.

1.7.1 Parameter groups and Suspect parameters

A parameter group is a set of parameters making part of the same topic and having the same transmission rate. A parameter group can be, for instance, the *'engine temperature'* which includes coolant temperature, fuel temperature, oil temperature, turbocharger oil temperature etc. The length of a parameter group is not limited to the length of a CAN frame. Usually a parameter group has a minimum length varying from 8 up to 1785 bytes [7]. Parameter groups larger than 8 bytes require a transport protocol to transmit those data split into more than one frame. A complete list of the standard parameter groups and parameters can be found in SAE J1939/71 (Figure 1.11 and Figure 1.10), one of the 13 documents composing the whole standard. In addition it is possible for manufacturers to define their own specific parameter groups. To each parameter group it is associated a Parameter Group Number (PGN) and to each paramater in a group it associated a Suspect Parameter Number (SPN). The PGN is contained in the ID of a J1939 frame (Table 1.2) with the Priority (0 high priority, 6 low priority), that marks the importance of the data transmitted, and the Source Address that identifies the ECU that has sent the frame. The description of the Data Page, the PDU Format and the PDU Specific would be very long but it is not necessary for the purposes of this introduction to SAE J1939.

The SPN describes the parameter in detail by providing the following informations: data length in bytes, data type, resolution, offset, range, reference tag. Every param-

Priority	**Reserved**	**Data page**	**PDU format**	**PDU specific**	**Source address**
3 bit	1 bit	1 bit	8 bit	8 bit	8 bit

Table 1.2: ID structure of a j1939 frame

eter can assume two main data type: *Measured* if the parameter is an analog variable (Figure 1.11) that can vary continously, *Status* if the parameter is a digital variable (Figure 1.12) and a specific meaning is associated to every possible value that it can assume. In order to convert a *Measured* parameter to physical units, the following formula must be applied:

$$p_{physical} = resolution \times p_{raw} + offset$$

where $p_{physical}$ is the value of the parameter converted into physical units while p_{raw} is the raw value read in the Data field. If the $p_{physical}$ falls out of the out of the range prescribed for its SPN the value is considered as not valid.

The meaning of each value that a Status parameter can assume is specified in the description on the standard.

pgn65262 - Engine Temperature 1 - ET1 -

Transmission Repetition Rate:		1 s	
Data Length:		8 bytes	
Data Page:		0	
PDU Format:		254	
PDU Specific:		238	
Default Priority:		6	
Parameter Group Number:		65262 ($00FEEE_{16}$)	
Bit Start Position /Bytes	Length	SPN Description	SPN
1	1 byte	Engine Coolant Temperature	110
2	1 byte	Fuel Temperature	174
3-4	2 bytes	Engine Oil Temperature 1	175
5-6	2 bytes	Turbo Oil Temperature	176
7	1 byte	Engine Intercooler Temperature	52
8	1 byte	Engine Intercooler Thermostat Opening	1134

Figure 1.10: Description of PGN 65262 in SAE J1939/71

spn110 - Engine Coolant Temperature - Temperature of liquid found in engine cooling system.

Data Length:	1 byte
Resolution:	1 deg C/bit , -40 deg C offset
Data Range:	-40 to 210 deg C
Type:	Measured
Suspect Parameter Number:	110
Parameter Group Number:	[65262]

Figure 1.11: Description of SPN 110 in SAE J1939/71

spn563 - Anti-Lock Braking (ABS) Active - State signal which indicates that the ABS is active. The signal is set active when wheel brake pressure actually starts to be modulated by ABS and is reset to passive when all wheels are in a stable condition for a certain time. The signal can also be set active when driven wheels are in high slip (e.g., caused by retarder). Whenever the ABS system is not fully operational (due to a defect or during off-road ABS operation) , this signal is only valid for that part of the system that is still working. When ABS is switched off completely, the flag is set to passive regardless of the current wheel slip conditions.

00 ABS passive but installed
01 ABS active

Bit Length:	2 bits
Type:	Status
Suspect Parameter Number:	563
Parameter Group Number:	[61441]

Figure 1.12: Description of SPN 563 in SAE J1939/71

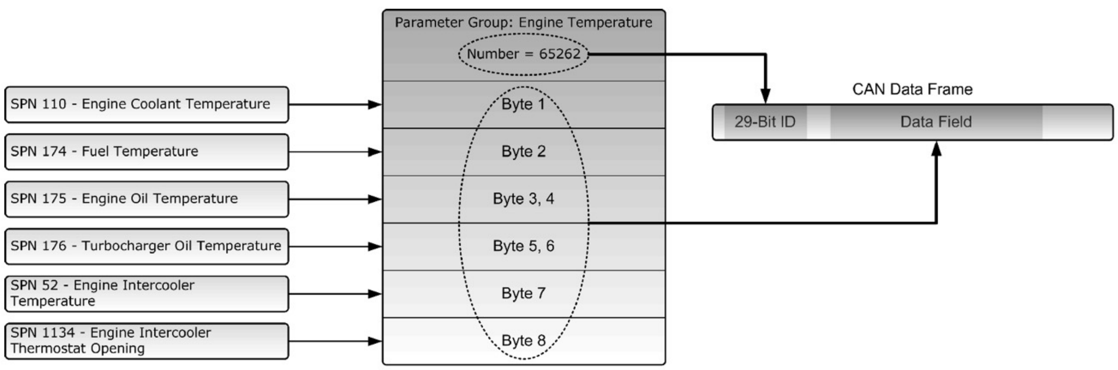

Figure 1.13: SPN and PGN

1.8 CAN sniffing

Nowadays it is possible to find several physical interfaces on the market that connect your PC to CAN bus networks (Figure 1.14) and commercial software that allows you to receive and transmit frames on the network (Figure 1.15).

Figure 1.14: PEAK USB interface

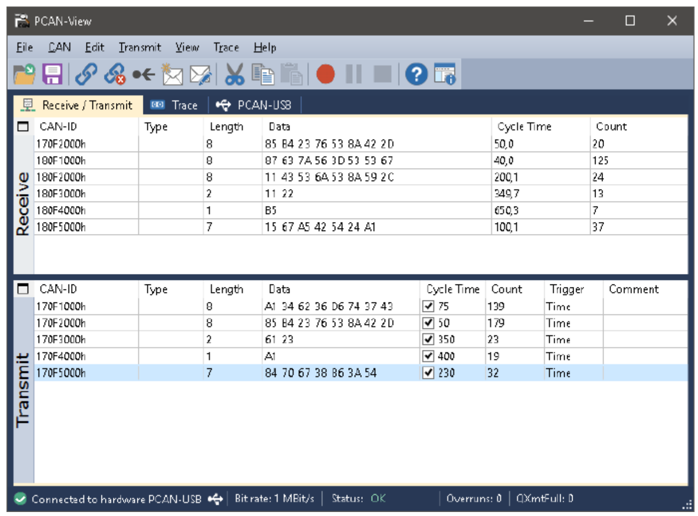

Figure 1.15: PCAN View

The conversion of raw CAN bus data to physical, readable data can be done with the use of a CAN DBC file (Figure 1.16). This file format was originally developed by Vector GmbH, a society producer of hardware and software solution for CAN bus systems, but it has then become a standard adopted also from CAN software of other companies. A CAN bus DBC file is simply a database format structured around CAN Messages (e.g. PGNs) and Signals (e.g. SPNs) which contains information about the ID, the position and length of the parameters within the Data field, the offset, the resolution, the Data type etc. necessary for converting raw CAN bus data. For standardized cases

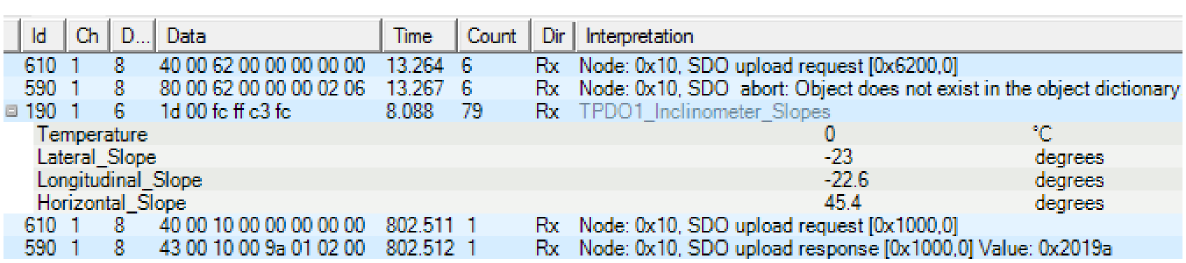

Figure 1.16: CAN data decoded with DBC file

like the SAE J1939, it is possible to buy a DBC file containing all the informations about PGNs and SPNs of J1939/71 and use it across many vehicles. On the other hand the database can be customized by manufacturers who adopt their proprietary CAN protocol systems or who have for example extended the original J1939 DBC file with conversion rules for their own PGNs. These DBC aren't usually available and so it is possible to adopt some reverse engineering processes to have access to some of their informations.

Chapter 2

The telescopic handler

The telescopic handler is a machine commonly spread in the agricultural and industrial field. Its main characteristic is to have a telescopic boom made of different square sections that slide one into the other. It can recall the forklift since it is commonly equipped with forks but its telescopic boom makes it more a crane than a forklift. The reason of its success is its versatility given by its boom that can extend forwards and upwards from the vehicle and the several attachments that the operator can fit at the end of the boom such as a bucket, pallet forks, muck grab, or winch [15]. In industry the most common attachment for a tele-handler is pallet forks and the most common application is to move loads to and from places unreachable for a conventional forklift. In agriculture it is generally used with a bucket or with forks for hay bales replacing the tractor front end loader. Some agricultural telescopic handlers can also be fitted with three point linkage and power take-off.
Many companies, like Merlo, Manitou, JCB, Dieci, Bobcat produce the frontal tele-

Figure 2.1: Merlo frontal telescopic handler

scopic handler (Figure 2.1). This kind of machine is so called because it does not have a rotating turret that allows the boom to rotate around the longitudinal axis of the vehicle. Some models are equipped with frontal stabilizer in order to increase the stability when the load is heavy or working radius is particularly large. Some special machines, called 'Roto', instead have the possibility to make the boom rotate around the longitudinal axis of the vehicle thanks to a rotating joint between an upper and a lower frame. This characteristic gives to the operator the possibility to reach any point around itself without relocate the machine. They can be compared to mobile cranes and typically have four stabilizers at the corners of the lower frame.
Nowadays many models are available on the market with a rated capacity in a range of 20 to 60 tons and a maximum reachable height between 6 and 35 m.

2.1 Stability monitoring

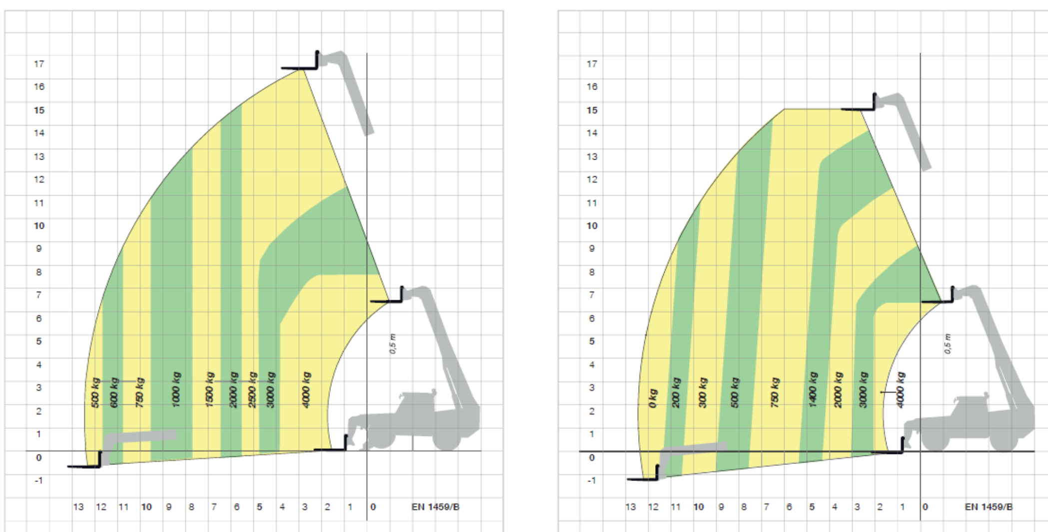

Figure 2.2: Load chart on stabilizers (left) and on tyres (right) with forks

The biggest limitation of the telescopic handler derives from its telescopic boom: as it extends, it acts as a lever and causes the vehicle to become increasingly unstable. This means that the lifting capacity quickly decreases as the working radius (distance between the front of the wheels and the centre of the load) increases. Each machine has its own load charts which indicates the maximum allowable weight that the boom can lift according to the boom extension and the boom inclination angle. Each load chart refers to a specific attachment and support condition of the machine (on wheels or on stabilizers)(Figure 2.2). All the load charts refers to the machine in static condition but the dynamic effect due to the inertial effect of the boom movement can increase the overturning moment. International standards impose to provide the telescopic handler with sensors that monitor the vehicle status and warn the operator and/or limit the allowed movements of the boom whenever the stability of the machine is at risk.

Chapter 3

Data logger

In the last years, the necessity to reduce the number of work-related accident has increased the sensibility of heavy duty machine producers to make their products always safer. This goal has been pursued installing a large amount of sensors monitoring the status of the machine and preventing hazardous operations. Even if these device have consistently reduced the number of accidents the risk still remains and accidents happens quite often. In order to investigate the causes that have led to the accident nowadays many international standards suggest the installation of data-recorder, also called data-logger, on board. They are a sort of 'Black boxes', like the ones installed on the air planes, that record the evolution, in a time interval, of some key parameters of the machine that can be useful to determine the causes and the dynamic of the accident. Those data can be exported and analysed by the machine's producer and used to determine if the origin of the accident derives from an hazardous operation or from a machine's defect or failure. It is necessary to distinguish two type of devices of this kind that are installed on a machine: a data logger and a black box. The first one is entirely designed by the producer of the machine who is usually the only one having access to the information recorded while the second one is a standardised device locked down that can be read only by the police in case of accident and whose data can be used at the court in case of civil or penal claims. Some countries can be considered as pioneer in the use of these technologies, such as Singapore that in 2015 adopted a law imposing the installation a data-logger on every crane operating on its territory [9] and to send periodic report to the authorities signalling all those situations that have compromised the stability of the machine . The Singapore law is based on the

European Standard EN 13000:2010 that is described in the next section.

3.1 EN 13000:2010

Before starting the description of this document, it is necessary to underline that this standard does not apply to telescopic handlers but it is the only standard mentioning the data logging of an industrial machine very similar to a telescopic handler and so it makes sense to report it.

3.1.1 Scope

This document has been prepared to give one means for mobile cranes to conform with the principal health and safety requirements of the Machinery Directive. This European Standard is supposed to help the manufacturers to the design, install, maintain and test mobile cranes. In particular it defines the main characteristics that a data logger, also called event recorder, on a mobile crane must have.

3.1.2 Event recorder

On mobile cranes all relevant data must be recorded by a event recorder, to allow the investigation of loading conditions in case of an accident. Size and frequency of overloading conditions may be recorded for evaluation of crane accidents, e.g. as result of fatigue. The manufacturer develops the concept for the data to be recorded in order to reconstruct the load case depending on the crane concept.
the event recorder shall meet the following functional criteria:

- the data shall be recorded automatically, independent of the crane operator.

- each situation which leads to an overloading of the crane (> 100% of the set load chart), shall be recorded. The size of the overloading shall be recorded.

- in addition all data which are relevant to reconstruct the last load case shall be recorded.

- a suitable interface to export the data shall be available.

- the manipulation of the recorded data shall be prevented.

- the function of the event recorder shall be automatically checked each time the crane is put into operation. Any malfunction shall be indicated to the crane operator.

The table below shows the operational parameters that must be recorded by the data logger

1	Date and time
2	Crane configuration
3	Permitted load, actual load, percentage of usage of rated capacity
4	Radius of load
5	Slew angle
6	Main boom angle, fly jib angle (if applicable)
7	Boom length ,fly jib length (if applicable)
8	Sequence of extension (for telescopic cranes)
9	Status of limit switches
10	Status of override key activation

Table 3.1: Operational parameters to be monitored

3.2 MERLO VisuaLogger

3.2.1 Overview

Merlo has recently decided to provide their machineries with a data logger that records all the main parameters of the machine, that can help to reconstruct the accident's dynamics, from the CAN. Basically it periodically saves the value that the different parameters assume and store them for a certain amount of hours in such a way that after the accident, when the data are exported, it is possible to analyse the behaviour of the machine during and some hours before the accident.
The period of time that the data logger is able to record and the parameters that the data logger records can not be reported in this document for confidential reasons but this limit does not affect the comprehension of how the system works.

In order to easily rebuild the accident' s dynamic and help those who have to read the data extracted from the logger, it has been decided to develop an intuitive software with a GUI (Graphical user interface). This GUI takes as input the data logger file and the model of telescopic handler on which it has been recorded and returns as output an animated virtual representation of the geometrical configuration (angle of the boom, extension of the boom, tilting of the chassis etc.) of the machine in a specific instant of time recorded by the logger (Figure 3.1). Even if this GUI was coded with Matlab App Designer, it does not require an expensive Matlab licence to run it but it is enough to download the Matlab Runtime that is completely free.

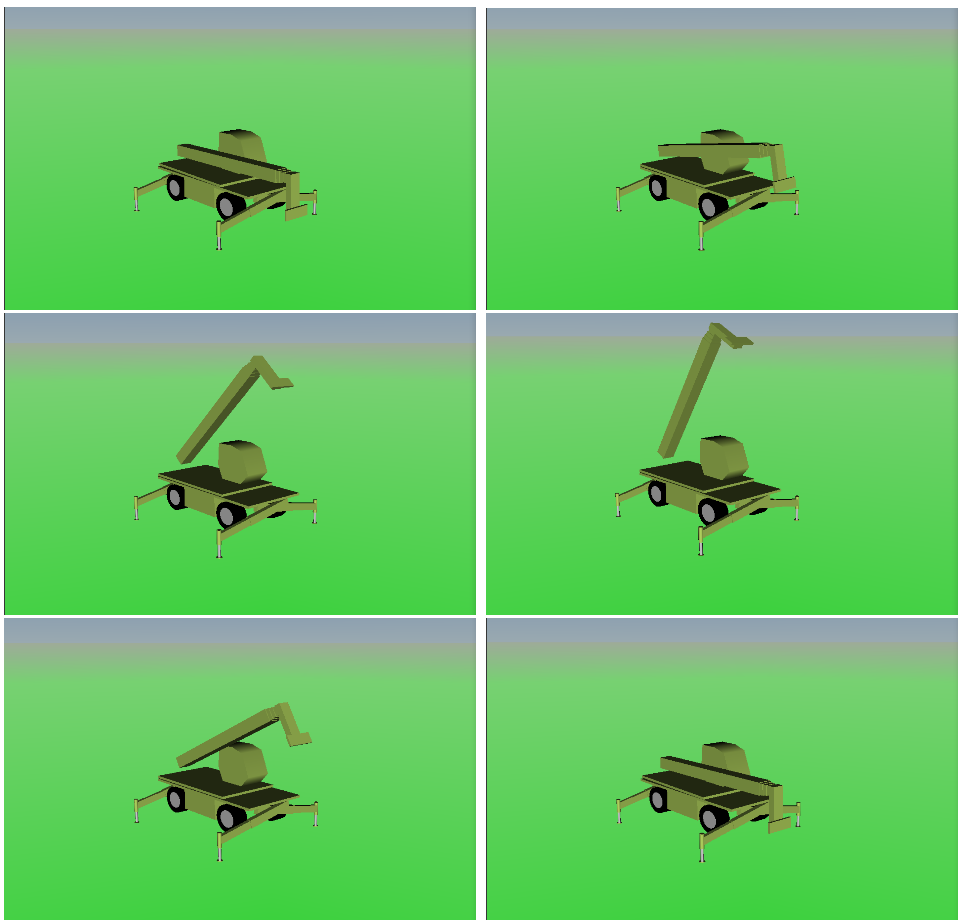

Figure 3.1: Some frames extracted from an animation

3.2.2 Virtual model

The realization of this GUI was made easy by the possibility that the "Simulink 3d animation" library of Matlab offers to create a virtual world interacting with a VRML file.

VRLM is a file format (like 3DS, STEP, OBJ etc.) used to represent three dimensional interactive vector graphics. VRML files are usually known as "worlds" and have the .wrl extension. Each world can contain different 3d shapes, also called "nodes", which are mainly identified by their shape, size, position, rotation, center of rotation and color (Figure 3.2 and 3.3). VRML files can be created with dedicated softwares (like the V-Realm editor integrated in Matlab) or also with a common text editor thanks to the easy and open syntax (Figure 3.2b). All the different parameters of a shape can be modified directly from Matlab and it is therefore possible to create animations changing the position of the object at each time instant and showing the virtual representation with a VRML viewer (Figure 3.1).

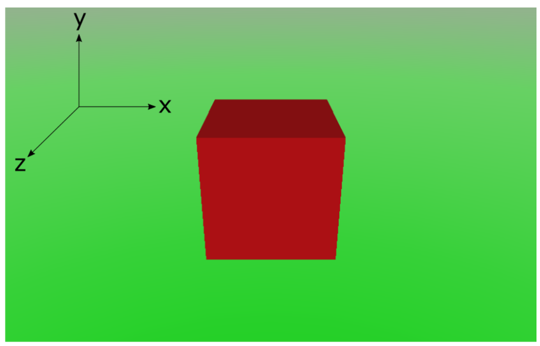

(a) File opened with a VRML editor

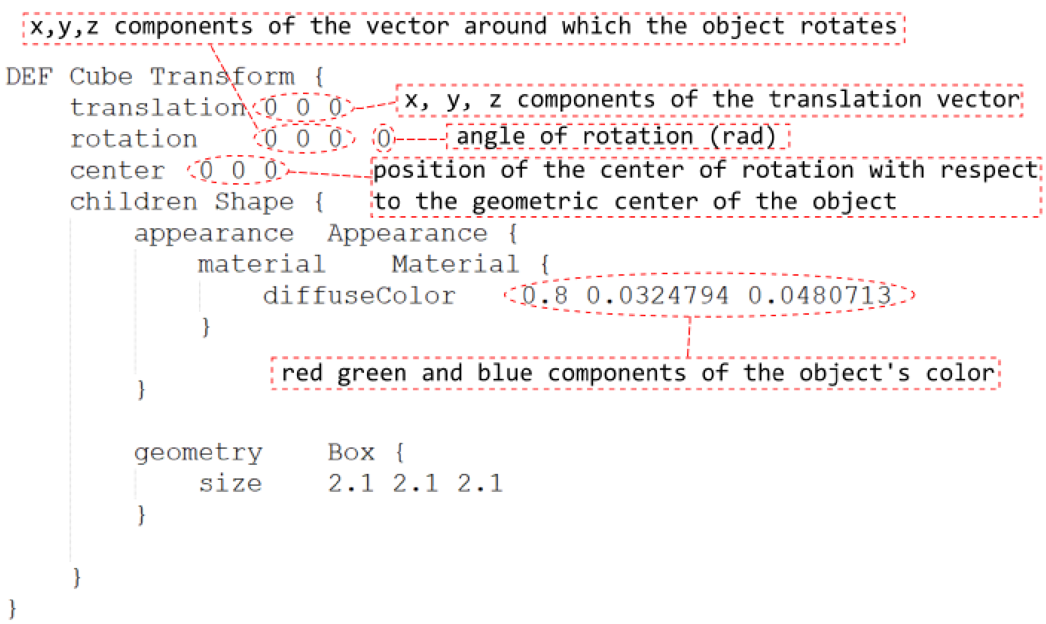

(b) File opened with a text editor

Figure 3.2: VRML file containing a cube

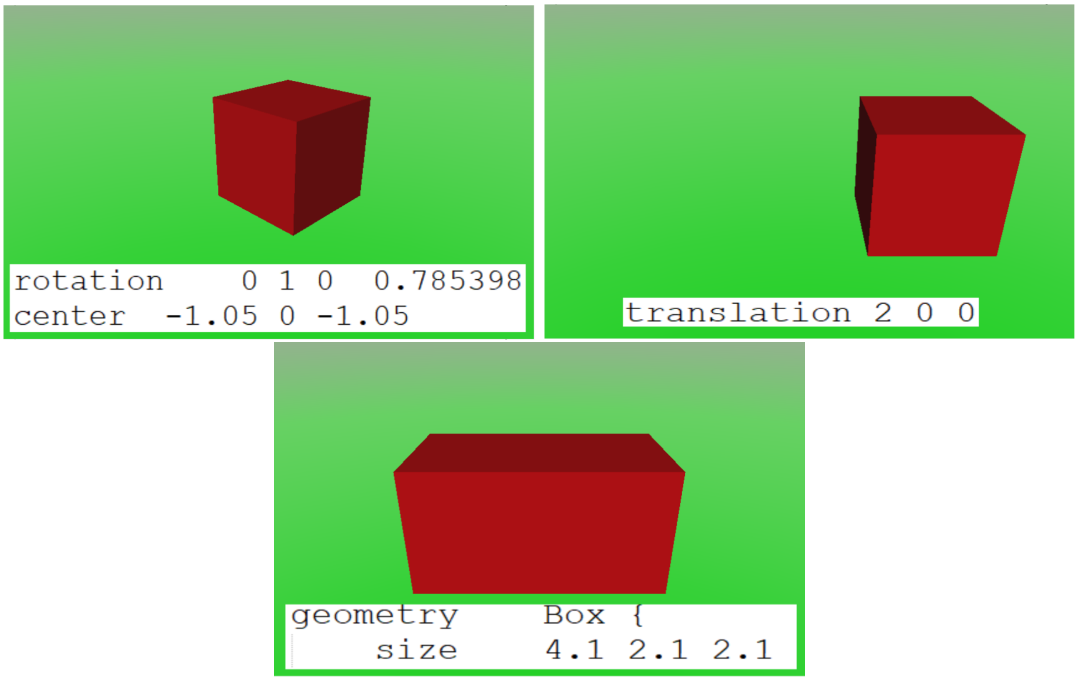

Figure 3.3: Different possible modification to the file in Figure 3.2

Due to the great variety of the Merlo machines and the impossibility to have a 3d model for each of them the structure of the machine was simplified with a few number of parts made out of simple geometries, whose dimensions can be easily adapted to the dimensions of different machines which are available on brochures (Figure 3.4).

Three main VRML models have been made to cover the entire range of telescopic handlers:

1. **Roto**: for all the rotating models
2. **Panoramic with stabilizers**: for the frontal telescopic handlers with stabilizers
3. **Turbofarmer**: for the frontal telescopic handlers without stabilisers

Table 3.2 shows the list of the parameters that have been chosen to characterize the geometry of rotating (Figure 3.6) and non rotating machines (Figure 3.7).

As it is possible to see in Figure 3.5 Roto 38.16 and 60.24 have different dimensions and a different number of extensions (2 the Roto 38.16 and 3 the Roto 60.24) even if the starting .wrl file is the same. The parameters for each model of machine have been stored in a excel file that is read by the GUI and it can be modified in order to add new models that will be developed in the future. The format of the excel tab that the GUI reads is reported in Figure 3.3.

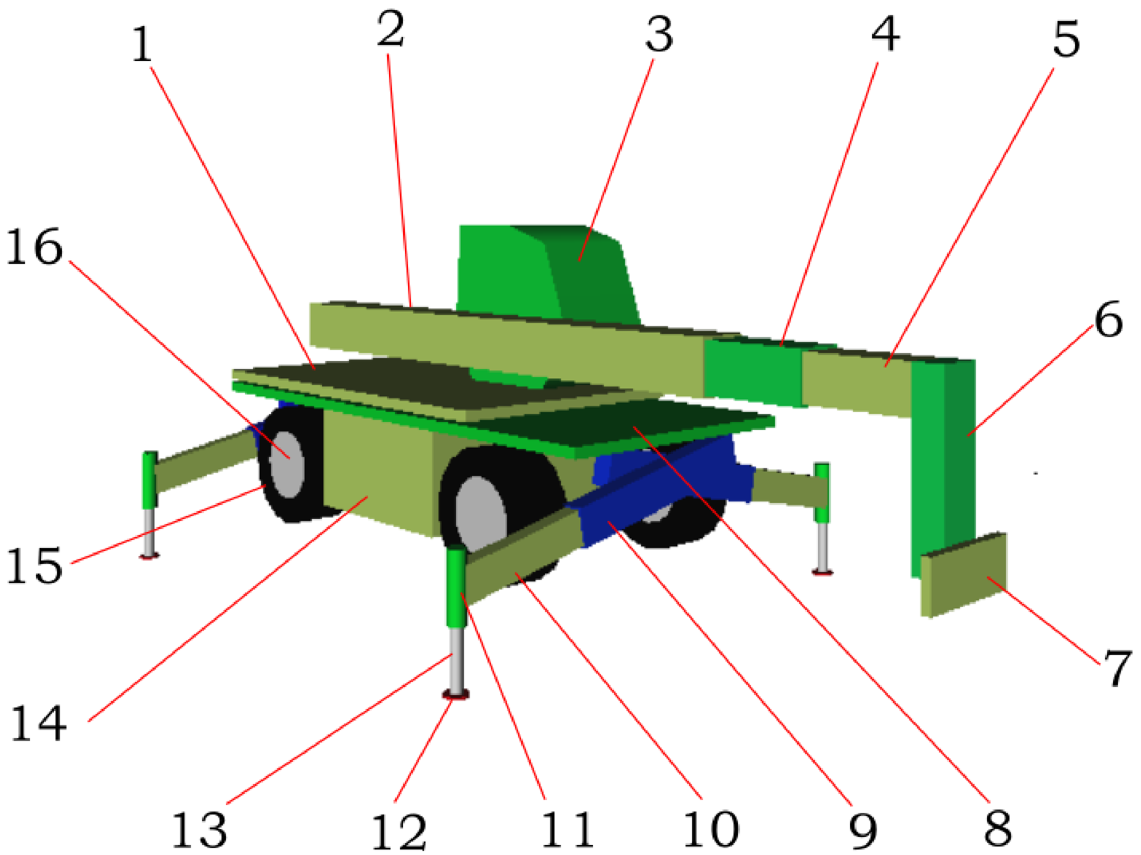

Figure 3.4: (1) turret base - (2) first section of the boom - (3) cab - (4) second section of the boom - (5) third section of the boom - (6) support arm - (7) raft - (8) chassis - (9) stabilizers support - (10) stabilizer extension - (11) stabilizer piston - (12) stabilizer foot - (13) stabilizers cylinder - (14) engine - (15) tyre - (16) rim

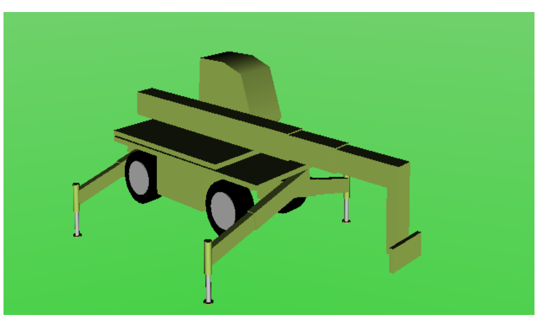

(a) Roto 38.14

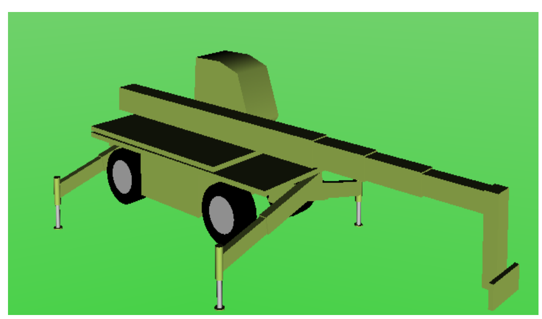

(b) Roto 60.24

Figure 3.5: Different models of Roto created adapting the same .wrl file

Obviously in order to limit the number of parameter that characterize a certain model it has been decided to neglect some differences within the different models:

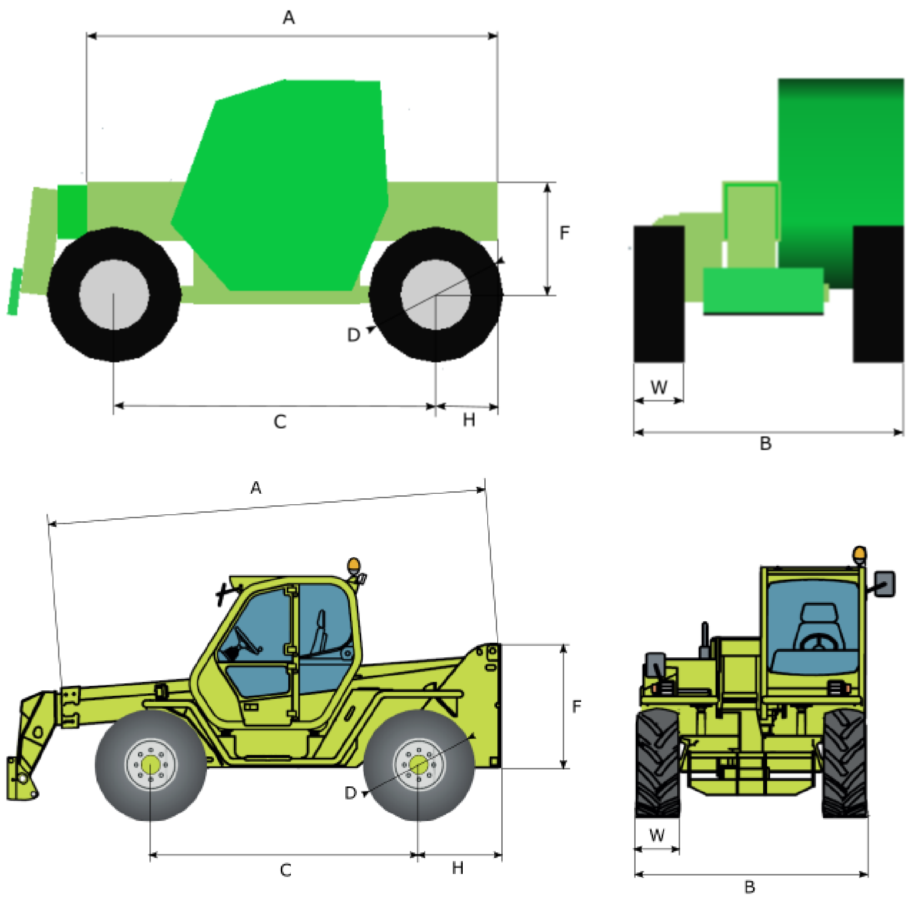

Figure 3.6: Parametrisation for all non rotating telescopic handlers

- the cab is not the same for all the machines
- the 400, 600, MCSS series of Roto have three different kinds of stabilizers
- the size and shape of the raft and of the depends on the kind of machine

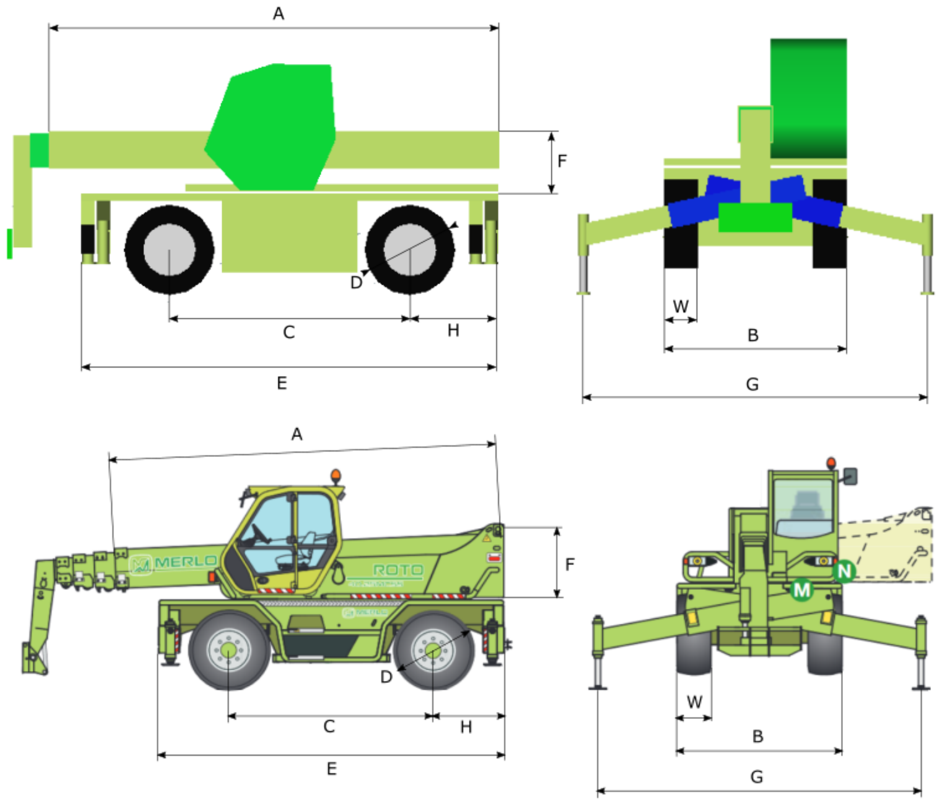

Figure 3.7: Parametrisation for all rotating telescopic handlers

Main parameters	
A	lenght of the first boom' s section
B	chassis' width
C	wheelbase
D	tyre diameter
E	chassis' lenght
F	vertical distance between the rear wheel axis and the boom joint
G	maximum extension of stabilisers
H	horizontal distance between the rear wheel axis and the boom joint
W	tyre width
n	number of etensions

Table 3.2: Parameters characterising the machine

model	VRML model	n	A (mm)	B (mm)	C (mm)	D (mm)	E (mm)	F (mm)	G (mm)	H (mm)	W (mm)
Roto 38.14	roto	2	4845	2240	2760	1076	4645	956	3750	942.5	407
Panoramic 38.12	panoramic with stabilizers	2	4200	2220	2750	1076	4100	1065	0	815	407
Turbofarmer 35.7	turbofarm er	1	3710	2250	2740	1178	3910	802	0	585	407
...	...	...	...	...	...	...	..	...	...	...	...

Table 3.3: Example of machines' database

3.2.3 GUI

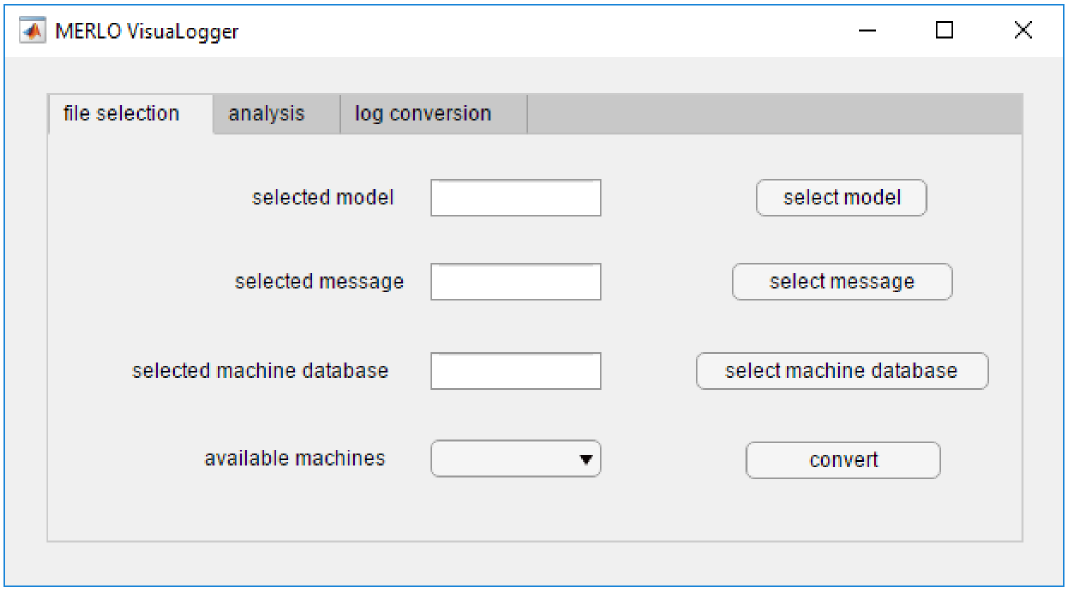

Figure 3.8: 'file selection' window

The GUI is composed of three main windows called *'file selection'*, *'analysis'* and *'log conversion'*. At the first run of the GUI the window *'file selection'* (Figure 3.8) appears. The button *'select model'* allows the user to select the VRML file (Roto, Panoramic with stabilizers, turbofarmer) suitable for the model of machine on which the data were recorded. With the button *'select message'* it is possible to select the log file to be analysed. The database with the main parameters of each model (Tab. 3.2) can be selected with button *'select machine database'*. Once these three fields have been filled it must select the model from the list box and press *'convert'*. The list box contains a list of all the machines available in the database. After this setup phase it is possible to pass to the analysis of the record clicking on the *'analysis'* window (Figure 3.9). A VRML viewer window, with the virtual representation of the selected model, opens when the button *'open virtual world'* is pressed. That configuration refers to the starting moment of the record. With the use of the slider it is possible to select a specific time instant to analyse and the viewer will adapt the configuration to the one of that specific instant. The scale of the slider is auto-adjusted according to the duration of the record. Moreover it is also possible to animate the virtual representation by pressing the *'play'* button and select the time interval of the animation typing the wanted value in the corresponding text field. The *'log conversion'* window (Figure 3.10) allows the user to convert ASCII log files recorded from the can bus into data logger-like files. The

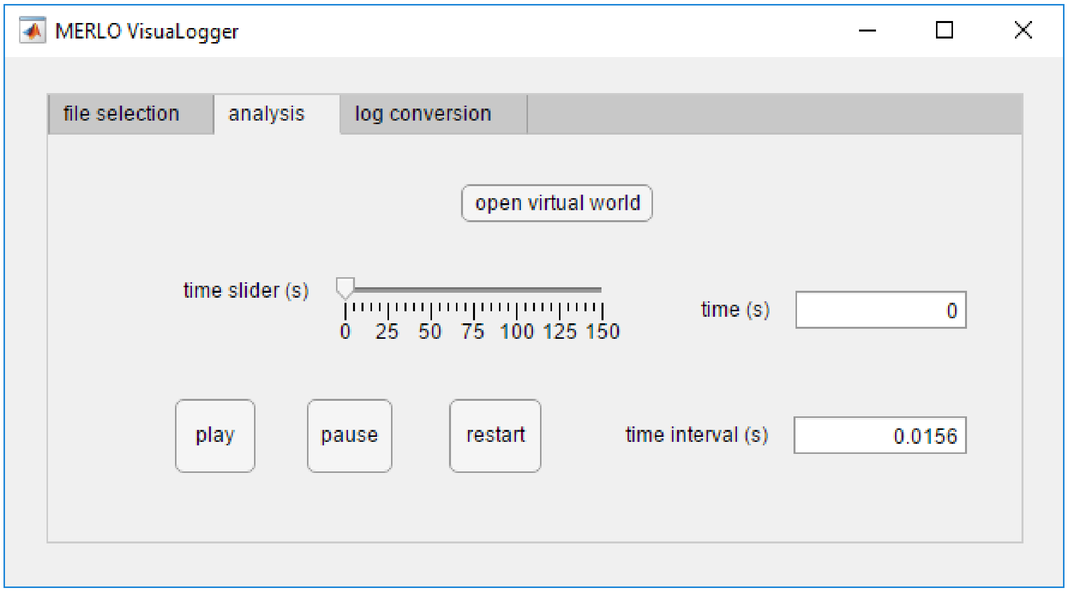

Figure 3.9: 'analysis' window

ASCII log files contain the list of all the CAN frames ID transmitted on the CAN bus during the duration of the record with the relative Data field and timestamps. Using the dbc file (Section 1.8), containing the informations about Merlo defined PGNs and SPNs, it is possible to extract, from the ASCII file, the temporal evolution of all the parameters saved by the data logger and, therefore, to convert a CAN bus record into a data logger record. To do so it is enough to press the button *'convert log'* after having selected the ASCII log with the button *'select log'* and the Merlo dbc with the *'select CAN database'* button. This operation generates a file with the same format of the data logger' s one which can therefore be analysed in the same way.

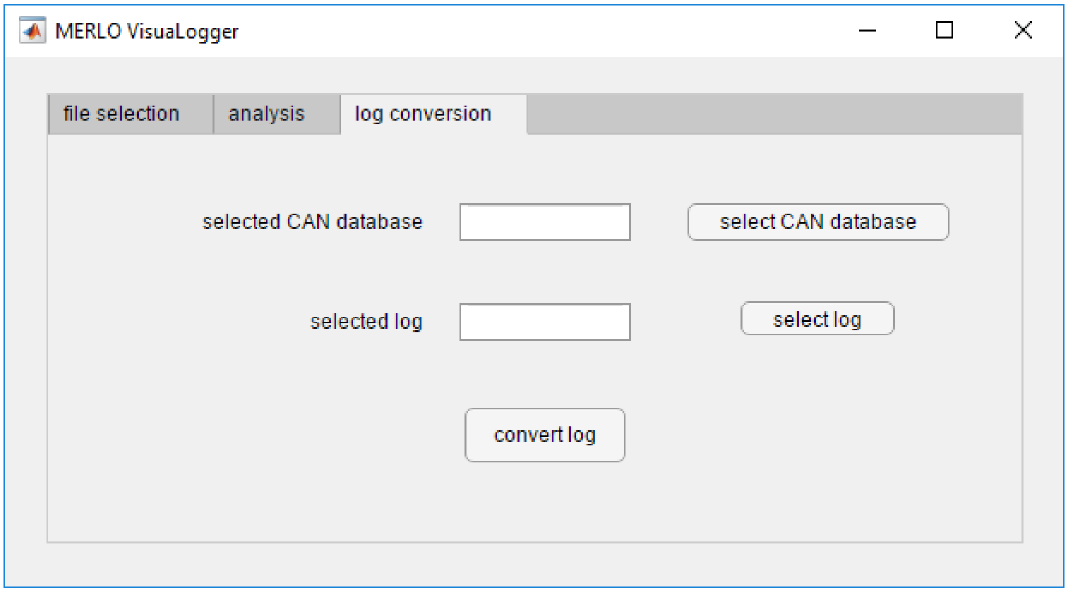

Figure 3.10: 'log conversion' window

Chapter 4

Stability requirements of telescopic handlers

This chapter aims to give an introduction to the actual international standards that deal with the safety requirements of telescopic handlers in terms of stability. The main international standards that cover this topic are:

- *CEN/TS 1459-8:2018: Rough-terrain trucks - Safety requirements and verification*

- *ISO 22915-14:2010: Industrial trucks — Verification of stability part 14: Rough-terrain variable-reach trucks*

- *ISO 22915-10:2008: Industrial trucks — Verification of stability part 10: Additional stability tests for trucks operating in the special condition of stacking with load laterally displaced by powered devices*

- *ISO 22915-20:2010: Industrial trucks — Verification of stability part 20: Additional stability test for trucks operating in the special condition of offset load, offset by utilization*

- *EN 15000:2008: Safety of industrial trucks - Self propelled variable reach trucks - Specification, performance and test requirements for longitudinal load moment indicators and longitudinal load moment limiters*

In the next sections it will be proposed a resume of the key aspects of each of the previous documents.

4.1 CEN/TS 1459-8:2018

4.1.1 Introduction

This document is intended to underline and explain the safety requirements and its verification, imposed by the Machine Directive 2006/42/EC and Tractor regulation 167/2013 for telescopic handlers. This document applies to the whole machine, to the single permanently mounted equipment but not to the removable attachment [8].
This standard defines the safety requirements for: Brakes, Electrical and electronic systems, Controls, Power systems and accessories, Stabilizing devices, Operator's station, Operator access, Protective devices, Stability requirements, Visibility, Lighting, Fire protection, Noise and Electromagnetic compatibility. In this document the focus will be only on Stability requirements and the test necessary for their verification.

4.1.2 Terms and definition

The main terms and definition introduced in the CEN/TS 1459-8:2018 concerning the stability of the machine are:

- **rough terrain variable reach (RTVR) tractor**: tractor with a permanently mounted non-slewing boom or with a slewing movement of less than 5° either side (Figure 4.1).

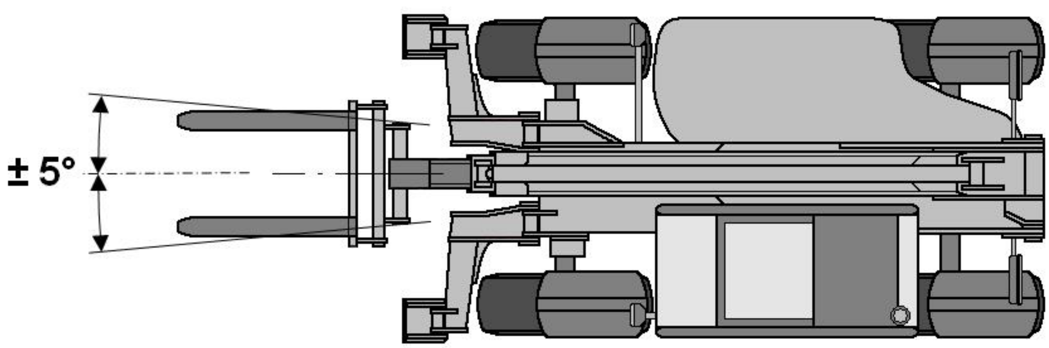

Figure 4.1: Rough terrain variable reach tractor

- **actual capacity (Q)**: maximum load, based on components strength and machine stability, that the RTVR tractor can carry, lift and stack to a specified height, at a specified standard load centre distance and reach. The actual capacity depends on: lift height, reach of the boom, standard load centre distance, load handling device (fork arms or attachment fitted) and stabilizing devices.

- **rated capacity (Q1)**: maximum load permitted at the standard load center distance that the telescopic handler is able to lift and transport on forks in normal conditions with the boom fully retracted.

- **rated capacity at maximum height or elevation (Q2)**: maximum load permitted at the standard load center distance that the RTVR can lift and transport on forks in normal conditions at the maximum lift height (H max).

- **rated capacity at maximum reach (Q3)**: maximum load permitted at the standard load center distance that the RTVR can lift and transport on forks in normal conditions at the maximum reach (d max).

- **reach (d)**: distance between a plane tangent to the front of the outside diameter of the front tyres and another described by the vertical projection of the center of gravity (G) of the load to the ground.

- **lift height (H)**: vertical distance between the upper face of the fork arms and the ground.

- **standard load centre distance (D)**: horizontal distance between the center of gravity of the load and the front of the fork shanks and vertical distance between the center of gravity of the load and the upper face of the fork arms. Typical values of standard load center distance are reported in Table 4.1.

4.1.3 Stability requirements

All the telescopic handlers shall pass the test imposed by ISO 22915-14. For specific operating conditions, foreseen by the manufacturer, the additional test of ISO 22915-10 and/or ISO 22915-20 shall apply. Moreover every machine should be fitted with a longitudinal moment indicator (LLMI) and a longitudinal load moment control, (LLMC) as imposed by EN 15000, and with a inclinometer of lateral slope visible by the operator in the cab.

Rated capacity Q in kg		Standard load center distance D in mm				
		400	**500**	**600**	**900**	**1200**
0	< 1000	x				
$\geqslant 1000$	< 5000		x			
$\geqslant 5000$	$\leqslant 10000$			x		
> 10000	< 20000			x	x	x
$\geqslant 20000$	< 25000				x	x
$\geqslant 25000$						x

Table 4.1: Typical standard load center distance

4.1.4 Verification of structural integrity

This document prescribes a static and a dynamic test in order to demonstrate the overall structural integrity in static and dynamic conditions of the loaded RTVR tractor.

Static test

RTVR tractors shall be tested at a minimum of 125% of Q1, Q2, Q3 at the corresponding positions. The test must be done on firm level ground and it is advisable to secure the machine to ground to prevent the risk of overturning.
If the telescopic handler safely supports the test load for 10 minutes without permanent deformations or obvious structural defects the test shall be considered as passed.

Dynamic test

RTVR tractors shall be tested at 100% of Q1, Q2, Q3 in a complete operating cycle, at full throttle as specified by the manufacturer, from a stationary position with a fully retracted and lowered boom to the relevant position, related to the tested capacity (Q1, Q2, Q3), and vice versa. At maximum engine speed as specified by the manufacturer:

- bring Q1 to fully retracted and maximum lifted position;

- bring Q2 to maximum height;

- bring Q3 to maximum reach.

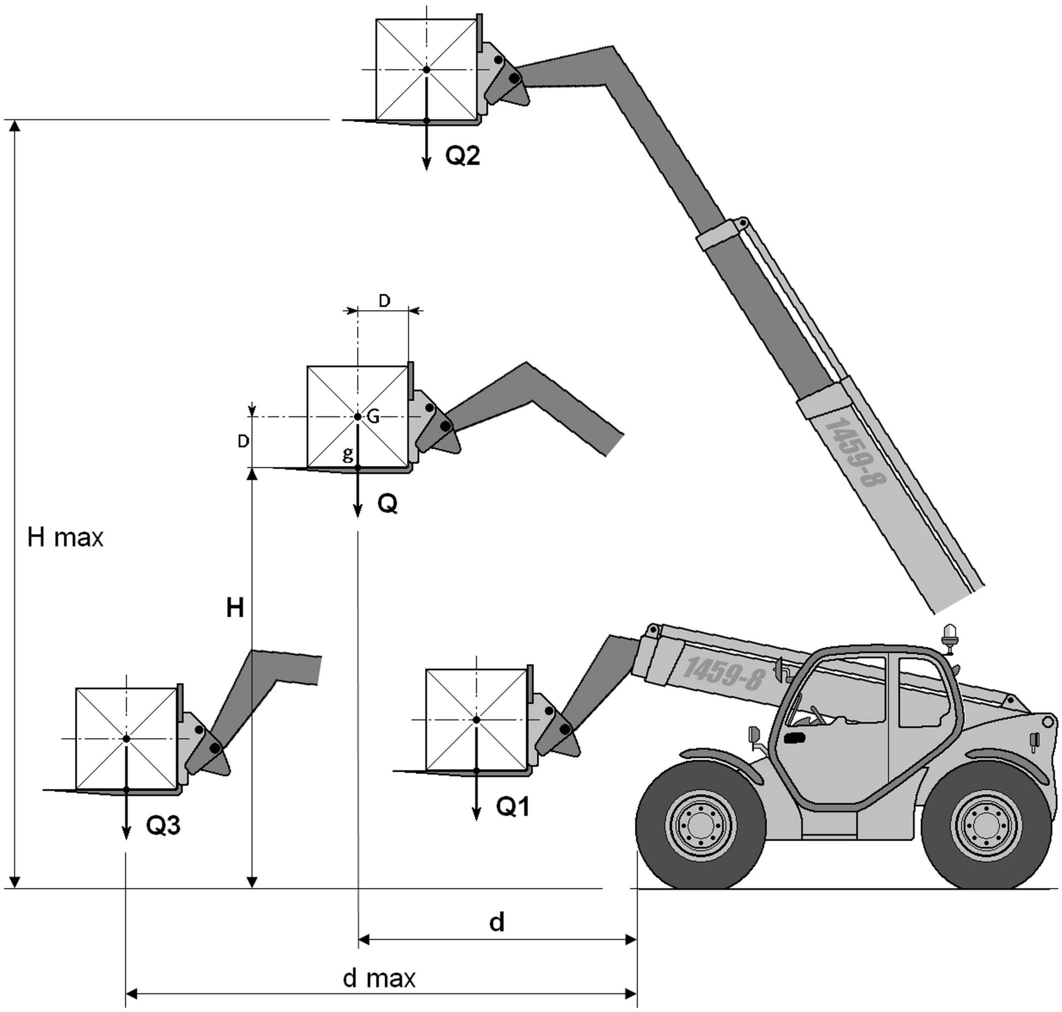

Figure 4.2: Parameters for the designation of the actual capacity of the telescopic handler with fork

Also for this test it is advisable to secure the tractor to the ground. The test is passed if no permanent deformations or obvious defect are appreciated.

4.2 ISO 22915-14:2010

4.2.1 Scope

This chapter of ISO 22915 defines the test for verifying the stability of telescopic handlers, equipped with fork arms or with load carrying or non-load carrying attachments [5]. It can not be applied to those machine used to handle freight containers or to lift people or suspended loads.

4.2.2 Terms and definitions

The terms and definition for the purposes of this document are the same defined in ISO 22915-1:

- **tilt table**: rigid table with the possibility to tilt at least on one side (around the axis X-Y in Figure 4.3) to test the lateral and longitudinal stability of the machine on that table.

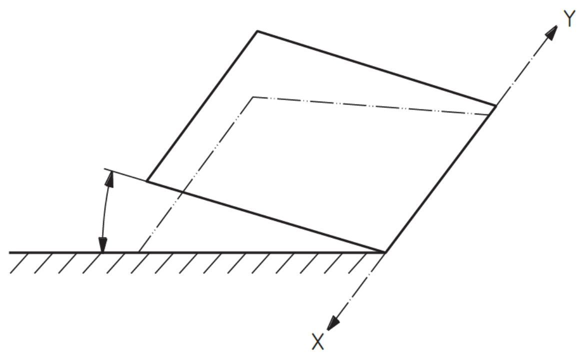

Figure 4.3: Tilt table

- **tilt axis**: axis about which the truck tips over when a sufficient static or dynamic force is applied above the center of gravity of the machine.
- **tip-over**: loss of stability when the truck completely tips over.
- **steer axle**: axis coincident with the rotation axis of one of the steering wheel of the machine (B-B in Figure 4.4).
- **load axle**: axis passing through the center of the two front wheels when they are not steered (C-C in Figure 4.4).
- **longitudinal centre plane of truck**: plane perpendicular to the ground and passing through the longitudinal axis of the machine (A-A in Figure 4.4).

4.2.3 Test

The standard introduces five different tests characterised by a number between 1 and 5. For Test 1 and Test 2 the telescopic handler shall be positioned on the tilt table with its load axle, C-C, parallel to the tilt axis, X-Y, of the tilt table. For Test 3, 4 and 5

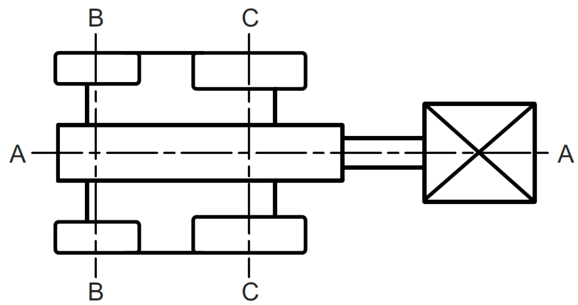

Figure 4.4: Representation of different axles

the machine shall be positioned on the tilt table in a turning position with the line , M-N, parallel to the tit axis, X-Y, of the tilt table. If the tested telescopic handler has an articulating steering axle, the wheel on the steer axle closest to the tilt axis, X-Y, shall be parallel to X-Y. The position of M and N for different kind of RTVR tractors is showed in Tables 4.3 and 4.4 where it is also possible to find a graphic representation of the machine's position on the tilt table for each test.
Test 1, 2 and 3 shall be conducted with a test load on the forks while for Test 4 and 5 the forks must be free. In Test 1 and 3 the boom shall be arranged in the least stable combination of lift and reach, with the fork arms parallel to the tilt table for the entire duration of the test. The center of gravity of the load on the forks shall fall on the longitudinal center plane of the machine. In Test 3 it is possible not to respect this condition if the tested machine is equipped with a lateral slope correction device.
For Test 2 and 4 the upper face of the fork arms, measured at the heel of the fork arm when fully tilted rearward, shall be positioned

- 300 mm above the tilt table if the machine's rated capacity (Q1) is below or equal to 10 t

- 500 mm for RTVR tractors whose rated capacity overcomes 10 t

Test 5 shall be conducted with the boom fully retracted and fully extended, at maximum boom angle and with the fork arms parallel to the tilt table. For telescopic handlers equipped with operator-selectable stabilizers and/or manual axle locking, Test 1 and 3 shall be conducted, if possible, on tyres, on stabilizers, with locked and unlocked axle. Test 3 shall be performed with a maximum lateral slope correction of 7%. Lateral correction is allowed only by means of operator-selectable stabilizers or lateral levelling. All the other tests shall be performed without the lateral slope correction. All this informations are summarized in Table 4.2.

Test criteria		**Test 1**	**Test 2**	**Test 3**	**Test 4**	**Test 5**
Direction of test	Longitudinal	x	x			
	Lateral			x	x	x
Direction ofload-handling device	Load leading	x	x			
	Load trailing					
Mode of operation	Travelling		x		x	
	Stacking/retrieving	x		x		x
Load at load centre	With	x	x	x		
	Without				x	x
Lift/reach position	Max. and min. boom extension at max. boom angle					x
	Least stable combi-nation	x		x		
	Travel		x		x	
Stabilizer device and/or axle locking device	With	x		x		
	Without	x	x	x	x	x
Lateral slope correction				x		
Position of fork arms	Horizontal	x		x		x
	Full rearward		x		x	
Tilt-table angle for actual capacity	⩽10 000 kg	7 %	22 %	12 %	50 %	10 %
	>10 000 kg	6 %		10 %	45 %	

Table 4.2: Test conditions

Test criteria	Test 1	Test 2	Test 3	Test 4	Test 5
Truck position on tilt table	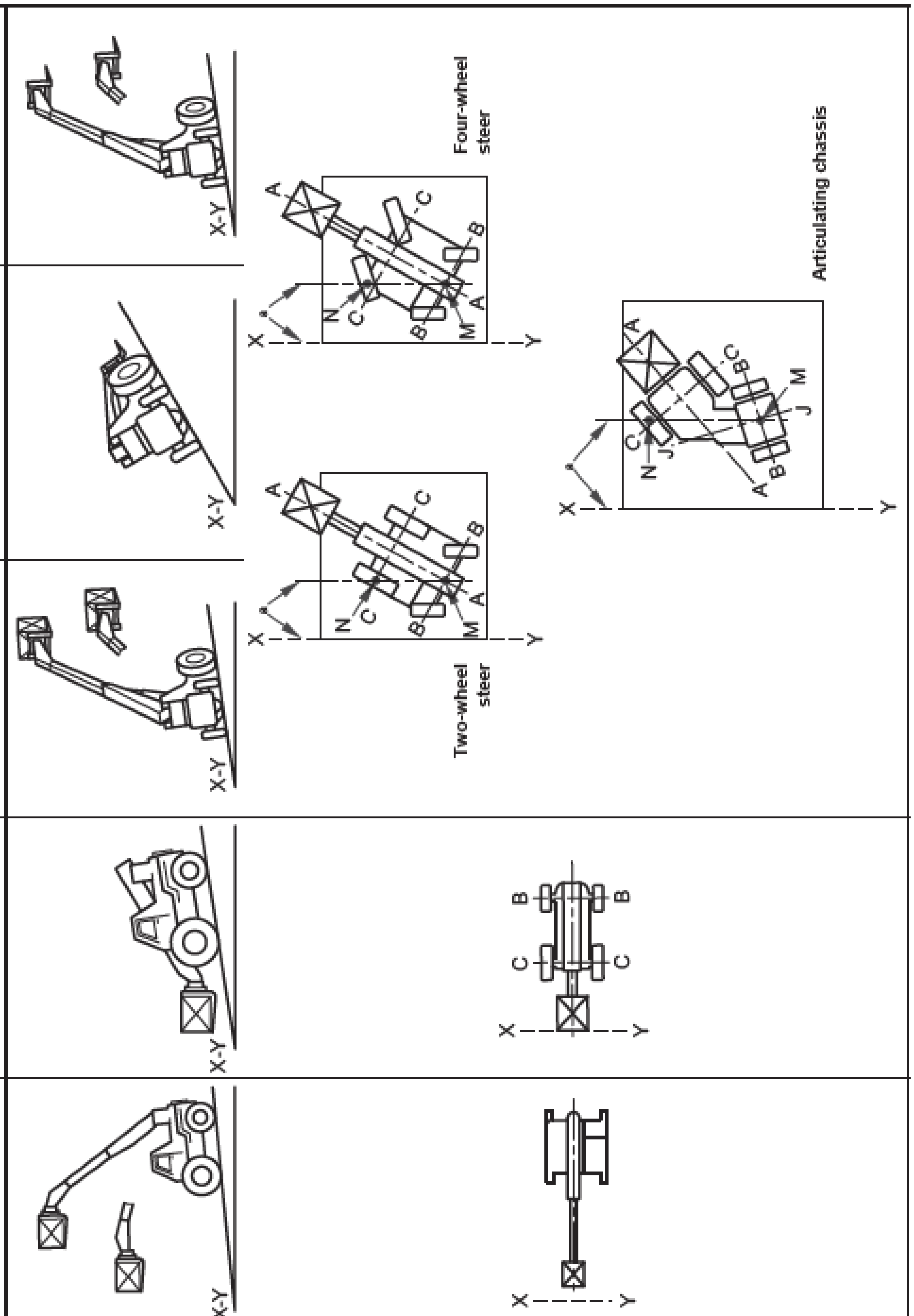				

Table 4.3: Machine's position on the tilt table Part 1

Test criteria	Test 1	Test 2	Test 3	Test 4	Test 5
Truck position on tilt table			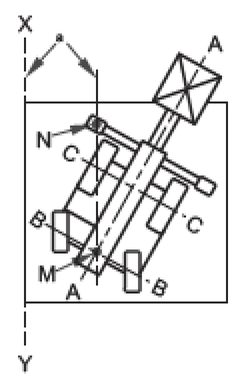 **Stabilized**	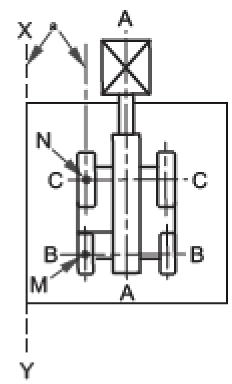 **Axles locked**	

[a] Parallel.

Table 4.4: Machine's position on the tilt table Part 2

4.3 ISO 22915-10:2008

4.3.1 Scope

This part of ISO 22915 prescribes an additional test for verifying the stability of a RTVR tractor equipped with a powered load-handling device, commonly called sideshift, which can displace the centre of gravity of the load to a substantial, predetermined extent from the longitudinal centre plane of the truck [4].
A displacement is considered to be a substantial displacement if it is greater than:

- 100 mm, for a machine with a machine with a rated capacity $<$ 5000 kg
- 150 mm, for a machine with a rated capacity $\geqslant$ 5000 kg and $\leqslant$ 10000 kg
- 250 mm, for a machine with a rated capacity $>$ 10 000 kg and $<$ 20 000 kg
- 350 mm, for a machine with a rated capacity $\geqslant$ 20 000 kg

4.3.2 Terms and definition

For the purposes of this document all the terms and definitions given in section 4.2.2 and the following apply.
special operating condition: stacking whereby loads are substantially displaced laterally by a powered device (Figure 4.5)

4.3.3 Position of the load

Before conducting the test, both the mechanism that offsets the load and the centre of gravity of the test load shall be positioned centrally to the longitudinal centre plane of the machine.
During the test, the load shall be laterally moved by substantial displacement, S (Figure 4.5), in the direction of least stability and to the fullest extent allowed by the mechanism, with forks raised to their maximum elevation.

4.3.4 Verification of stability

The stability of the truck with the load fully offset and at maximum elevation shall be verified in accordance with Test 3 of ISO 22915-14 (see section 4.2).
The capacity under this special operating condition, as determined by this additional

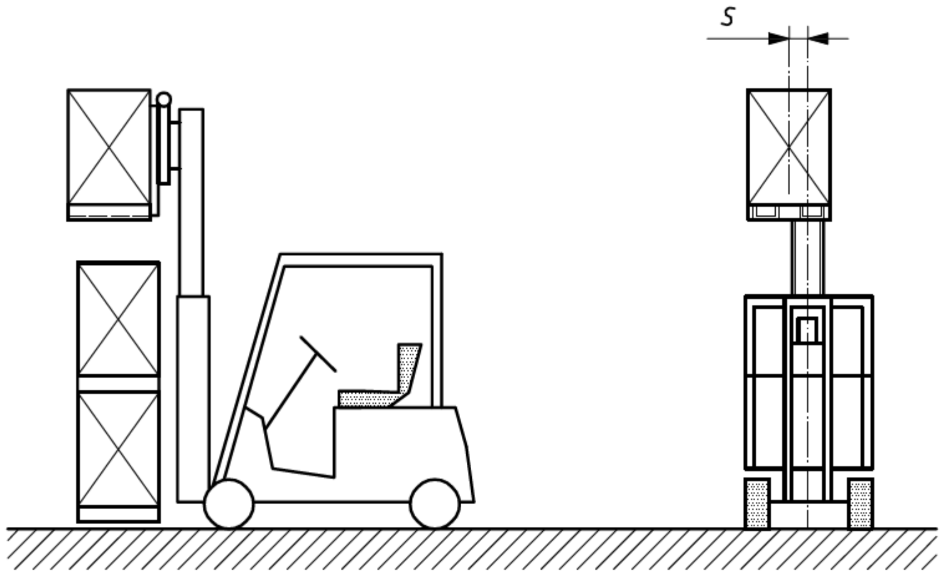

Figure 4.5: Special operating condition

stability test, and the lateral substantial displacement shall be indicated on an information plate in view of the operator.

4.4 ISO 22915-20:2008

4.4.1 Scope

This part of ISO 22915 defines an additional test in order to verify the stability of a RTVR truck whose utilization creates the special operating condition whereby there is a substantial offset between the load centre of gravity and the truck's longitudinal centre plane [6].

4.4.2 Terms and definition

For the purposes of this document all the terms and definitions given in section 4.2.2 and the following apply.

special operating condition: stacking whereby loads are substantially displaced laterally. The displacement is created by the utilization and not by a powered device (Figure 4.6).

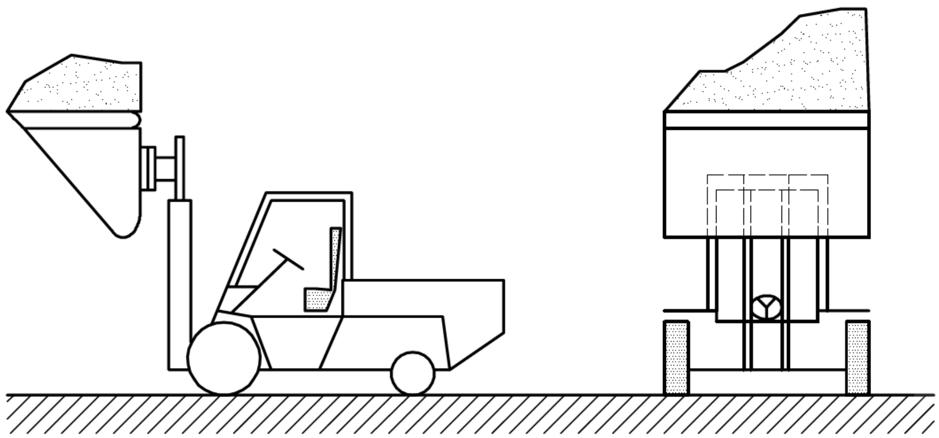

Figure 4.6: Special operating condition

4.4.3 Position of the load

The load's centre of gravity shall be offset laterally by the maximum amount is expected to find in actual operation. The test shall be conducted on the least stable side of the truck. The load shall be raised to the maximum elevation.

4.4.4 Verification of stability

The stability of the truck with the load fully offset and at maximum elevation shall be verified in accordance with Test 3 of ISO 22915-14 (see section 4.2). The capacity under this special operating condition, as determined by this additional stability test, and the load offset shall be indicated on an information plate in view of the operator.

4.5 EN 15000:2008

4.5.1 Scope

This Standard defines the technical requirements, verification and test procedure for the longitudinal load moment indicators (LLMI) and longitudinal load moment control (LLMC) systems operating in the forward direction for telescopic handlers [1]. This Standard focuses on LLMI and LLMC systems in case of loading or placing operations on consolidated, stable and level ground.
This Standard does not take into account the risk due to lateral instability, or instability during the travelling of the machine. The LLMI and LLMC do not warn of the

overturning risk while the machine is travelling.

4.5.2 Terms and definitions

The main technical terms used in this Standard are:

- **longitudinal load moment**: moment produced by the load, the attachment and the lifting means which acts at the load centre of gravity to overturn the machine in the forward direction.

- **longitudinal load moment indicator (LLMI)**: device warning the operator of the increasing longitudinal load moment due to a change in the load handling geometry.

- **longitudinal load moment control (LLMC)**: device that limits the possible operations in case a change in the load handling geometry would increase the longitudinal load moment beyond allowable limits.

- **load handling geometry**: relationship of points, lines and angles, described by the position of the load (boom, carriage and attachment) centre of gravity and the tipping line (the line on the ground connecting the center of the front wheels or front stabilizers' contact area).

4.5.3 Requirements for the LLMI

The LLMI shall continuously warning the operator starting at a pre-determined limit of the longitudinal load moment and being maintained with the activation of the LLMC. The warning should stop only when the longitudinal load moment returns below the pre-determined limit at which the warning started. The warning must be both audible and visible.

4.5.4 Requirements for the LLMC

The LLMC shall stop any change in the handling geometry which would increase the longitudinal load moment. After the stop the only movement that reduce the longitudinal load moment shall be possible. The stopping of the movement shall not lead to instability. It shall be possible to override the LLMC in just two cases:

- when the boom is fully retracted, LLMC and the audible warning of LLMI may be disconnected.

- when a the operator run control with a 2-hand hold complying with EN574

Temporary lifting of the rear wheels is permitted during the test.

4.5.5 Verification

Verifications shall be carried out on a representative number of machines and on each model equipped with LLMI and LLMC. The test shall be done with the machine on wheels and on stabilizers. The telescopic handler shall remain stable throughout the execution of the test. The proper functioning of the LLMI/LLMC shall be tested with a variety of load and reaches including the maximum allowed loads and reaches according to the load chart. The test should follow a precise procedure:

- engine at low idle

- fully actuate the lowering control of the boom

- accelerate the engine to maximum speed

- allow the LLMC to stop the descent at various lift points

- it shall be possible to bring the load to ground in safe condition after trigger of the LLMC

A test is valid even if rear wheels temporary lifted.
Figure 4.7 shows the main phases of a typical test for the validation of the LLMC.

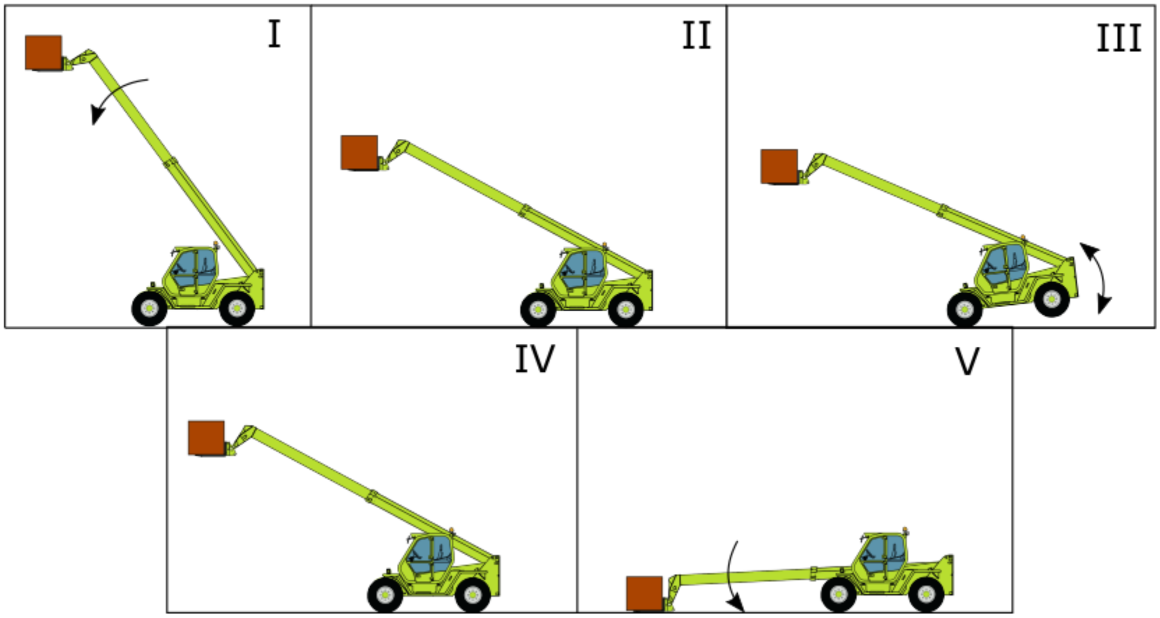

Figure 4.7: Execution phases of the test

Chapter 5

Study of the vehicle dynamics and stability: analysis of the experimental data

This second main part of the thesis is dedicated to the study of the longitudinal dynamics and stability of a telescopic handler. This study has been promoted by Merlo in order to develop a new dynamic stability control system able to make the machines overcome the test prescribed in the EN 15000:2008. In order to avoid the risk of overturning the machine during the test there are two main approaches that it is possible to adopt:

- make the machine inherently stable by reducing the maximum allowable tilting speed of the boom. This approach can be applied on a 'blind' machine (a machine without any sensor giving information about the mass of the load and its position) reducing the total cost but on the other hand it does not allow fast movement of the load. In fact this approach limits fast movements also when those would be completely safe because the maximum allowable boom tilting speed is estimated testing the machine in the worst conditions (lowering the boom fully extended and with an heavy load).

- compute the dynamic longitudinal load moment taking into account the inertial effect of the boom tilting and limit the boom tilting speed or blocking it when it overcomes a limit value. This solution lets the machine move the boom with the maximum allowable tilting speed in every condition of load and boom extension but on the rebound it is quite expensive because it requires to know the mass of the load and its position.

Merlo adopts mainly two different stability control systems depending on the kind of machine. The basic models with a limited maximum boom length are inherently stable so they do not suffer from dynamic stability problems. Their stability system only prevents movement that could bring the load in some zones of the load chart where the static stability would not be granted.
All the other models are equipped with a patented system called CDC (Controllo Dinamico del Carico - Dynamic Load Control) that follows the second approach previously described. Knowing the mass of the load, the tilting angle of the boom, the extension of the boom and the kind of equipment mounted on the raft this system is able to adapt the stability diagram of the machine according to the kind of equipment and compute the dynamic longitudinal load moment. When the dynamic longitudinal load moment overcomes a safe value the movement of the boom is blocked.
Merlo has encharged the Politecnico di Torino to develop a dynamic stability control system to adopt on machines that are not equipped with the CDC. Since the price of these kind of machines is relatively low it is not possible to install the CDC because it would be too expensive in relation to the final price of the machine. The high cost of the CDC derives form the fact that it requires to install several sensors to know the mass of the load, the kind of equipment, the extension of the boom and the angle of the boom, so the new system must limit the number of sensors of the machine but at the same time it must allow the machine to move the boom faster than the actual system. This new control system will be based on the installation of an inertial measurement unit (IMU) on the boom and one on the chassis. For this reason the next section will explain what is an IMU and how it can be used to find the inclination angle of the chassis and of the boom.
In order to accurately design and tune the new control system it was decided to adopt a numerical approach, developing a numerical multibody model of a telescopic handler by using the commercial software Adams view, and verifying the real dynamic behaviour of the machine by means of a series of tests done at the headquarter of the Merlo on a real machine. In this document it will be described the process of analysis of the experimental data and of characterisation of the telescopic handler's longitudinal dynamic behaviour .

5.1 Inertial measurement unit

An IMU is an electronic device that can measure angular rate and accelerations [13]. Is is typically composed of a 3-axis accelerometer and a 3-axis gyroscope. This kind of IMU is considered to have 6-axis. Three additional axis can be added by integrating also a magnetometer in order to get a 9-axis IMU. 9-axis IMU are the only ones giving the possibility to measure all the 6 degrees of freedom (DOF) of a single rigid body, which include three degrees of translation along each axis (x, y, z) and three degrees of rotation about the three axis (pitch, roll, yaw) (Figure 5.1). 6-axis sensors are also widely used but do not allow to find the yaw angle.
IMUs were originally adopted on Inertial Navigation Systems which use the IMU data to compute the altitude, the angular rates, linear velocity and position relative to a global reference frame (Figure 5.2). IMU became essential also in the guidance and control systems adopted on unmanned vehicles and also for security electronic systems on motorcycles. Nowadays thanks to the spread of tiny low cost IMUs they are in many consumer products. Almost all smartphones and tablets have an IMU to orientate the screen view.

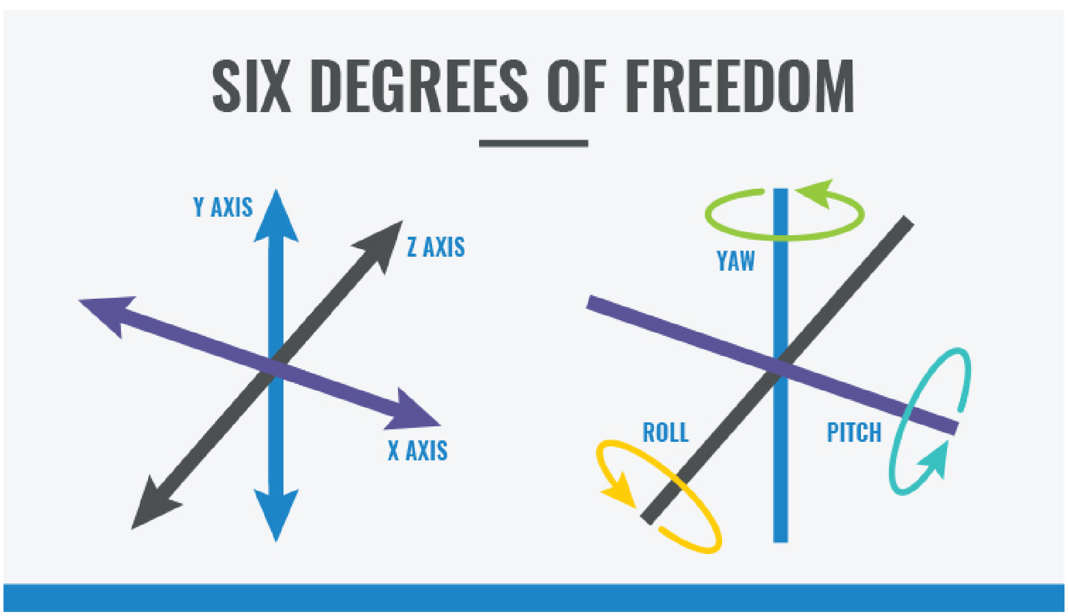

Figure 5.1: Degrees of freedom of a body in the space

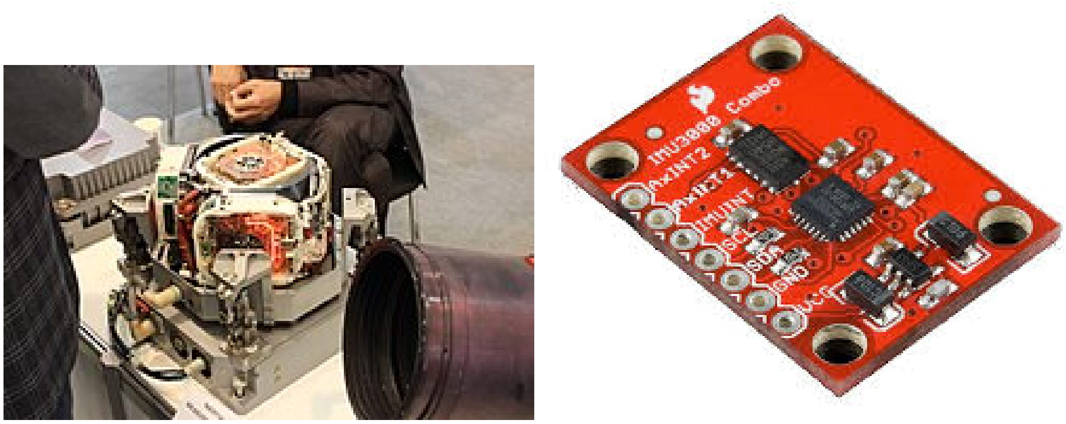

(a) Aircraft IMU (b) Drone IMU

Figure 5.2: Different kind of IMUs

5.1.1 Derivation of the roll and pitch angle

The output data of an IMU is a discrete temporal evolution of the acceleration along the three axis (x,y and z) and the angular velocity around those axis. Since the goal of the tests performed at the Merlo head-quarter was to investigate the oscillations of the boom angle and of the chassis along the longitudinal axis the extracted data have been used to evaluate the temporal evolution of the pitch angle of the different IMUs mounted on the vehicle (see Section 5.3). The common procedure to find the pitch (θ_x) and the roll (θ_y) angle suggests to estimate those angles by using the data from the accelerometer, finding $\theta_{x,acc}$ and $\theta_{y,acc}$, and the gyroscope, finding $\theta_{x,gyr}$ and $\theta_{y,gyr}$, and then integrate the two results with a complementary filter. The accelerometer is sensitive to the gravitational acceleration and this means that in static condition it is the only acceleration measured by the sensor. This information is at the basis of the extrapolation of the pitch and roll angle from the acceleration data because, knowing that the gravitational acceleration always points towards the center of the earth, the orientation of the IMU reference frame with respect to the gravity vector can be derived from the measured value of the acceleration along the different axis as showed in Figure 5.3. The equations 5.1 and 5.2 show how it is possible to find the rotation angle around the x-axis and the y-axis. They are based on the hypothesis that the acceleration measured by the accelerometer always point toward the earth's center. The index i that appears in those equations refers to each discrete recorded time instant.

From the left scheme of figure 5.3 it is possible to understand why it it is impossible to estimate the yaw angle from the accelerations values, in fact if the IMU rotates

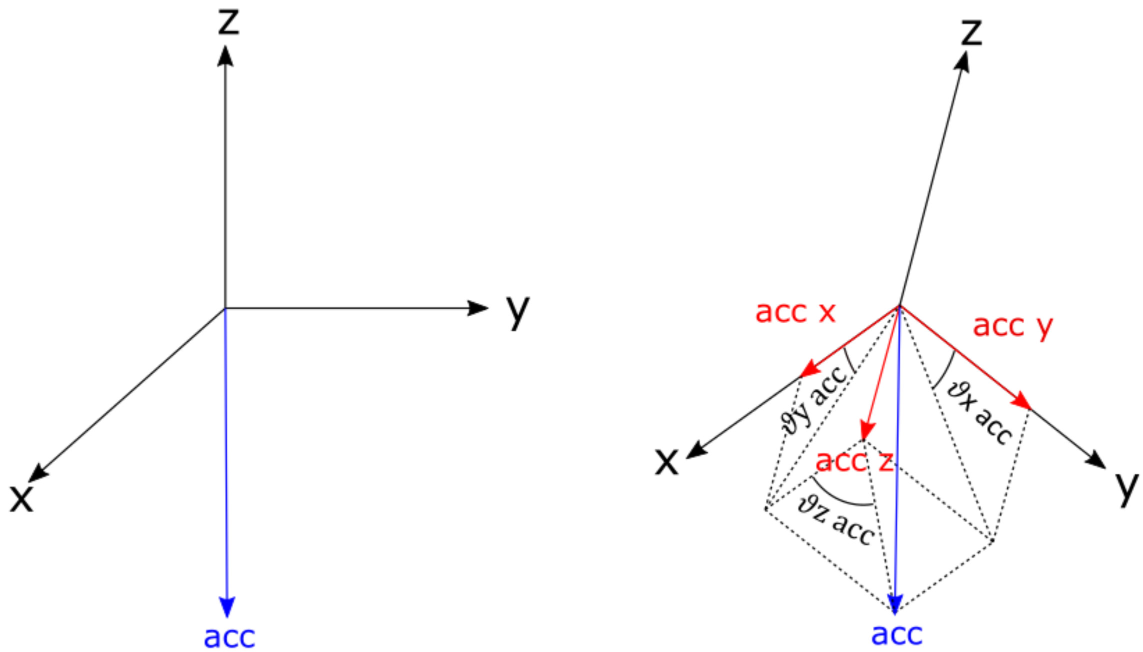

Figure 5.3: Angles derived from accelleration

around the z-axis no changes in the measured accelerations along the three axis can be appreciated. In order to be able to estimate the yaw angle it must use a 9-axis IMU that contains also a magnetometer. In this document it will not be described how to find the yaw angle because it was not necessary to find it since it is not supposed to vary during the test.

For slow acceleration of the IMU the main acceleration measured by the accelerometer is always close to the gravitational one and so the measure of the angle given by the accelerometer is quite precise. On the other hand whenever the IMU undergoes strong accelerations the vectorial sum of the gravity vector and the external one strongly differs both in direction and modulus from the gravitational vector reducing the precision of the computed angle value.

$$\theta_{x,acc,i} = \arctan \frac{acc_{y,i}}{\sqrt{acc_{z,i}^2 + acc_{x,i}^2}} \tag{5.1}$$

$$\theta_{y,acc,i} = \arctan \frac{acc_{x,i}}{\sqrt{acc_{z,i}^2 + acc_{y,i}^2}} \tag{5.2}$$

On the other hand in order to find the value of the rotation angle from the gyroscope data it is necessary to integrate the angular velocities along a certain period of time as showed in following equations:

$$\begin{aligned}
\theta_{x,gyr,i} &= \theta_{x,acc,i} \qquad \text{if } i = 1 & (5.3)\\
\theta_{x,gyr,i} &= \theta_{x,gyr,i-1} + \omega_{x,i}\Delta t \qquad \text{if } i > 1 & (5.4)\\
\theta_{y,gyr,i} &= \theta_{y,acc,i} \qquad \text{if } i = 1 & (5.5)\\
\theta_{y,gyr,i} &= \theta_{y,gyr,i-1} + \omega_{y,i}\Delta t \qquad \text{if } i > 1 & (5.6)
\end{aligned}$$

Since the θ_{gyr} is obtained by integration of the angular velocity it is not possible to know the initial orientation of the IMU. For this reason the initial orientation is given imposing $\theta_{gyr,1} = \theta_{acc,1}$.

Once that θ_{gyr} and θ_{acc} have been evaluated, they must be integrated to find the best approximation of the real evolution of the angles. In fact neither the angle obtained from the gyroscope (θ_{gyr}) nor the angle obtained from the accelerometer (θ_{acc}) provide a good approximation of the real evolution of the desired angle. The accelerometer data are strongly affected by high frequency noise that produces jitter and it is for this reason that θ_{acc} gives a good approximation of the slow movement but fails in reproducing the exact dynamic behaviour. On the rebound the θ_{gyr} approximates very well the dynamic behaviour but fails in reproducing slow movements due to the drift error deriving from the temporal integration of the measure errors. The best trade off to integrate those two results is given by the complementary filter (Figure 5.4). The

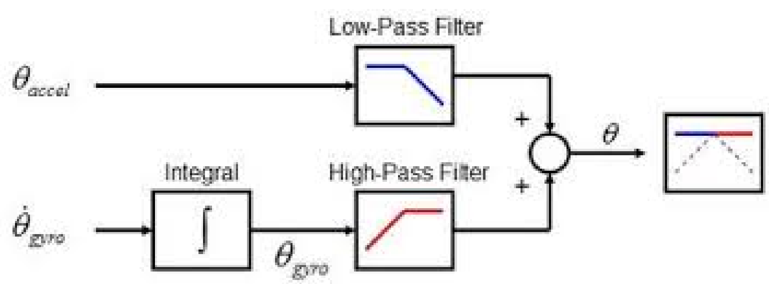

Figure 5.4: Schematic representation of the complementary filter

complementary filter basically filters the θ_{gyr} with an high pass filter and the θ_{acc} with a low pass filter and then integrate the filtered signals ($\theta_{gyr,f}$ and $\theta_{acc,f}$) with a specific formula. The low-pass filter removes the high frequency jitter on θ_{acc} while the high-pass filter removes the drift from θ_{gyr}. More details about the complementary filter will be given in section 5.1.2 but before this it must describe how a low-pass filter and an high-pass filter works.

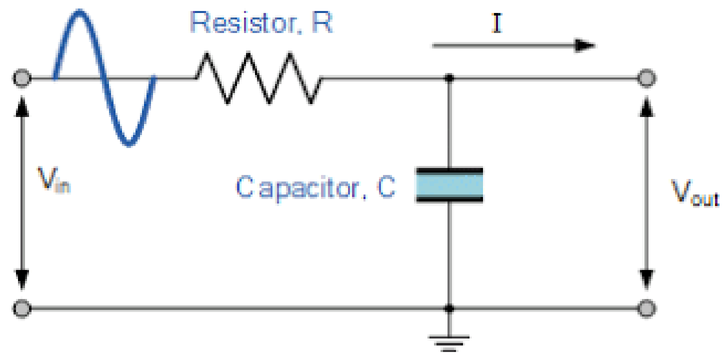

Figure 5.5: A simple RC circuit

Low-pass filter

A low-pass filter (LPF) is a filter that leaves almost unchanged the signals with a frequency lower than a selected cut-off frequency (f_c), also called corner frequency, and attenuates signals with frequencies higher than f_c [12]. The effect of a low pass filter can be analysed taking as example an RC electric circuit. From the diagram in Figure 5.5 according to Kirchoff's laws, the first Ohm's law and the definition of capacitance it is possible to write:

$$v_{in}(t) - v_{out}(t) = Ri(t) \tag{5.7}$$

$$Q_c(t) = Cv_{out}(t) \tag{5.8}$$

$$i(t) = \frac{dQ_c(t)}{dt} \tag{5.9}$$

Where $v_{in}(t)$ and $v_{out}(t)$ are the tensions measured at the left and right poles of the circuit, $i(t)$ is the current intensity through the resistance R, Q_c is the charge stored in the capacitor with a capacity C. Putting the previous equation together it is possible to write:

$$v_{in}(t) - v_{out}(t) = RC\frac{dv_{out}}{dt} \tag{5.10}$$

The product between the resistance R and the capacity C gives the time constant of the filter τ that is directly related to the cut-off frequency according to equation 5.11.

$$f_c = \frac{1}{2\pi RC} = \frac{1}{2\pi\tau} \tag{5.11}$$

The frequency response of a LPF (the variation of the amplitude and phase shift of v_{out} according to the frequency of v_{in}), is usually analysed by means of a Bode diagram (Figure 5.6). A Bode diagram is a combination of two different plots showing the variation of the Magnitude (also called Gain) and the Phase shift, between the output

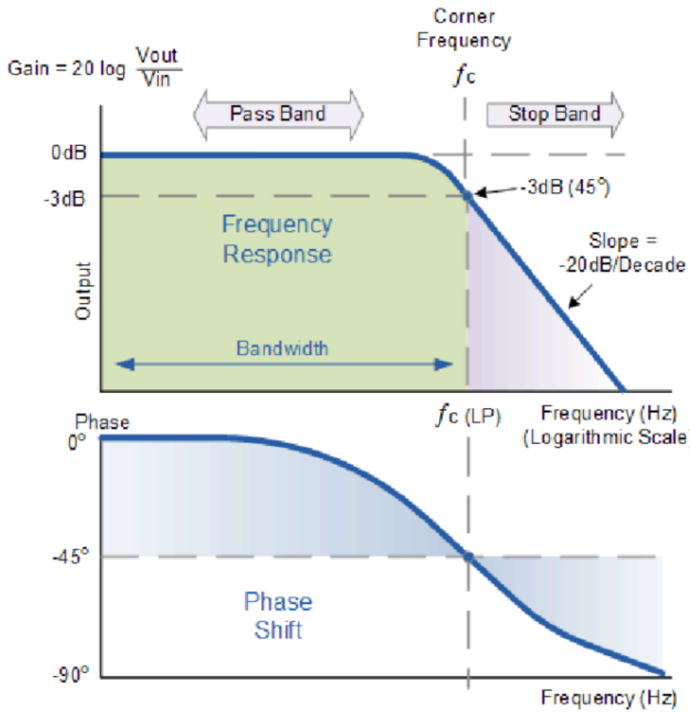

Figure 5.6: Bode diagram of a low-pass filter

and the input signal, in the frequency domain on a logarithmic scale. The Magnitude is expressed in decibels that is defined as 20 times the logarithm of the ratio between the output and input signal ($20\log(\frac{v_{out}}{v_{in}})$ for the RC filter example). The Phase shift is expressed in degrees.

On the Gain-frequency plot it is possible to distinguish the cut-off frequency and the Slope of the curve. The cut-off frequency is that value of frequency at which the filter attenuates the input power by 3 dB ($20\log(\frac{v_{out}}{v_{in}}) = -3$) and it divides the frequency spectrum into two bands: the *Pass band* that leaves almost unchanged the amplitude of the input signal ($20log(\frac{v_{out}}{v_{in}}) \approx 0 \longrightarrow v_{out} \approx v_{in}$) and the *Stop band* where the input signal is attenuated. More precisely the *Stop band* is characterised by a certain Slope of the curve. Since the Gain-frequency curve is not straight its characteristic Slope is the one to which the curve tends for very high frequencies values ($f \to \infty$). In case of a first order filter (like the RC of the example) the slope of the curve tends to -20 decibels per decade. One decade is a unit for measuring frequency ratios on a logarithmic scale. One decade corresponds to a ratio of 10 between two frequencies.

For higher order low-pass filter the Bode diagram remains almost unchanged in the *Pass band* zone but the slope of the *Stop band* becomes more steep. For example a second order low pass filter has a Slope of -40 decibels per decade.

In many cases the signal to be filtered is not continuous but assume a finite number of discrete values along a certain period of time. In this case the equation 5.10 can be discretised assuming that samples of the input and output are taken at equally spaced time instants separated by Δt seconds. Representing the samples of $v_{in}(t)$ with the sequence of a generic input variable $(x_1, x_2, ..., x_n)$ of the filter, and those of $v_{out}(t)$ with a generic output variable $(y_1, y_2, ..., y_n)$, and substituting in the 5.10 it is possible to find:

$$x_i - y_i = RC\frac{y_i - y_{i-1}}{\Delta t} \tag{5.12}$$

Equation 5.12 can be rearranged in the following formulation

$$y_i = x_i\left(\frac{\Delta t}{RC + \Delta t}\right) + y_{i-1}\left(\frac{RC}{RC + \Delta t}\right) \tag{5.13}$$

Introducing the *smoothing factor* as $\alpha_{LPF} = \frac{\Delta t}{RC+\Delta t}$ the equation 5.13 becomes:

$$y_i = \alpha_{LPF}x_i + (1 - \alpha_{LPF})y_{i-1} \tag{5.14}$$

Adapting this equation to filter the θ_{acc} we obtain:

$$\theta_{acc,i,f} = \alpha_{LPF}\theta_{acc,i} + (1 - \alpha_{LPF})\theta_{acc,i-1,f} \tag{5.15}$$

In this case τ does not derive from the product of a resistance and a capacity but will be derived from the cut-off frequency recalling that $\tau = \frac{1}{2\pi f_c}$. f_c is chosen according to the range of frequencies that it is reasonable to expect that the IMU vibrates with.

High pass filter

An high-pass filter (HPF) works in the opposite way with respect to a low-pass filter. In fact it leaves almost unchanged signals with a frequency higher than a certain cut-off

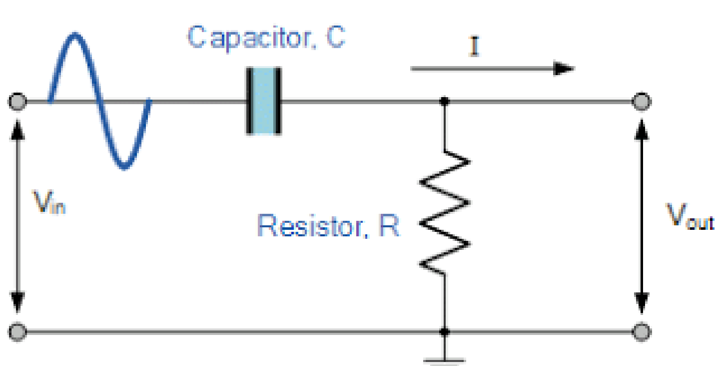

Figure 5.7: A simple RC circuit

frequency and attenuates those signals with a frequency below the cut-off frequency [14]. Also this kind of filter can be analysed taking as example a RC circuit (Figure 5.7). In this case the positions of the resistance (R) and of the condenser (C) have been inverted with respect to the scheme of the LPF (Figure 5.5). From the diagram in Figure 5.5 according to Kirchoff's laws, the first Ohm's law and the definition of capacitance:

$$v_{out}(t) = Ri(t) \tag{5.16}$$

$$Q_c(t) = C\left(v_{in}(t) - v_{out}(t)\right) \tag{5.17}$$

$$i(t) = \frac{dQ_c(t)}{dt} \tag{5.18}$$

Putting the previous equation together it is possible to write:

$$v_{out}(t) = RC\left(\frac{dv_{in}(t)}{dt} - \frac{dv_{out}(dt)}{dt}\right) \tag{5.19}$$

Also in this case the time constant of the filter (τ) is given by the product between the resistance R and the capacity C. Since the equation 5.11 is valid also for a high-pass filter, the circuits in Figure 5.7 and 5.5 have the same cut-off frequency if they have the same resistance (R) and the same capacity (C).

Observing the Bode diagram of an HPF (Figure 5.8) it is clear that the phase-frequency plot is the same of an LPF but the Gain-frequency plot is mirrored along a vertical axis passing through the cut-off frequency with respect to the LPF' s one. Equation 5.19 can be discretized assuming that samples of the input and output are taken at equally spaced time instants separated by Δt seconds. Representing the samples of $v_{in}(t)$ with a generic input variable sequence $(x_1, x_2, ..., x_n)$, and those of $v_{out}(t)$ with the generic output variable$(y_1, y_2, ..., y_n)$, and substituting in the equation 5.19::

$$y_i = RC\left(\frac{x_i - x_{i-1}}{\Delta t} - \frac{y_i - y_{i-1}}{\Delta t}\right) \tag{5.20}$$

Equation 5.20 can be rearranged in the following formulation

$$y_i = \frac{RC}{RC + \Delta t} y_{i-1} + \frac{RC}{RC + \Delta t}\left(x_i - x_{i-1}\right) \tag{5.21}$$

Introducing the *smoothing factor* as $\alpha_{HPF} = \frac{RC}{RC+\Delta t}$ the equation 5.21 becomes:

$$y_i = \alpha_{HPF} y_{i-1} + \alpha_{HPF}(x_i - x_{i-1}) \tag{5.22}$$

Adapting the previous equation to filter the angle derived from the gyroscope (θ_{gyr}) we obtain:

$$\theta_{gyr,i,f} = \alpha_{HPF}\theta_{gyr,i-1,f} + \alpha_{HPF}(\theta_{gyr,i} - \theta_{gyr,i-1}) \tag{5.23}$$

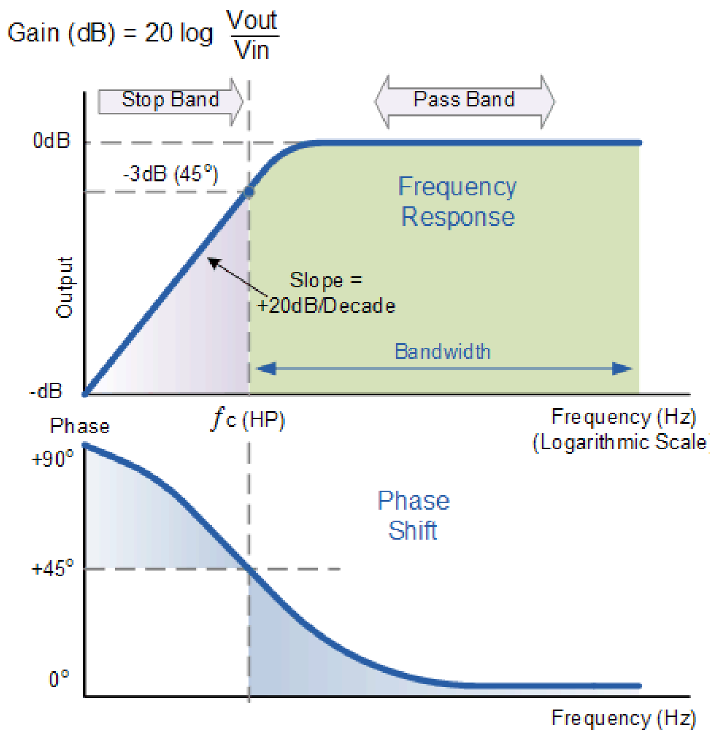

Figure 5.8: Bode diagram of an high pass filter

5.1.2 Complementary filter

The idea behind complementary filter is evaluate slow moving signals with θ_{acc} and fast moving signals with θ_{gyr} and combine them passing the accelerometer signals through a low-pass filter and the gyroscope signals through a high-pass filter. The key-point at the base of the characteristic equation of the complementary filter (equation 5.24) is that if the cut-off frequency of the two filters is the same, the frequency response of the low-pass and high-pass filters add up to 1 at all frequencies.

$$\theta = c_f \theta_{acc,f} + (1 - c_f)\theta_{gyr,f} \tag{5.24}$$

c_f is a coefficient that can assume a value between 0 and 1 that measures how much the angle given by the accelerometer must weight on the final value of the angle. A description of how this coefficient has been chosen in the analysis of the data recorded on the telescopic handler is described in section 5.4.

5.2 Terms and definitions

Before starting describe how the tests were performed and analyse the results it is necessary to define some terms and give some definition that will be used in the next sections:

- **boom**: it includes the whole tilting arm with all its sliding square sections and the raft, that device fitted at the end of the boom to mount interchangeable attachments. The boom does not include the attachment (like bucket, forks etc.).
- **boom extension (b_e)**: it is the difference between the actual length of the boom and the length of the boom completely retired.
- **lower frame**: it is what remains of the machine if the wheel, the boom and the attachment are removed.
- **load**: it includes the forks and the load over them.
- **weight on forks (w_f)**: it is the weight of the load on the forks.

5.3 Test setup

During two main test days at Merlo headquarter we had the opportunity to perform several times the test prescribed by the EN 15000:2008 (see Section 4.5) with different values of boom extension and weight on the forks (see Table 5.1.). The tested machine, a Merlo panoramic 40.14 (Figure 5.9) is equipped with the CDC. This system can be tuned modifying some parameters that regulate the reactivity of the system to situations that could lead to the overturn of the machine. CDC 'LOW' means that the system is regulated on the safe side blocking the movement of the boom as soon as it appears a low risk of overturning. CDC 'HIGH' means that the system is regulated on a lower safety level blocking the movement of the boom only in those situations with an high risk of overturning.
Those tests made us identify both the dynamic behaviour of the machine and the way the CDC operates to prevent the overturning of the machine.

In order to clearly investigate the behaviour of the machine during the tests four IMUs were mounted on it. Each IMU is characterised by a number from 1 to 4. IMU 1 was mounted below the frontal axis, IMU 2 on the top of the boom, IMU 3 above the

n	b_e **(mm)**	w_f **(kg)**	**CDC**
1	0	0	HIGH
2	7500	0	HIGH
3	7500	0	HIGH
4	0	1000	HIGH
5	2000	1000	HIGH
6	4000	1000	HIGH
7	6000	1000	HIGH
8	7500	1000	HIGH
9	2000	1000	LOW
10	3000	1000	LOW
11	4000	1000	LOW
12	5000	1000	LOW
13	6000	1000	LOW
14	1000	2000	LOW
15	2000	2000	LOW
16	3000	2000	LOW
17	4000	2000	LOW
18	2000	2000	HIGH
19	4000	2000	HIGH

Table 5.1: Test list

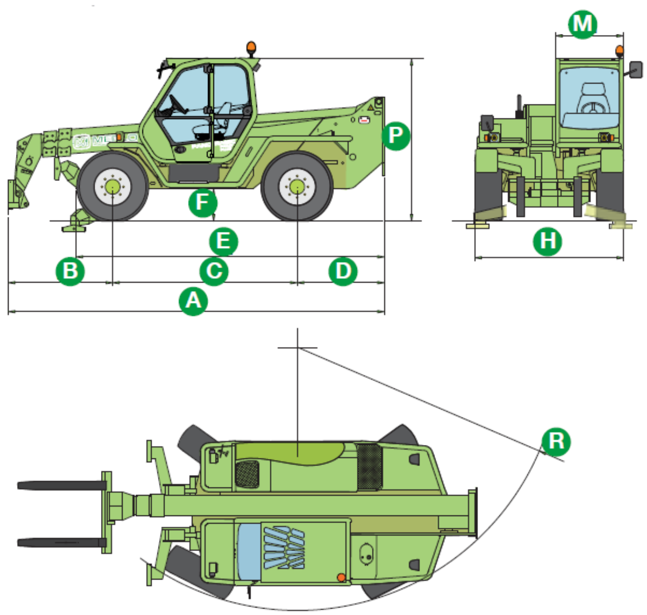

dimensions p 40.14			
A (mm)	5590	**F (mm)**	480
B (mm)	1540	**H (mm)**	2220
C (mm)	2750	**M (mm)**	1010
D (mm)	1300	**P (mm)**	2440
E (mm)	4585	**R (mm)**	3920

Figure 5.9: Selected model for the test

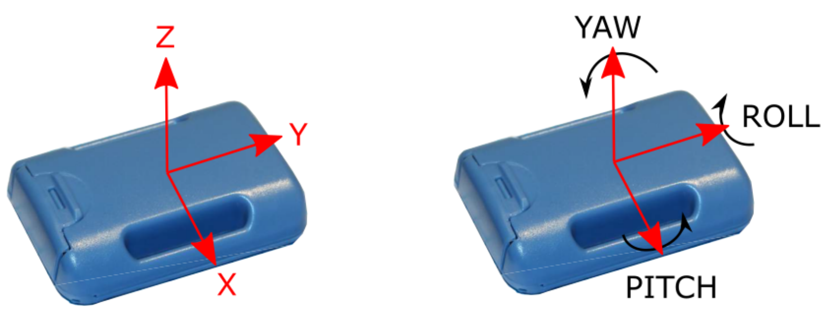

Figure 5.10: IMU reference frame

rear axis, IMU 4 on the lower frame close to its the centre of mass. The IMU chosen for the measurement have 9-axis and so they can measure the 6 degrees of freedom of a body. They record data from the digital sensors which are time stamped (sampling frequency = 50 Hz) using a real time clock and stored to a microSD card in simple text format [2]. Figure 5.10 shows how the reference frame is orientated on the IMU.

Moreover the machine is also equipped with an optical encoder that measures the inclination of the boom with respect to the lower frame and a sensor that returns the longitudinal and the transversal inclination of the lower frame. These sensors are essential for the CDC and return their measures on the CAN bus of the machine with a sampling frequency of 10 Hz.

Using data extracted form the IMUs and the CAN bus it is possible to extract the

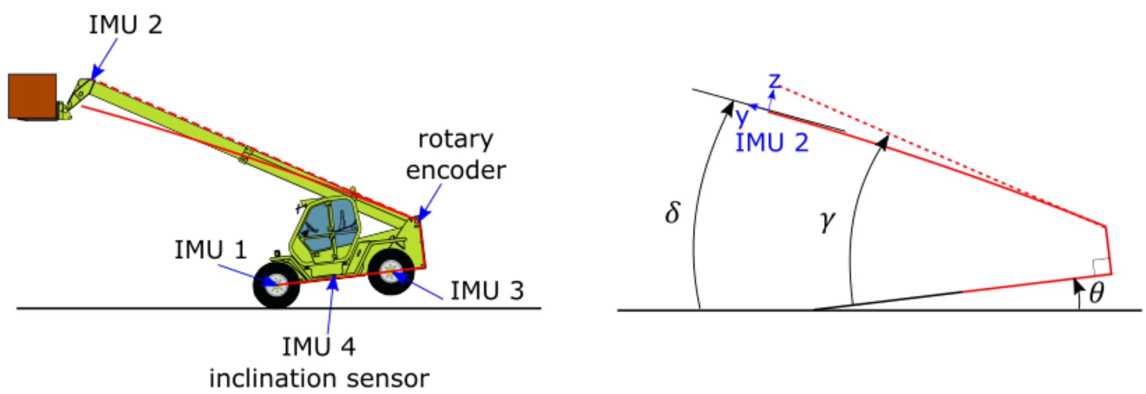

Figure 5.11: Geometric scheme of measured angles

following angles:

- γ: angle between the plane parallel to the upper side of the external section of the boom and the plane passing through the center of the four wheels.
- δ: angle between the x-y plane of IMU 2 and the plane parallel to the ground.
- θ: angle between the plane passing through the center of the four wheels and the plane parallel to the ground.

The angle θ can be measured by the IMU 1, IMU 3, IMU 4 and by the on-board sensor, δ only by the IMU 2 and γ by the on-board encoder.
Figure 5.11 shows how it is is possible to simplify the machine geometry to better describe the angles object of analysis. The red line passes through the center of the wheels and then joins the dotted line coincident with the upper side of the external section of the boom. The solid curved line represent how the ideal dotted line deforms due to the flexibility of the boom.

5.4 Comparison of θ measured by the IMUs on the lower frame

The choice to install three IMUs on the lower frame is justified by the necessity to understand which place is the most suitable to minimize the interference of the vibrations that the engine and the hydraulic pumps have on the IMU measurements. For this reason the first thing to do is to compare the angle θ measured by each of the IMUs on the lower frame.

Before doing so it is necessary to describe how the parameters of the complementary filter have been tuned to extract θ from the IMU data. Observing the evolution of the angle θ given by the inclination sensor it is possible to note that, during the execution of the test, when the CDC stops the lowering of the boom, the rear axle lifts up and ,when it touches the ground again, the entire machine starts to oscillate with a main frequency close to 0.5 Hz and an amplitude that does not overcome 10°. This information made us decide to chose a cut-off frequency of 20 Hz and a $c_f = 0.98$ for the complementary filter used to extrapolate the angle θ from the IMU data. The choice to use such an high c_f is justified by the fact that such values of amplitude and frequency lead to accelerations low enough to make the angle θ computed with the acceleration data very close to the real one. On the other hand the cut-off frequency of 20 Hz derives from the necessity to avoid, as much as possible, the slight attenuation provided by the low-pass filter for frequencies below the cut-off one and at the same time to smooth the high frequency jitter.

Plotting the evolution of θ during a part of the entire time interval recorded by the IMU it is possible to clearly distinguish the different tests and the pauses between one test and another (Figure 5.12). Some tests, like Test 16, 17 and 19, show a multiple series of oscillation because when the first oscillation is completely damped the dynamic load moment decrease and the CDC removes the block on the boom and lets the operator start moving the boom again. Obviously as soon as the CDC adverts the risk of overturning it blocks the boom an other time. During our tests it was said to the operator to go on lowering the boom every time the CDC made it possible. The CDC definitively blocks the movement of the boom when the load risks to fall in an unsafe zone of the static load diagram.

Analysing each single test it is possible to note that for tests with small oscillations of the lower frame (e.g. Test 4 and Test 5) the angle θ from IMU 4 has some anomalous oscillations with respect the other two IMUs (Figure 5.13b). On the other hand during larger oscillations of the machine (e.g. in Test 16 and 17) the response of the three sensors is pretty close (Figure 5.13a). These considerations exclude the possibility to install the IMU on the back of the machine since the signal is less stable than the one recorded elsewhere. Signals from IMU 1 and IMU 3 are quite similar and this suggest that any place between the center of mass of the lower frame and the frontal axle is

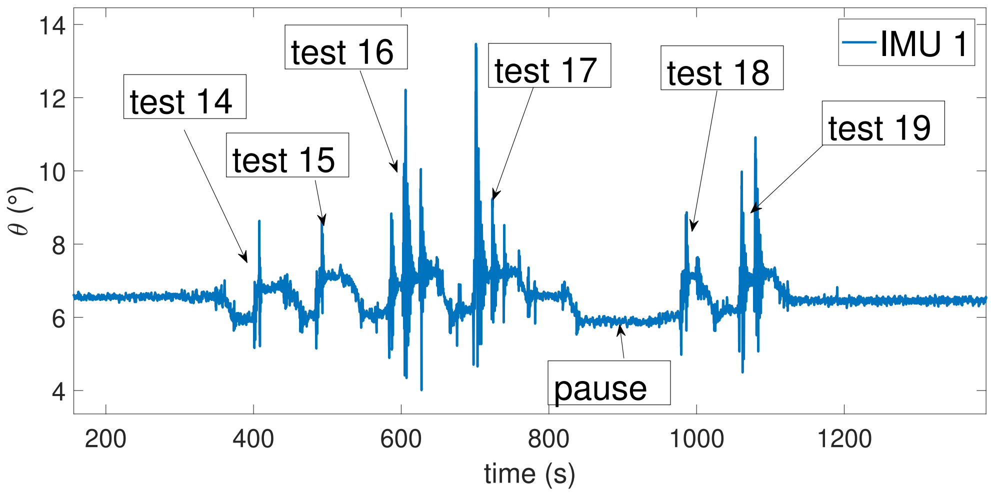

Figure 5.12: Evolution of θ during some different tests

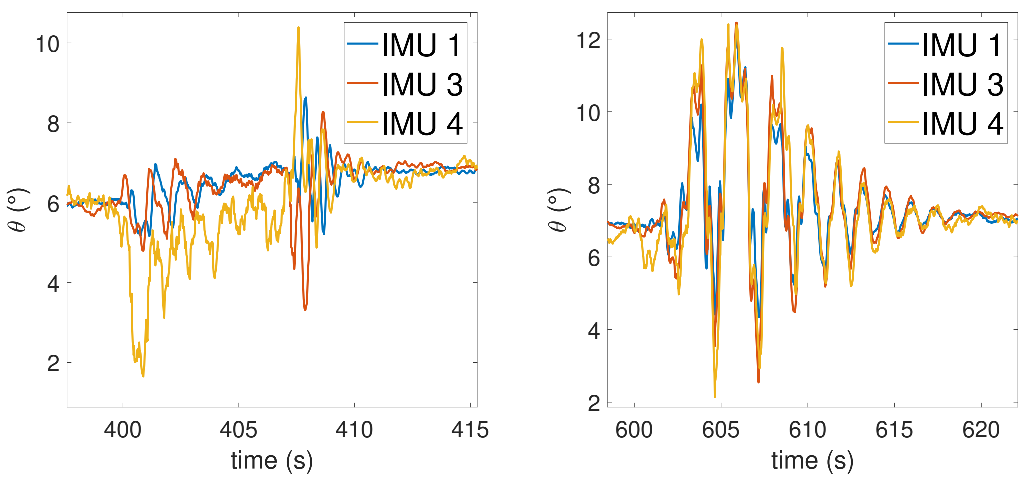

(a) Test 14

(b) Second oscillation of Test 16

Figure 5.13: Comparison of θ measured by different IMUs

suitable for the installation of an IMU.

5.5 Comparison of θ measured by IMU 1 and the inclination sensor

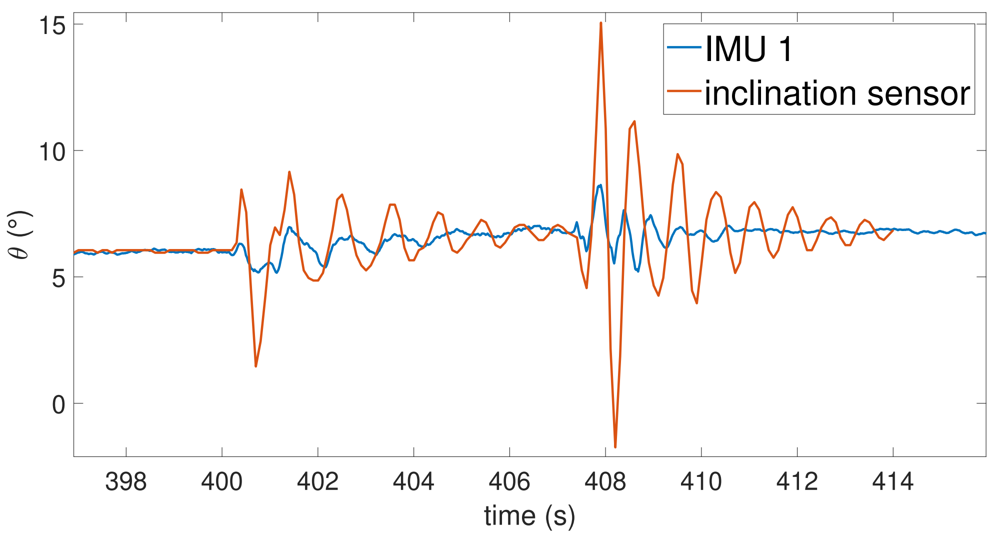

Figure 5.14: Comparison of the second oscillation of Test 6

One of the goals of the tests was to understand if the data coming out of the on-board inclination sensor could be used for the new dynamic stability control system or not. For this reason the evolution of the angle θ given by the inclination sensor was compared with the one of the IMUs during all the different test. The result was that the inclination sensor returns an amplitude of the oscillation of θ larger than the one computed starting from the IMU data for every test. In Figure 5.14 it is possible to observe the comparison of Test 14 but the result is the same also for all the other test. This strong difference has underlined the need for an IMU on the lower frame to know its longitudinal inclination. Even if this choice increases the cost of the final system, the installation of an IMU can't be avoided because, in case of a wrong read of the inclination sensor, the stability of the machine and the life of the operator is at risk.

5.6 Analysis of the boom tilting

The flexibility of the boom is a parameter that strongly influences the effectiveness of the new control system. For this reason it is important to analyse the flexural behaviour of the boom with data coming from the IMU 2, IMU 1 and the encoder measuring the

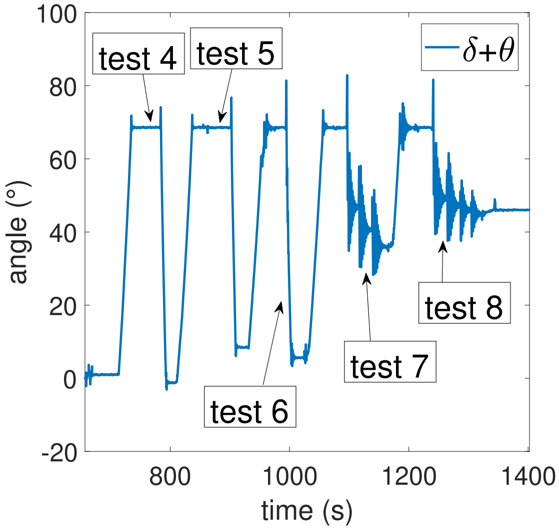

Figure 5.15: $\delta + \gamma$ from IMU 1 and IMU 2 records

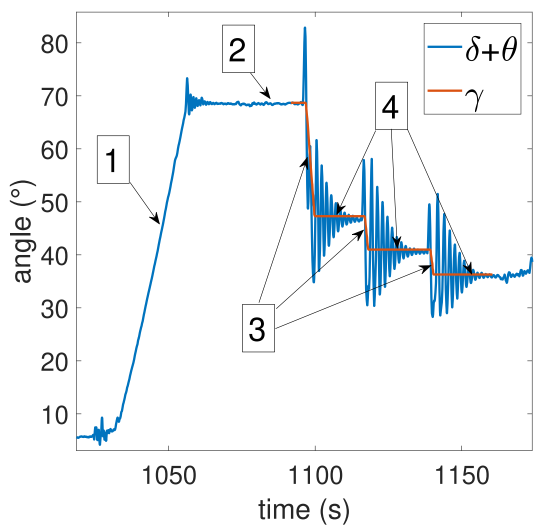

Figure 5.16: Different phases of Test 7

inclination of the boom.

In order to highlight the flexural behaviour it makes sense to compare $\delta + \theta$ with γ. In fact, if the boom was perfectly rigid, then $\delta + \theta = \gamma$ while every time $\delta + \theta \neq \gamma$ it means that the boom is flexing. In Figure 5.15 it is possible to see how the angle $\delta + \theta$ varies during different tests while Figure 5.16 highlights all the different phases of a test: the boom lift after the previous test (1), stabilization after the lift (2), boom lowering (3), CDC block(4).

Figure 5.17 shows the comparison between angle γ measured with the on-board rotary encoder and angle $\delta + \theta$ for Test 1, 2, 7 and 12. δ is measured with IMU 2 while θ with IMU 1. The test selected in Figure 5.17 are representative of the main differences between δ and $\delta + \theta$. During Test 1 (Figure 5.17a) as soon as the lowering of the boom starts the two curves diverge due to the deflection of the boom. During Test 2, that was ran with the boom extended of 7500 mm, the deflection of the boom has been much larger than in test 1 that was performed with the boom was fully retracted.

It is also interesting to note that when the boom lowering is blocked, after some oscillations of the boom, the angle $\delta + \theta$ is greater than δ of around 5°. This condition is represented in Figure 5.18 and means that the boom remains deflected upwards. This phenomenon could be explained with the attempt of the company to make anticlastic the boom of their telescopic handlers. The anticlasticity is a property typic of the tower cranes' arm that compensates its deflection due to the load with an opposite deflection

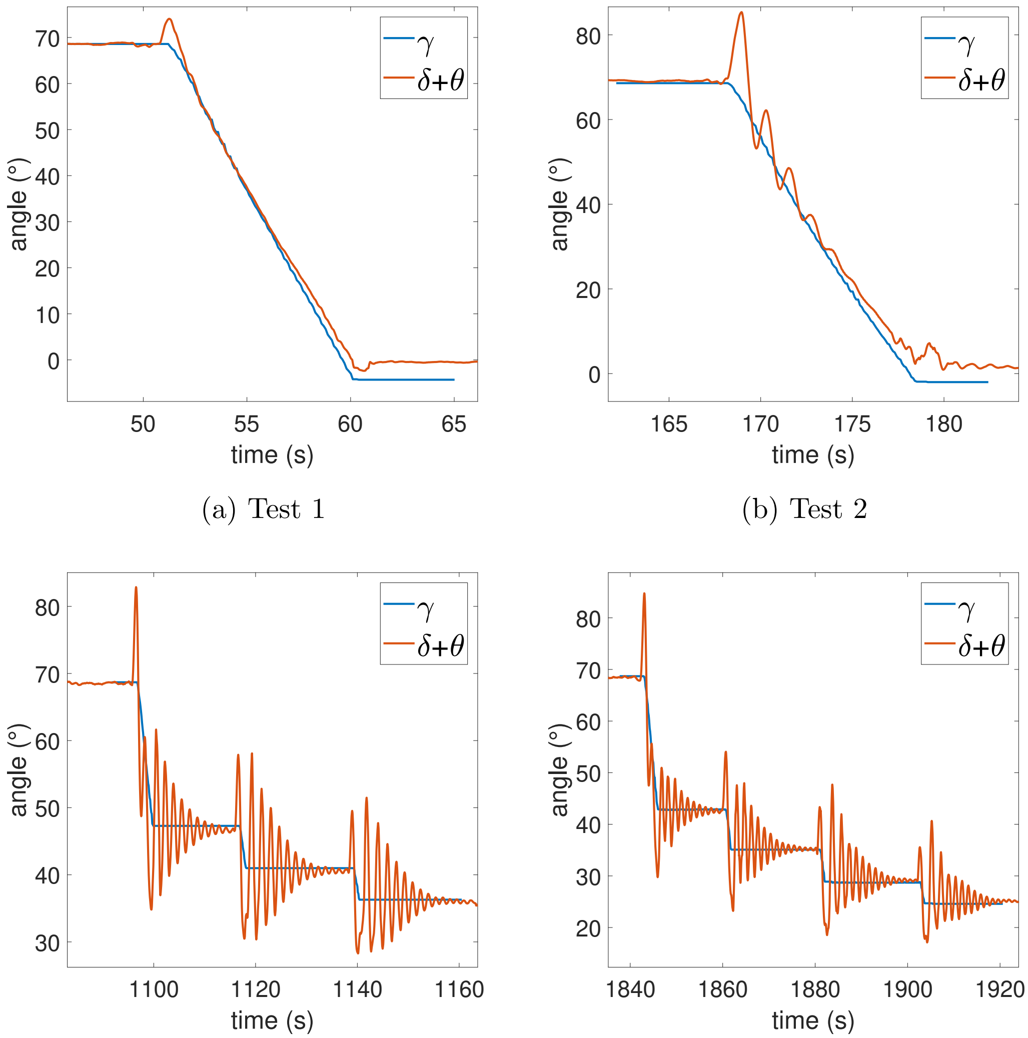

(a) Test 1 (b) Test 2

(c) Test 7 (d) Test 12

Figure 5.17: Comparison between γ and $\delta + \theta$

obtained with a particular design of the welded joints. This is the only explanation that it has been possible to give to justify that phenomenon but it has not been confirmed by the company.

Figure 5.17c and 5.17d, relative to test performed with $w_f = 1000$ kg show that when the CDC blocks the boom lowering the machine starts vibrating with wide amplitude. The study of the vibrations and the influence of boom extension and weight on forks will be treated in the next section.

In contrast with Test 1 and 2 , in Test 7 and 12 the mean value of $\delta + \theta$ differs from γ of not more than 2°. This analysis has confirmed the goodness of the measurement since

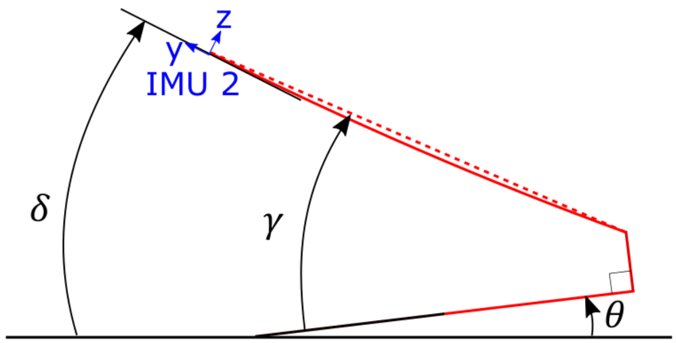

Figure 5.18: Condition $\delta + \theta > \gamma$

both the dynamic and static behaviour of the machine are well identified. The little unexplained offset between $\delta + \theta$ and γ is no cause of alarm mostly because the gap is quite big ($\approx 5°$) only for those tests that have not really compromised the stability of machine while it is smaller for more risky tests.

5.7 Vibration analysis

One of the key parameters of the new control system is the oscillating frequency of the boom. In particular the control system needs to know how the oscillating frequency varies according to the position of the load and its mass.
Observing the evolution of the angle δ during all the test it is possible to observe that on several occasions δ shows the typical free response of a one Degree Of Freedom (DOF) damped system. This happens when the boom has been blocked, both in the the lowering and the lifting phase, especially during those test inducing an high risk of overturning (high weight on forks and boom fully extended) and thus wide oscillations on δ and θ.
The oscillation of θ during the test are characterized by one main frequency of oscillation but they are much more chaotic than those of δ. Only for some of the test that have really compromised the stability of the machine (Test 7, 8, 12, 13, 16, 17) it is possible to observe a cleaner response characterised by two main frequencies.
Figure 5.19 and 5.20 show the time and frequency response to the second block of the boom lowering during test 12 respectively of δ and θ. The representation of the evolution of δ in the frequency domain shows a peak of the amplitude for a frequency equal to 0.713 Hz. θ instead, has two main resonance frequencies: the first equal to

0.625 Hz and the second equal to 1.964 Hz.
The frequency domain representation has been obtained via a Fast Fourier Transform (FFT) algorithm.

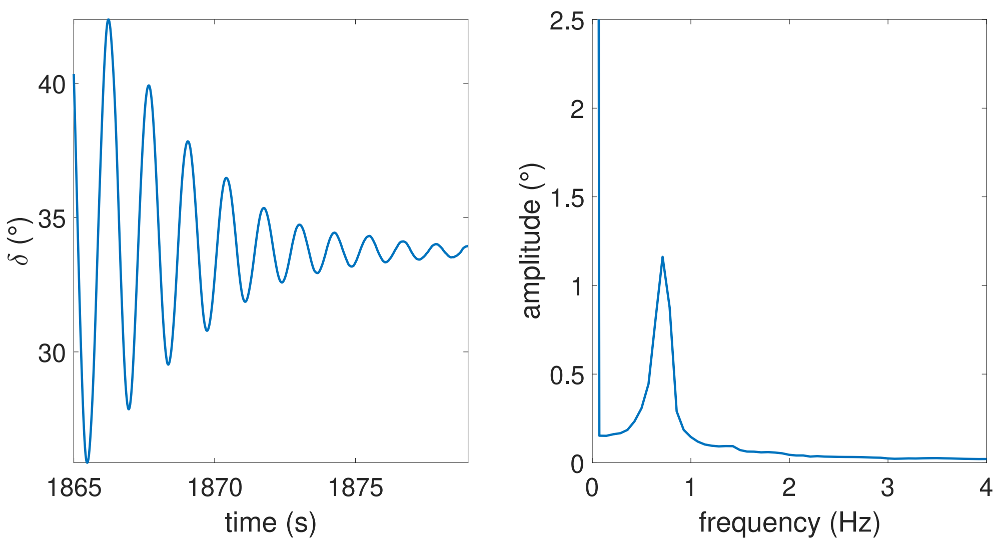

Figure 5.19: Second oscillation of Test 12

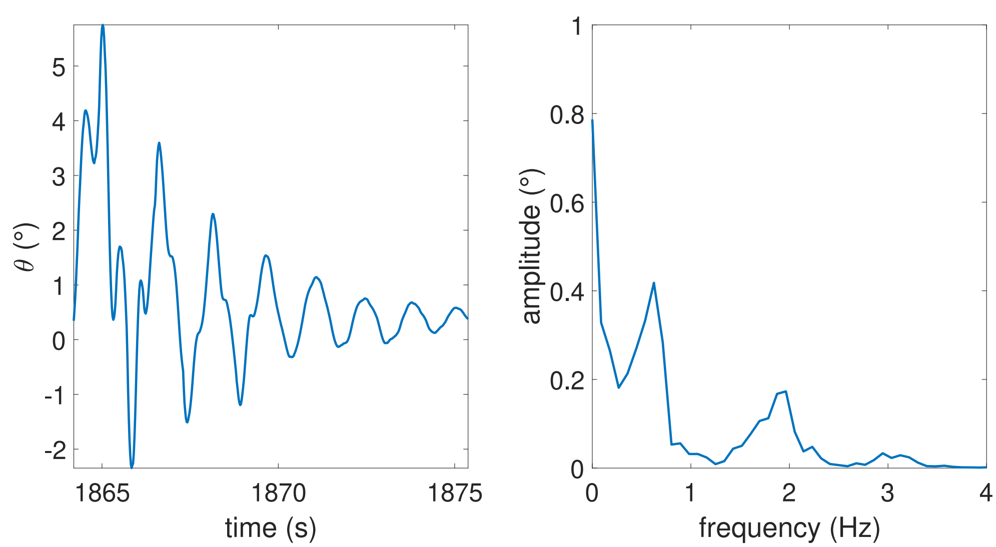

Figure 5.20: Second oscillation of Test 12

The result of the Fourier analysis of all the oscillations of δ, measured during the different test, has allowed us to understand how the main resonance frequency (f_δ) varies according to b_e and w_f. The results are reported in Figure 5.21 and show how f_δ is inversely proportional both to the boom extension and the weight on the forks.

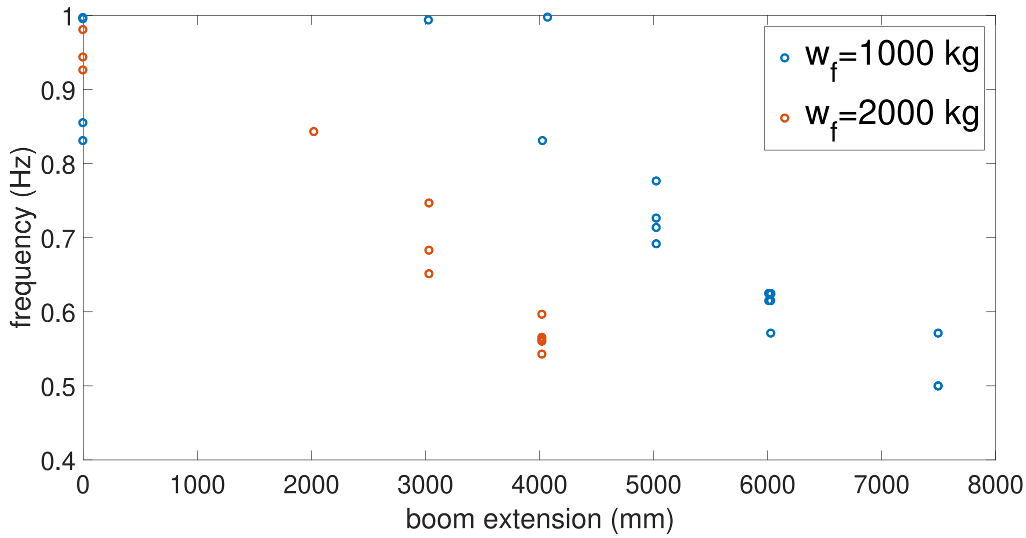

Figure 5.21: Influence of b_e and w_f on f_δ

In order to give a rough approximation of the dependence of f_δ on the b_e the points coming from tests done with 1000 kg and 2000 kg have been approximated with two different straight lines. For this approximation the values of f_δ obtained for a null boom extension have not been taken into account because they would have negatively influenced the precision for higher values of boom extension. The coefficients of the first order polynomial approximations obtained for $w_f = 1000kg$ and $w_f = 2000kg$ have then been linearly interpolated to find the polynomial coefficients valid also for other values w_f (Figure 5.22). This is clearly a very rough approximation to estimate the variation of f_δ according to b_e and w_f. This kind of analysis has been mainly done to try to influence the choice of the first attempt values of the key parameters of the control law.

The results reported in Figure 5.23 and 5.24 show the influence of the boom extension and w_f on the first ($f_{\theta,1}$) and the second ($f_{\theta,2}$) main resonance frequency of θ on during the different tests. Any attempt to find a polynomial approximation of the points on those plots would be null since the point are very scattered. It is only possible to say that the $f_{\theta,1}$ is always comprised between 0.3 and 1 Hz and $f_{\theta,1}$ between 1.6 and 2 Hz.

This analysis of the vibrations occurring during the different tests has highlighted the main resonance frequencies of δ and θ for a limited set of b_e and w_f but it has not provided a reliable method to estimate their influence on the resonance frequency. For this reason in the next chapters it will be described how an analytical and a numeric

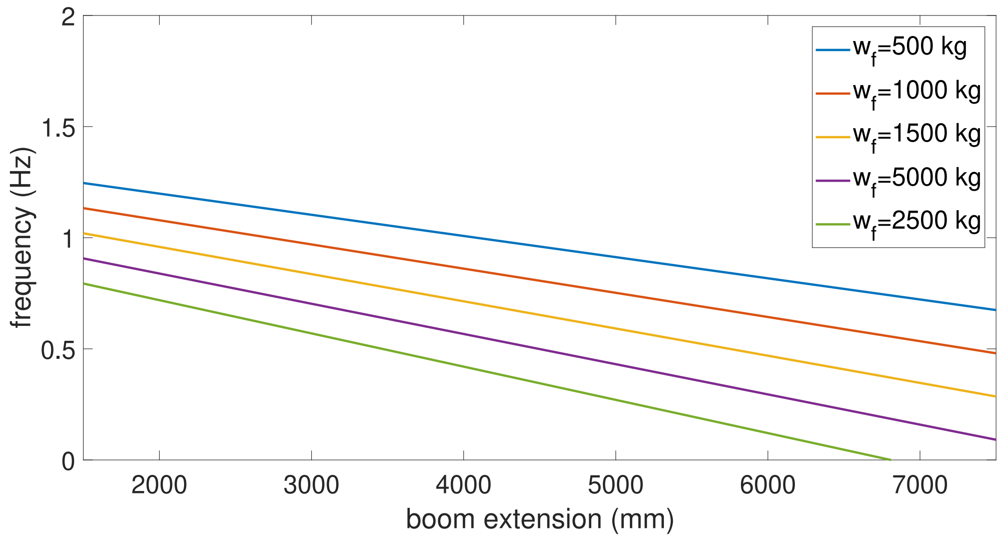

Figure 5.22: Linear approximation of f_δ for different w_f values

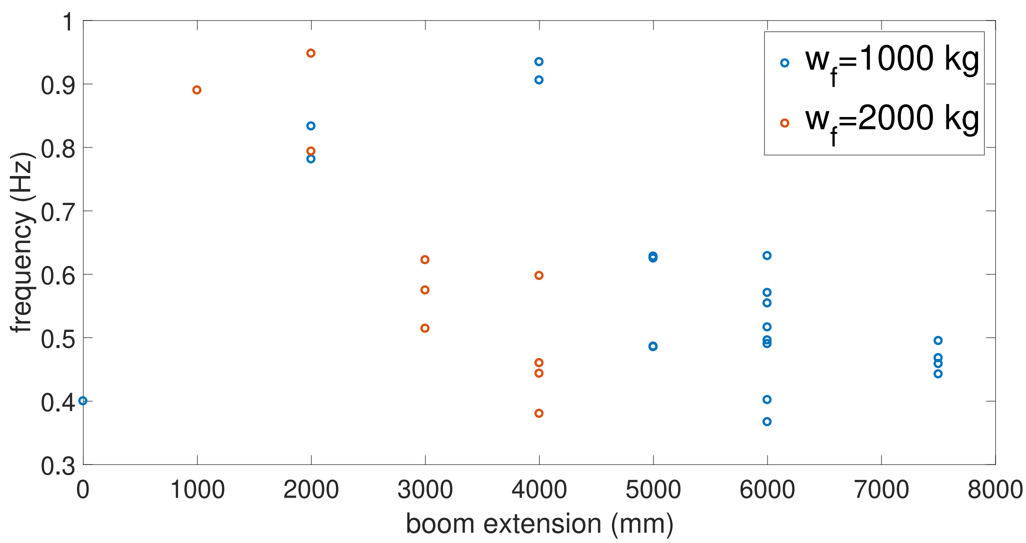

Figure 5.23: Influence of b_e and w_f on $f_{\theta,1}$

model of the machine have been developed to fit the experimental results and estimate the behaviour of the machine in condition different from the ones of the tests.

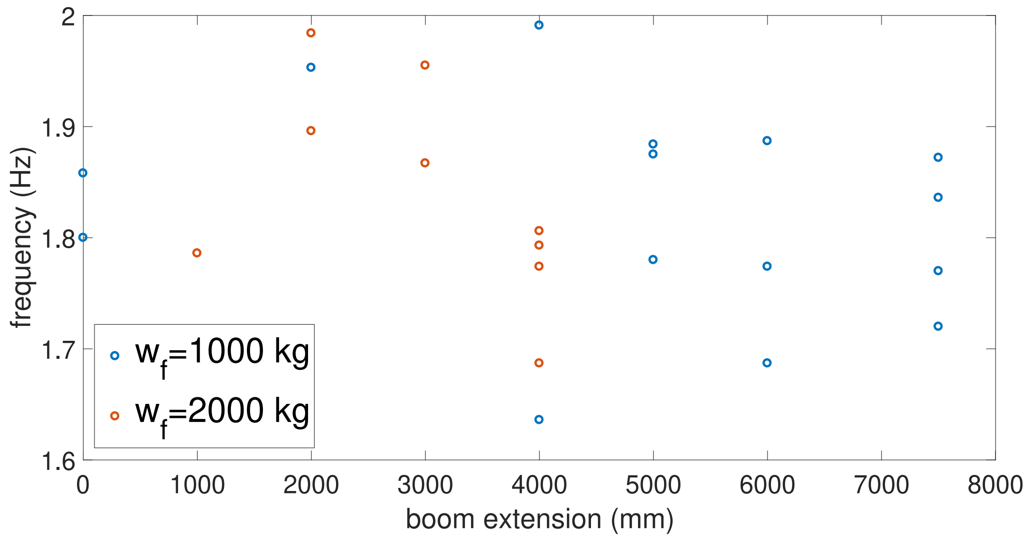

Figure 5.24: Influence of b_e and w_f on $f_{\theta,2}$

Chapter 6

Analytic model

As previously introduced, the analytic model described in this chapter aims to emulate the real dynamic behaviour of the machine on the longitudinal plane observed during the test prescribed by the EN 15000. In particular the main goal is to find a linear natural equivalent system on which perform a modal analysis. The computed natural frequencies will then be compared with those found with the experimental test in order to tune the parameters of the model. The principal assumptions behind the model are:

- the entire boom is considered as a rod connecting the joint between the lower frame and the boom to the center of mass of the load. This rod is perfectly rigid but the flexural behaviour of the boom is taken into account by a rotational spring acting on the joint connecting the boom to the lower frame.

- a linear spring simulates the behaviour of each wheel. The spring is linked both to the lower frame and the ground and can work both in compression and traction. The spring is perfectly conservative.

- the lower frame is perfectly rigid and can not translate horizontally with respect to the ground.

- the load is a cube of 1 m^3 on the forks and its size remains the same for all the values of mass that it can assume.

The simplified geometrical scheme of the machine is reported in Figure 6.2. The model has three DOF (x,θ,ϕ) and is made of three main bodies: the lower frame, the boom and the load. Table 6.1 reports the main parameters and variables of the model. For what concerns the geometric parameters only a, c and d can be extracted from data available on the brochure. l is function of α and of b_e and of some other fixed geometrical parameters (f, e, μ, q, s) characteristic of the boom that can be extracted from images on the brochure. The geometric scheme of the boom is reported in figure 6.1 and the following equations show how it is possible to extract l from the parameters mentioned above.

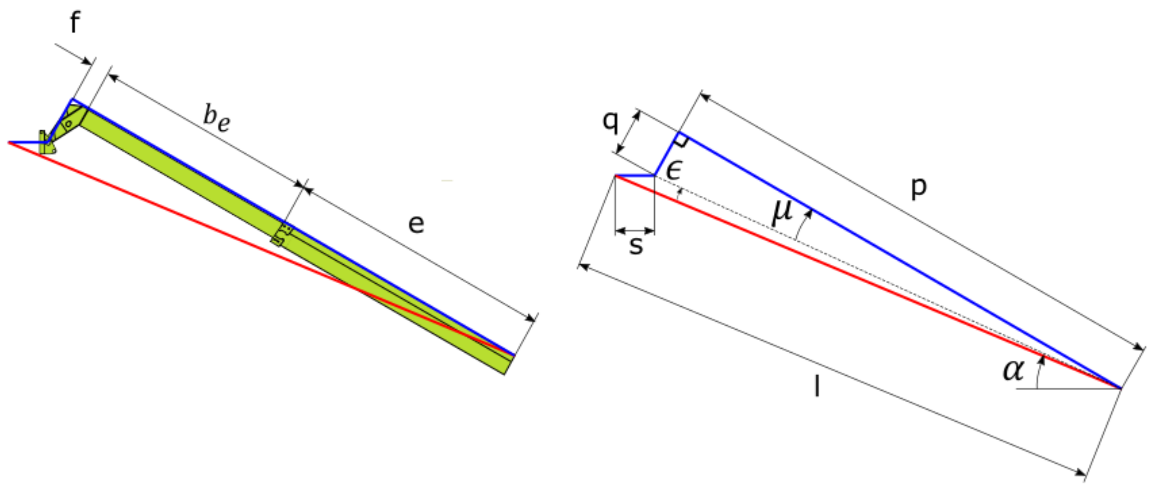

Figure 6.1: Geometric scheme of the boom

$$p = e + f + b_e \tag{6.1}$$

$$\mu = \arctan\left(\frac{q}{p}\right) \tag{6.2}$$

$$\epsilon = \arctan\left(\frac{s\tan(\alpha)}{\sqrt{p^2+q^2}}\right) \tag{6.3}$$

$$l = s\cos(\alpha) + \sqrt{p^2+q^2}\cos(\epsilon) \tag{6.4}$$

b and r can be found with some computation based on data directly given by Merlo (see Section 6.1). α is directly related to γ, the angle that can be measured by the on-board encoder, according to the following equation: $\alpha = \gamma - \epsilon - \mu$.
m_b and m_f are reported on brochure while m_l is a variable whose influence on the resonance frequencies of the model is one of the main objects of study of this document. I_b is estimated supposing that the boom is a common rod ($I_b = \frac{m_b l^2}{12}$) while I_f is computed by a multibody simulation software on the basis of a simplified CAD (Computer Aided Design) model of the machine described in the next chapter.
k_1, k_2 and k_b are unknowns. A sensibility analysis in chapter 8 describes how the value

of these parameters is extrapolated using the values of resonance frequencies found in the previous chapter.

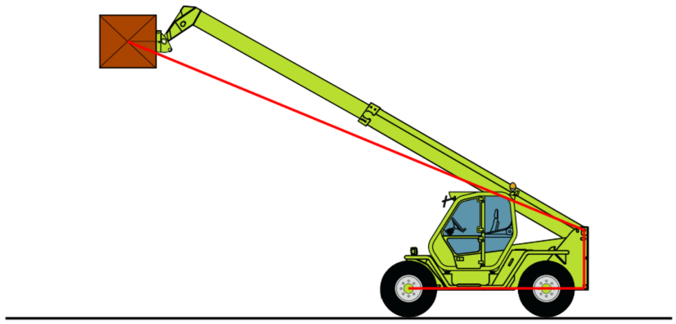

(a) Overlap or the simplified and real model

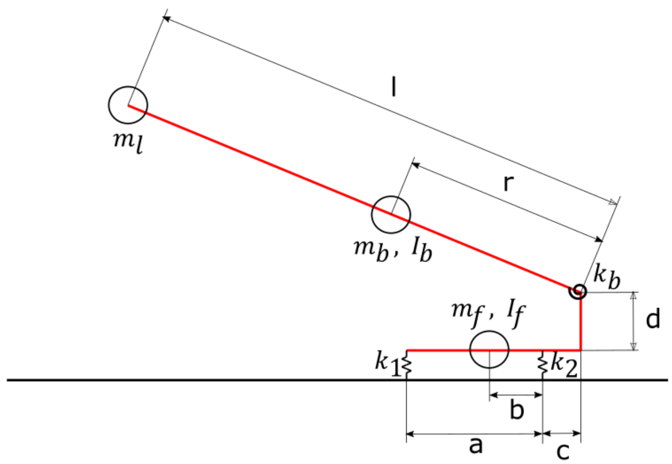

(b) Geometric, mass and stiffness parameters

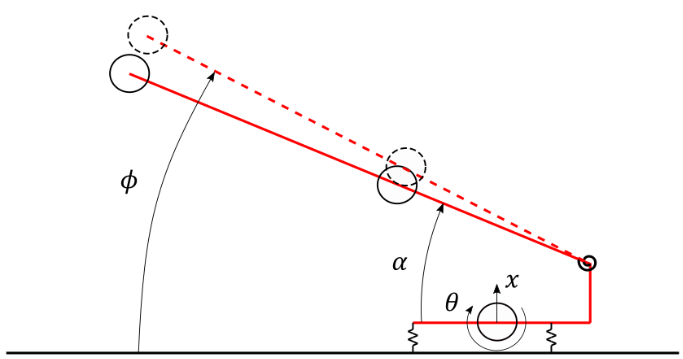

(c) Degrees of freedom

Figure 6.2: Simplified 3 dof model

Symbol	**Parameter**	**unit**
a	inter-axis distance between the front and rear axis	m
b	distance between the rear axis and the center of mass of the lower frame	m
c	horizontal distance between the rear axis and the revolute joint	m
d	vertical distance between the rear axis and the revolute joint	m
r	distance between the revolute joint and the center of mass of the boom	m
l	length of the boom line	m
b_e	extension of the boom	m
k_1	combined stiffness of the front wheels	N/m
k_2	combined stiffness of the rear wheels	N/m
k_b	stiffness of the revolute joint	Nm/rad
m_l	mass of the load	kg
m_b	mass of the boom	kg
m_f	mass of the lower frame	kg
I_b	moment of inertia of the boom	kgm^2
I_f	moment of inertia of the frame	kgm^2
α	angle between the boom line in static condition and the line passing through the two axis of the lower frame	rad
ϕ	angle between the boom line and a plane parallel to the ground	rad
θ	inclination angle of the lower frame	rad
x	vertical displacement of the lower frame's center of mass	m

Table 6.1: List of the parameters involved in the analytic model

6.1 Identification of b and r

In order estimate b, and r Merlo has measured the load on the front (F_f) and back tyres (F_b) with two different configurations of the machine:

1. machine on level ground, boom parallel to the ground and fully retired, no attachment
2. machine on level ground, boom parallel to the ground and fully extended, no attachment

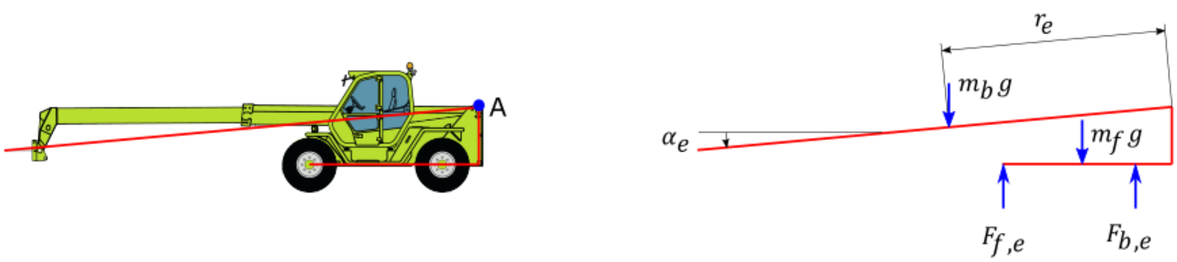

(a) Boom extended

(b) Boom retired

Figure 6.3: Free body diagram of the machine in static condition

The subscripts r and e stands for 'retired' and 'extended'.
Writing the rotation equilibrium equations around point A (see Figure 6.3a) for the two configurations it is possible to note that three parameters remain unknown: b, r_r, r_e.

$$A \quad r_r \cos(\alpha_r) m_b g + (b+c) m_f g - F_{b,r} c - F_{f,r}(a+c) = 0 \tag{6.5}$$

$$A \quad r_e \cos(\alpha_e) m_b g + (b+c) m_f g - F_{b,e} c - F_{f,e}(a+c) = 0 \tag{6.6}$$

Since it is not possible to identify three unknowns with two equations it was assumed: $r_r = \frac{l_r}{2}$. This hypothesis is quite reasonable and allows to find the two remaining unknowns solving the system of two equations.

$$b = \frac{F_{b,r}c + F_{f,r}(a+c) - (\frac{l}{2})\cos(\alpha_r)m_b g + cm_f g}{m_f g}$$

$$r_e = \frac{F_{b,e}c + F_{f,e}(a+c) - (b+c)m_f g}{\cos(\alpha_e)m_b g}$$

In order to find the value of r for all the other possible geometric configurations of the machine, r is supposed to vary linearly with l according to equation: $r(l) = m_{ar}l + q_{ar}$. The coefficient m_{ar} and q_{ar} solving the following system of equations:

$$\begin{cases} \frac{l_r}{2} = m_{ar}l_r + q_{ar} \\ r_e = m_{ar}l_e + q_{ar} \end{cases}$$

6.2 Equations of motion

The equations of motions have been written using the Lagrange equations for conservative systems:

$$\frac{d}{dt}\left(\frac{\partial L}{\partial \dot{q_k}}\right) - \frac{\partial L}{\partial q_k} = 0$$

$$L = T - V$$

Where L is the 'Lagrangian', T the kinetic energy and V the potential energy. q_k is the generalized k-th coordinate of the system with $k = 1...N$ where N is the number of DOF of the system. In this case the 3 generalized coordinates are: x,θ,ϕ.
According to these definitions it is possible to write:

$$T = \frac{1}{2}m_b\left[\dot{\phi}r\cos(\alpha)\right]^2 + \frac{1}{2}m_l\left[\dot{\phi}l\cos(\alpha)\right]^2 + \frac{1}{2}m_f\dot{x}^2 + \frac{1}{2}I_f\dot{\theta}^2 + \frac{1}{2}I_b\dot{\phi}^2$$

$$\begin{aligned} V =& \frac{1}{2}k_1\left[x + \theta(a-b)\right]^2 + \frac{1}{2}k_2\left[x - \theta(b)\right]^2 + \frac{1}{2}k_b\left(\phi - \alpha - \theta\right)^2 + m_f g x + \\ & m_b g\left[r\sin(\alpha) + x + d\right] + m_l g\left[l\sin(\alpha) + x + d\right] \end{aligned}$$

The portion of kinetic energy of the boom relative to the vertical translation and rotation of the lower frame has been neglected because it would introduce some gyroscopic terms linearly proportional to the velocities ($\dot{x}$,$\dot{\theta}$,$\dot{\phi}$) making the system non-natural. This approximation produces an error on the natural frequencies but it allows to use the classic modal analysis approach avoiding much more complicated and time demanding techniques to extrapolate resonance frequencies for non-natural systems.

$$\frac{\partial L}{\partial \dot{x}} = m_f \dot{x} \quad \Rightarrow \quad \frac{\partial}{\partial t}\left(\frac{\partial L}{\partial \dot{x}}\right) = m_f \ddot{x}$$
$$\frac{\partial L}{\partial \dot{\theta}} = I_f \dot{\theta} \quad \Rightarrow \quad \frac{\partial}{\partial t}\left(\frac{\partial L}{\partial \dot{\theta}}\right) = I_f \ddot{\theta}$$
$$\frac{\partial L}{\partial \dot{\phi}} = \left[(m_b r^2 + m_l l^2)\cos(\alpha)^2 + I_b\right]\dot{\phi} \quad \Rightarrow \quad \frac{\partial}{\partial t}\left(\frac{\partial L}{\partial \dot{\phi}}\right) = \left[(m_b r^2 + m_l l^2)\cos(\alpha)^2 + I_b\right]\ddot{\phi}$$
$$\frac{\partial L}{\partial x} = -k_1\left[x + \theta(a-b)\right] - k_2\left[x - \theta(b)\right] - g(m_f + m_b + m_l)$$
$$\frac{\partial L}{\partial \theta} = -k_1(a-b)\left[x + \theta(a-b)\right] + k_2 b(x - \theta b) + k_b(\phi - \alpha - \theta)$$
$$\frac{\partial L}{\partial \phi} = -k_b(\phi - \alpha - \theta)$$

The terms above can now be put together into the three equations of motions:

$$\begin{aligned}
m_f\ddot{x} + k_1\left[x + \theta(a-b)\right] + k_2\left[x - \theta(b)\right] &= -g(m_f + m_b + m_l) \\
I_f\ddot{\theta} + k_1(a-b)\left[x + \theta(a-b)\right] - k_2 b(x - \theta b) - k_b(\phi - \theta) &= -k_b\alpha \\
\left[(m_b r^2 + m_l l^2)\cos(\alpha)^2 + I_b\right]\ddot{\phi} + k_b(\phi - \theta) &= +k_b\alpha
\end{aligned}$$

The equation of motion can then be re-written in a matrix form:

$$[M]\,\ddot{q} + [K]\,q = p \tag{6.7}$$

Where:

$$[M] = Mass\,matrix = \begin{bmatrix} m_f & 0 & 0 \\ 0 & I_f & 0 \\ 0 & 0 & (m_b r^2 + m_l l^2)\cos(\alpha)^2 + I_b \end{bmatrix}$$

$$[K] = Stiffness\,matrix = \begin{bmatrix} k_1 + k_2 & k_1(a-b) - k_2 b & 0 \\ k_1(a-b) - k_2 b & k_1(a-b)^2 + k_2 b^2 + k_b & -k_b \\ 0 & -k_b & k_b \end{bmatrix}$$

$$p = \begin{Bmatrix} -g(m_f + m_b + m_l) \\ -k_b\alpha \\ +k_b\alpha \end{Bmatrix} \qquad q = \begin{Bmatrix} x \\ \theta \\ \phi \end{Bmatrix} \qquad \ddot{q} = \begin{Bmatrix} \ddot{x} \\ \ddot{\theta} \\ \ddot{\phi} \end{Bmatrix}$$

The harmonic solution of equation 6.7 can be expressed by either a sine or cosine function or an exponential function with imaginary exponent

$$q = q_0 e^{st} \tag{6.8}$$

Because the system is undamped, all solutions s are imaginary so the equation 6.8 can be rewritten as:

$$q = q_0 e^{i\omega t} \tag{6.9}$$

The acceleration is obtained from a double derivation with respect to time of equation 6.9:

$$\ddot{q} = -\omega^2 q_0 e^{i\omega t} \tag{6.10}$$

By introducing equations 6.8 and 6.10 into the homogeneous equation of motion the following equation is obtained:

$$\left([K] - \omega^2[M]\right) q_o = 0 \tag{6.11}$$

The equation 6.11 can be obtained by noting that to obtain a solution different from the trivial solution $q_0 = 0$, the determinant of the matrix of the coefficients must vanish:

$$\det\left([K] - \omega^2[M]\right) = 0 \tag{6.12}$$

The algebraic equation 6.12 is of degree N (number of DOF) and so it yields to N eigenvalues (ω_i^2) that satisfy the equation. All eigenvalues are real and positive; the natural frequencies (ω_i) then are real as well as the the the eigenvectors (ψ_i) which means that all the bodies move in phase, or with a phase lag of 180°. The eigenvectors give the mode shapes, i.e., the amplitudes of oscillation of the various bodies at the corresponding natural frequency and they can be obtained by substituting each eigenvalue in equation 6.11. The result is a set of N column vector with N components defined apart from a constant which can be rearranged in a square matrix called the modal matrix:

$$[\psi] = [\psi_1, \psi_2, ..., \psi_N] \tag{6.13}$$

The complete solution of the equation of motion is:

$$q(t) = \sum_{i=1}^{N} A_i \cos(\omega_i t + \Theta_i)\psi_i \tag{6.14}$$

Where A_i and Θ_i depend on the initial condition of q and $\dot{q}$.
In our case supposing $k_1 = k_2 = 500{\cdot}000\, N/m$ and $k_b = 2,2 * 10^6\, Nm/rad$ and with $b_e =$

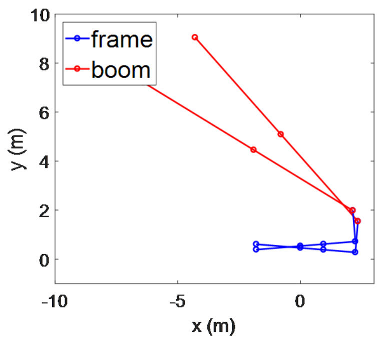

(a) Mode 1: $f_1 = 0.47$ Hz

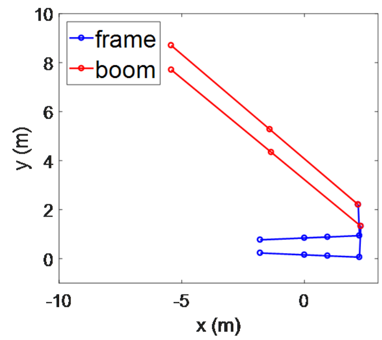

(b) Mode 2: $f_2 = 1.80$ Hz

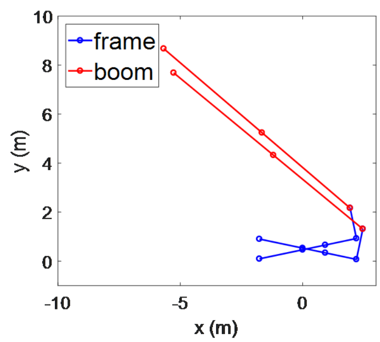

(c) mode 3: $f_3 = 3.53$ Hz

Figure 6.4: Mode shapes

$4000\,mm$, $\alpha = 30°$, $w_f = 1000\,kg$ we obtain three resonance frequencies: $f_1 = 0.47\,Hz$, $f_2 = 1.80\,Hz$, $f_3 = 3.53\,Hz$. In Figure 6.4 each i-th mode shape has been represented by imposing $\{q\} = \pm\{\psi_i\}$.

The first mode emulates the oscillations of the machine during the tests of EN 15000. For this reason it makes sense to compare the first resonance frequency of this model with the resonance frequency of boom extracted during the different tests. A Matlab script has been developed to solve the eigenvalue problem and obtain the previous results. The script has also been adapted to perform a parametric analysis to estimate the value the influence of k_1, k_2, k_b, b_e, w_f and α on the first resonance frequency of the system. The results of this analysis will be compared with those of the numerical multibody model in chapter 8.

Chapter 7

Multibody model

Beyond the analytic simplified model also a multibody numeric one was realized to characterize the dynamic behaviour of the machine during the test prescribed by EN 15000:2008. As for the analytic model the main goal of this numerical multibody model is to try to estimate the values of k_1, k_2 and k_b that allow to match the experimental results and to find the main resonance frequency of the boom also for condition different from those of the test (different values of w_f, α, and be).
The entire process process can be summarized into the following main steps:

1. simplification of the real model by subdividing it into a small number of bodies
2. creation of the different bodies composing the model with the built-in Adams 3d editor
3. assembly of the model using joints that limit the degrees of freedom of each body
4. application of the external forces on the model
5. run iterative simulations to study the influence of the different parameters on the first resonance frequency computed by linearising the model and performing a modal analysis

7.1 3d modelisation

The model has been entirely designed with the built-in Adams 3d editor trying to respect the main geometric parameters of the Merlo panoramic 40.14 that can be found on the brochure (Figure 5.9). The shape of some parts of the machine like the engine

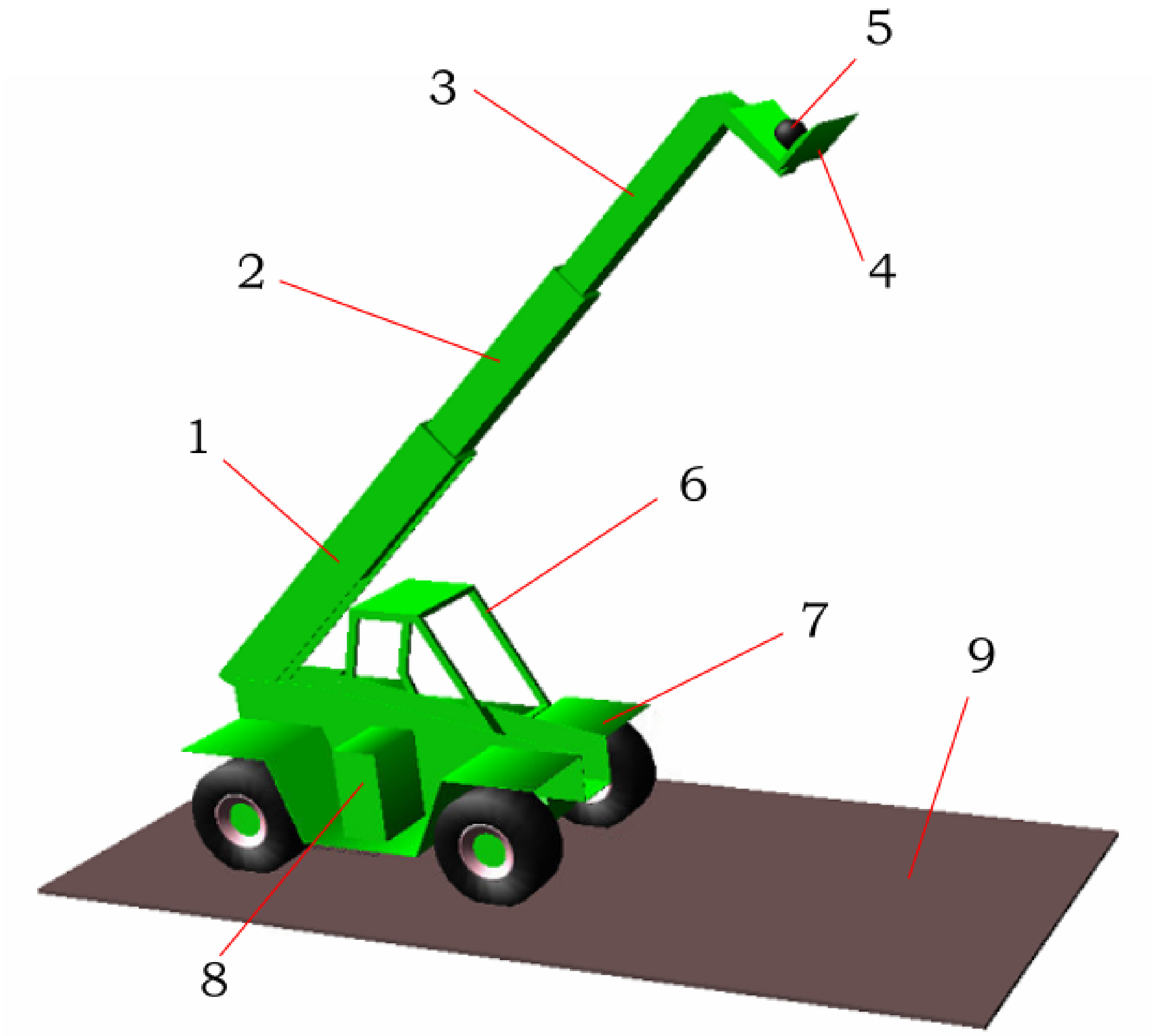

(a) (1) first section of the boom - (2) second section of the boom - (3) third section of the boom - (4) forks - (5) weight on forks - (6) cab - (7) frame - (8) engine - (9) support basement

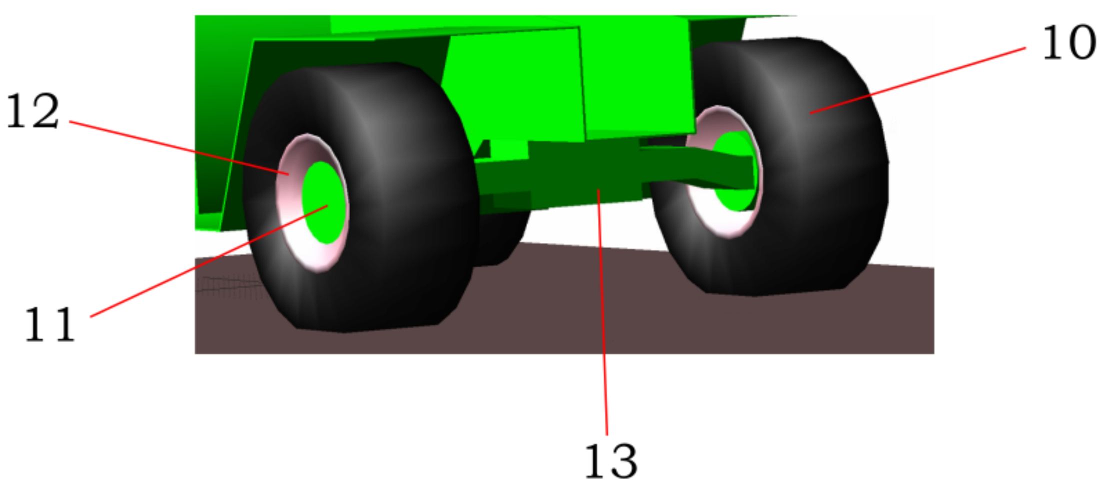

(b) (10) wheel - (11) hub - (12) rim - (13) axle

Figure 7.1: Model's bodies

compartment and the cab has been strongly simplified because the realisation of a more realistic representation would have been time demanding but it would have not made the results more reliable. The model is composed of: a telescopic boom made out of three main sections, the forks, the weight on the forks, a cab, a frame, the ground, an engine, four tyres, four rims, four hubs and two axles (Figure 7.1).
Obviously the real machine is made of more parts but their weight is split among all the different bodies of the virtual model. By chance the mass of the hydraulic jacks that allow the tilt and the extension of the boom is included in the mass of its first section. Adams offers the possibility to define the mass properties (mass and mass moment of inertia) of each body or to compute them on the basis of their density and geometry. Since the inertias of the different bodies were unknown it was decided to impose a value of density for each body in such a way that its total weight includes the weight of all the components that it represents and to let the software compute the inertias. Beyond the mass and geometrical properties each body is also characterised by a certain number of *markers*. A *marker* identifies a reference frame linked to a specific body that can have different functions. For example the position of all the points of the body is defined with respect to a *reference marker*. An other *marker*, always called *'cm'* identifies the position of the center of mass of the body while other ones may identify the position of a specific joint.

7.2 Joints

In order to emulate the dynamic behaviour of the machine during the execution of the test and to perform a modal analysis whose results can be compared with the one of the analytic model, the different bodies of the model have been linked with several joints. Those joints impose the constraints reported in the list below:

- the support basement is fixed to the global reference frame by means of a *fixed joint*. This kind of joint fixes the relative position and orientation of two bodies.

- the frame, the cab, the engine, the axles, the wheels, the hubs and the rims are fixed together by means of several *fixed joint*. This means all those bodies are treated like a single body.

- all the sections of the boom, the forks and the weight on them are fixed together with some *fixed joints*.

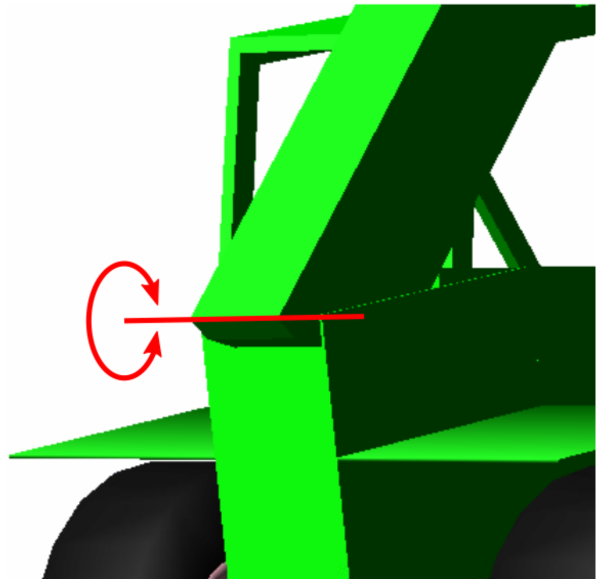

Figure 7.2: Axis of the revolute joint

- the first section of the boom is linked to the frame by a *revolute joint*. This joint allows the tilting of the boom with respect to the frame (Figure 7.2). Any other possible relative translation or rotation of the two bodies is blocked.

- the machine can only pitch while the roll and the yaw are blocked. This condition is obtained by imposing that the the z-axis of a marker on the lower frame must be parallel to the z-axis of a marker on the support basement. In this case the two z-axis must be parallel to the shorter side of the support basement. The joint that allows this kind of constraint is called *parallel joint*.

- the machine can only translate along a line perpendicular to the support basement. An *inline joint* force a marker on the front axle to translate only along a line obtained by connecting the center of that marker with the one of a marker on the support basement. That line is perpendicular to the support basement.

This group of joints reduce the number of degrees of freedom of the model to three.

7.3 Forces

Once defined the joints it is necessary to apply the forces acting on the model. In particular in this case we have:

- the gravity force acting on the entire model.

Figure 7.3: Springs on the front and rear axles

- two translational springs that simulate the stiffness of the front and rear wheels. They are linked to the basement and respectively to the centre of the front and rear axle (Figure 7.3).

- a rotational spring in order to take into account the flexibility of the boom. This element acts on the *revolute joint* that links the frame to the first section of the boom.

7.4 Parametrisation of the model

In the *Design Exploration* section of Adams it is possible to parametrize the model with the creation of some *Design variables*. Their value can be easily changed to study the behaviour of the machine in different configurations. The *Design variables* that parametrize some physical quantities of our model are:

- k_1: the stiffness of the translational spring on the front axle.
- k_2: the stiffness of the translational spring on the rear axle.
- k_b: the stiffness of the rotational spring.
- b_e:
  - the displacement of the third section of the boom with respect to the first along the direction of extension of the boom.
  - the double of the displacement of the second section of the boom with respect to the first along the direction of extension of the boom.

- w_f: the mass of the weight on the forks.
- γ: the inclination angle of the boom in static conditions with respect to the support basement.

7.5 Linear modes extrapolation

Adams offers the possibility to compute the linear modes of the model. Adams uses a condensation scheme to reduce a model to a minimal realization linear form for efficient solution similar to equation 6.7. For example adopting the same parameters of section 6.2 ($k_1 = k_2 = 500'000\, N/m$, $k_b = 2,2 * 10^6\, Nm/rad$, $b_e = 4000\, mm$, $\gamma = 35,4°$, $w_f = 1000 kg$) we find three modes shapes corresponding to three resonance frequencies: $f_1 = 0.41\, Hz$, $f_2 = 1.36\, Hz$, $f_3 = 2.55\, Hz$. Even if the values of the three resonance frequencies do not match those of the analytic model Figure 7.4 shows that the mode shapes of this numerical multibody model are very similar to those of the analytic one (Figure 6.4). The *Design evaluation tool* of Adams allows the user to perform a parametric analysis by automatically running multiple simulations varying the value of some selected *Design variables* in order to study their influence on a specific objective function. In our case the objective function is the the first resonance frequency of the linearised model.

The results of this parametric study will be compared with those of the analytic model and reported in the next chapter .

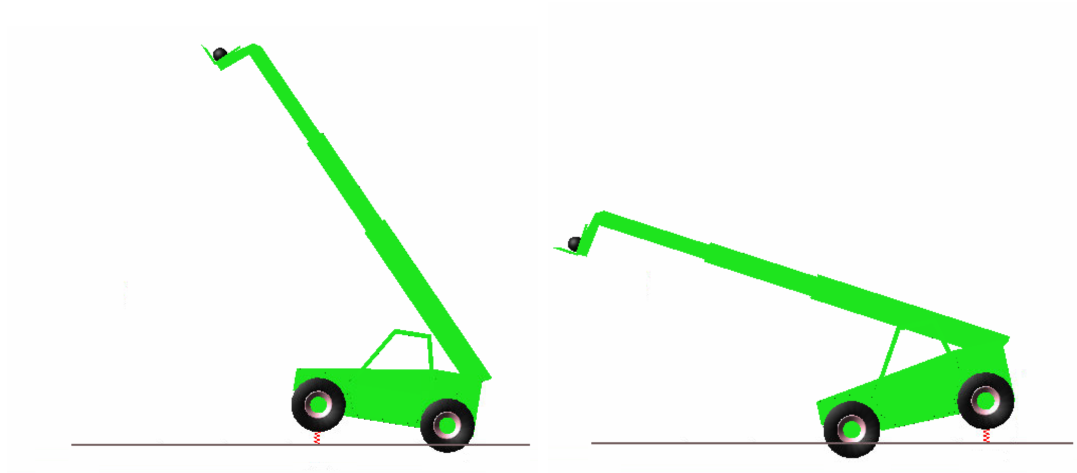

(a) Mode 1: $f_1 = 0.41$ Hz

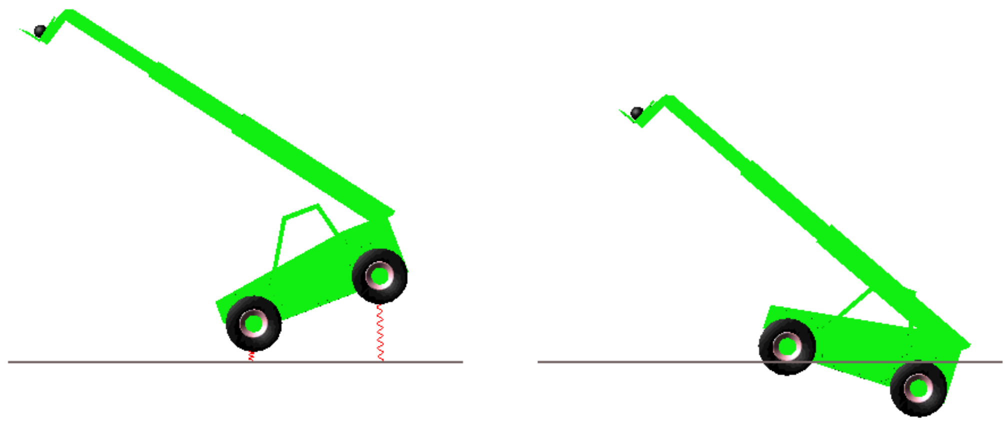

(b) Mode 2: $f_2 = 1.36$ Hz

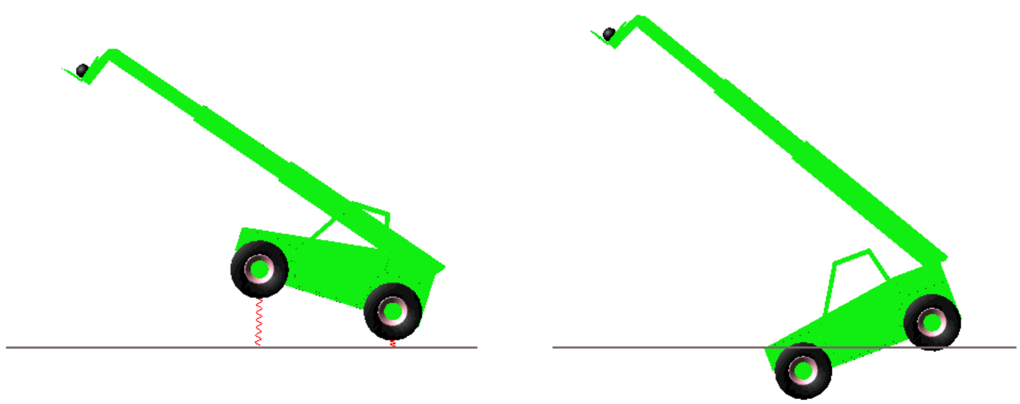

(c) Mode 3: $f_3 = 2.55$ Hz

Figure 7.4: Mode shapes

Chapter 8

Results

After having described how the analytic and the numerical model have been created it is necessary to analyse their results in order to estimate the value of k_1, k_2 and k_b. Since an easy test with the numeric and analytic model has revealed the non linearity of the the unknowns, it was decided to consider the entire boom as a wedged beam with a linear k_b depending only on the total length of the boom (L) and to suppose k_1 and k_2 depending on w_f. After having approximated $k_b(L)$ the results of the numeric model have been tuned to fit the experimental ones by changing k_1 and k_2 both for $w_f = 1000$ kg and $w_f = 2000$ kg. The same values of k_b, k_1 and k_2 have then been used also in the analytic model to evaluate the difference of that model with respect to the numeric one.

8.1 Comparison of test 11 and 17

A valid method to test the linearity of the different stiffness is to try to find the combinations of k_1 and k_b for which the first resonance frequency (f_1) computed with the analytic and numerical model match those extracted with the Fast Fourier Transformation algorithm during the oscillations of δ after the block of the boom lowering of test 11 and 17. Supposing the stiffness of the tyres perfectly constant k_2 has been considered equal to k_1 since the front and rear tyres are the same. An infinite number of combinations of k_1 and k_b brings the models to have f_1 equal to a specific value. An extra conditions, for example limiting the value of eigenvectors, should be added in order to limit to one the number of possible combinations of k_1 and k_b that make the model have f_1 equal to a specific target.

Since test 11 and 17 were performed with the same b_e, and so the same L but with different w_f, supposing that k_b is linear and depends only on L, there should be at least one combination of k_1 and k_b that make the computed (with the analytic or the numeric model) f_1 match the one found in test 11 and 17 considering the different configurations of the two tests in terms of b_e, γ and w_f.
Table 8.1 reports the main key parameters of those two tests. γ is the angle of the boom measured by the on-board encoder when the CDC or the operator blocks the boom lowering. Since during several tests the CDC has blocked the boom lowering more than one time, the column *'CDC block n°'* identifies which of the different oscillation's phases of each test has been analysed to extract the resonance frequency of δ.

Test n°	**CDC block n°**	b_e **(mm)**	w_f **(kg)**	γ **at CDC/operator block (°)**	f_1 **(Hz)**
11	1	4000	1000	12.7	0.8435
17	1	4000	2000	45.2	0.5650

Table 8.1: Key parameters of test 11 and 17

In order to find the combinations of k_1 and k_b that make the models match the results of test 11 and 17 a parametric analysis has been conducted studying how the variation of k_1 and k_b influences f_1.

Figure 8.1 shows the parametric analysis on the analytic (Figure 8.1a) and numeric (Figure 8.1b) model. The red points indicate a part of all the possible combination of k_1 and k_b that would allow to have $0.83 < f_1 < 0.84$ Hz adopting the parameters provided in table 8.1 for test 11. The blue points, instead, indicate a part of the combinations of k_1 and k_b that would allow to have $0.56 < f_1 < 0.57$ Hz adopting the parameters provided in table 8.1 for test 17. Those lines have an hyperbolic shape and so they continue with an asymptotic behaviour also beyond the limits of the plot. Only a limited number combinations of k_1 and k_b have been tested both for the analytic and numeric model. In particular, since the analytic eigen-problem solution is much faster than the numeric one, 1000000 combinations have been tested with k_1 ranging between 40000 N/m and 6000000 N/m and k_b ranging between 200000 Nm/rad and 30000000 Nm/rad while only 10000 combinations have been tested in the same range for the

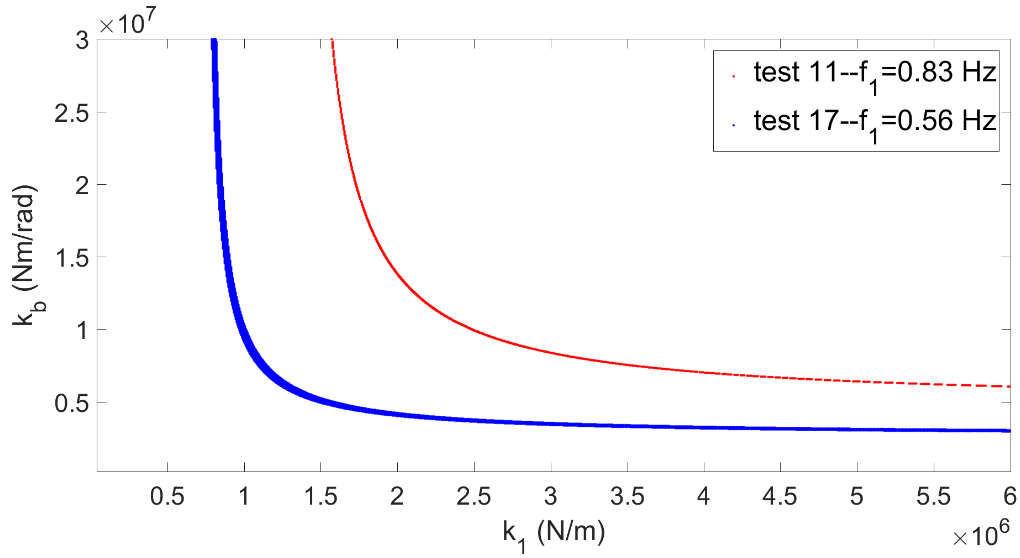

(a) Analytic model

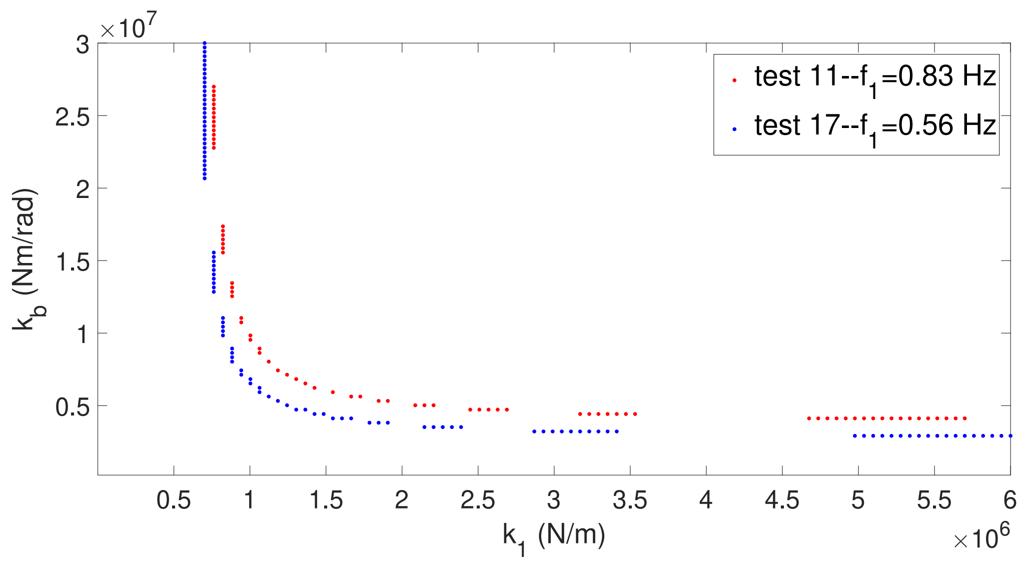

(b) Numeric model

Figure 8.1: Combination of k_1 and k_b that satisfy the condition in table 8.1

numeric model.
Unfortunately the two curves do not meet for the analytic nor for the numeric model and this means that there is not a combination of k_1 and k_b that satisfies the conditions of test 11 and test 17 at the same time . This inconsistency is probably justified by the non linearity of wheels and boom' s stiffness and by the poor approximation of the boom as a rod linked to the frame with a torsional stiffness. Moreover the dynamic effect given by the compressibility of the oil in the hydraulic jack that allows the tilting

of the boom has been completely neglected.

8.2 Approximation of the boom stiffness

As anticipated at the beginning of this chapter the non linearities revealed by the previous section have been charged only to the stiffness of the two axles. The boom has been approximated as a wedged beam and so its rotational stiffness is considered equal to $k_b = \frac{2EJ}{L}$ where E is the Young' s modulus of the beam's material, J is the area moment of inertia and L is the length of the boom. In our case the term $2EJ$ is unknown since the boom is made of different sections and for this reason it is considered as an unknown called $k_{b,0}$. In order to give a first-attempt value to $k_{b,0}$ the boom has been approximated as composed of a unique section equal to the second of the three rectangular profiles that compose the telescopic boom of the machine used during the test. It has a rectangular section (Figure 8.2) with: $H = 320\,mm$, $h = 300\,mm$, $B = 250\,mm$, $b = 230\,mm$. For this kind of section the area moment of inertia with respect to the horizontal axis is $J = \frac{BH^3 - bh^3}{12}$. Considering that section made of steel ($E = 2 * 10^5\ N/mm^2$) this approximation leads to have $k_{b,0} = 6,9 * 10^7\ Nm^2/rad$.

Also in this case an analysis similar to the previous one has been performed but

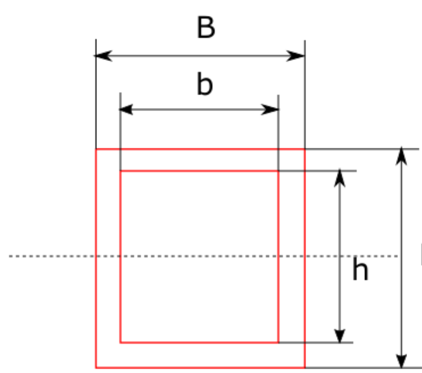

Figure 8.2: Hollow rectangular section

this time $k_{b,0}$ has been fixed and a parametric analysis has been performed varying k_1 and k_2 between 40000 N/m and 6000000 N/m. We searched for combinations of k_1 and k_2, that make the computed f_1 equal to the resonance frequency of δ measured for a series of test (Table 8.2). To do so the analytic model has been set with the same configuration (in terms of b_e, w_f, and γ) that the machine assumed when the CDC/operator block occurred during those tests. The values of k_1 and k_2, found with

Test n°	CDC block n°	b_e (mm)	γ at CDC/operator block (°)	f_1 (Hz)
10	1	3000	15.2	0.9912
11	1	4000	12.7	0.8435
12	2	5000	30.4	0.7133
13	2	6000	46.8	0.6242
8	1	7500	51.8	0.4923

Table 8.2: Key parameters of different tests performed with w_f = 1000 kg

$k_{b,0} = 6,9 * 10^7\ Nm^2/rad$ are reported in Figure 8.3a using a different colour for each test. As it is possible to see the lines relative to different test are quite distant and this suggest that, since the analysed tests were performed with the same w_f and k_1 and k_2 are only function of w_f, any single combination of k_1 and k_2 within the blue and yellow line would produce a strong divergence between the analytic and experimental results if $k_{b,0} = 6.9 * 10^7\ Nm^2/rad$. This fact has forced us to increase to $11 * 10^7\ Nm^2/rad$. Figure 8.3b shows that in this case the lines are much more close to each other, and so fixing a combination of k_1 and k_2 within the limits given by the blue and yellow line the divergence between the analytic and numeric results is reduced with respect to the previous case. An increase of $k_{b,0}$ would slightly reduce the gap between those lines but at the same time it would produce unreal values of k_b for the geometric and mass properties of the boom.

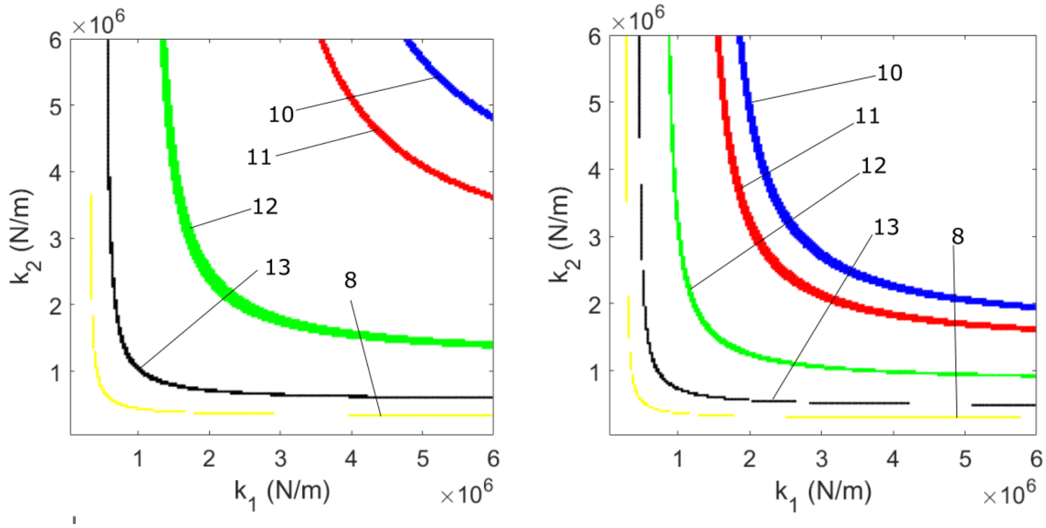

(a) $k_{b,0} = 6.9 * 10^7 \; \frac{Nm^2}{rad}$

(b) $k_{b,0} = 11 * 10^7 \; \frac{Nm^2}{rad}$

Figure 8.3: Combination of k_1 and k_2 that satisfy the condition in table 8.1

8.3 Approximation of the wheels stiffness

Fixed $k_{b,0} = 11 * 10^7 \; Nm^2/rad$ we searched for the values for the value of $k_1 = k_2$ for which the first resonance frequency f_1 of the numeric model best fit the resonance frequency of δ during the different tests done with $w_f = 1000kg$ (Table 8.2). We rapidly found a good match for $k_1 = k_2 = 1.1 * 10^6 \; N/m$. At this point we tried to reduce the gap between those results supposing $k_1 = \alpha_k * k_2$ and performing different simulations varying the value of α_k. A good trade-off is represented by $\alpha_k = 0,8$. Figure 8.4a reports the comparison of the numeric and experimental results with $k_2 = 1.1 * 10^6 \; N/m$ and $k_1 = \alpha_k * k_2 = 8,8 * 10^5 \; N/m$. After that we tuned k_2, keeping $k_1 = \alpha_k * k_2$ with the same value of α_k previously found,to make the numeric model make fit the results of tests performed with $w_f = 2000 \; kg$ (Table 8.3). In this case the combination that provide a good fitting of the experimental results (Figure 8.4b) is given by: $k_2 = 8 * 10^6 \; N/m$ and $k_1 = \alpha_k * k_2 = 6,4 * 10^5 \; N/m$.

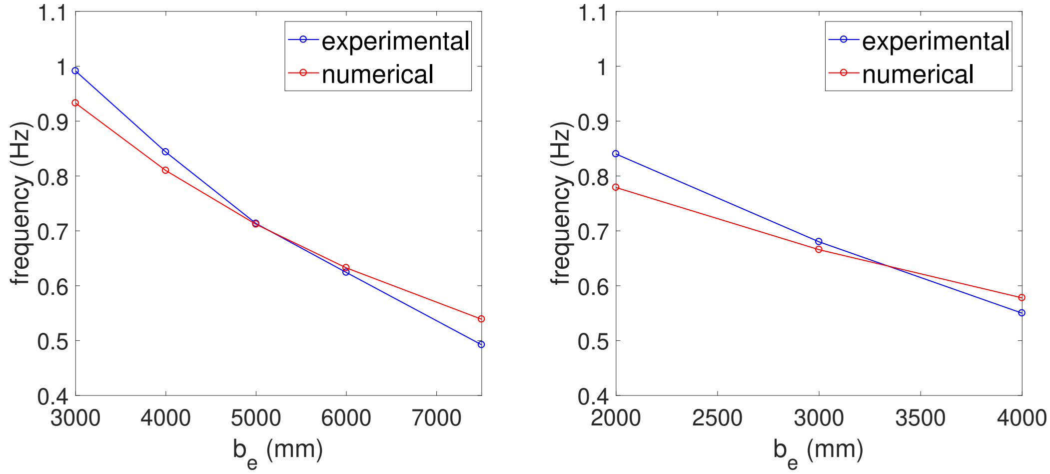

(a) $w_f = 1000\,kg$

(b) $w_f = 2000\,kg$

Figure 8.4: Comparison of the numerical and experimental results

Test n°	**CDC block n°**	b_e **(mm)**	γ **at CDC/operator block (°)**	f_1 **(Hz)**
18	1	2000	10.88	0.8427
16	2	3000	36.8	0.6826
19	2	4000	48.9	0.5597

Table 8.3: Key parameters of different tests performed with w_f = 2000 kg

8.4 Comparison of the numerical, analytic and experimental results

Figures 8.5a and 8.5b show the evolution of f_1 computed with the numerical and analytic model respectively for $w_f = 1000\,kg$ and $w_f = 2000\,kg$ for different values of b_e. For $w_f = 1000\,kg$ it has been possible to measure clear wide oscillations only in a range of b_e between 3000 and 7500 mm while for $w_f = 2000\,kg$ that range is limited from 2000 to 4000 mm.
Table 8.4 reports the relative error (equation. 8.1) of the analytic and numeric model with respect to the experimental results. It is possible to note that the approximation of the numeric model is quite precise with a maximum relative error of 8,7% while the

analytic model tends to under-estimate the real oscillation frequency of δ.

$$r_e = \frac{f_{1,model} - f_{1,experimental}}{f_{1,model}} \tag{8.1}$$

w_f **(kg)**	b_e **(mm)**	$r_{e,numeric}$ **(%)**	$r_{e,analytic}$ **(%)**
1000	3000	-6.3%	-23.7%
1000	4000	-4.1%	-16.7%
1000	5000	-0.2%	-8.5%
1000	6000	1.3%	-3.8%
1000	7500	8.7%	7.3%
2000	2000	-7.8%	-36.7%
2000	3000	-2.1%	-23.5%
2000	4000	4.8%	-10.6%

Table 8.4: Relative errors of the numeric and analytic models with respect to the experimental results

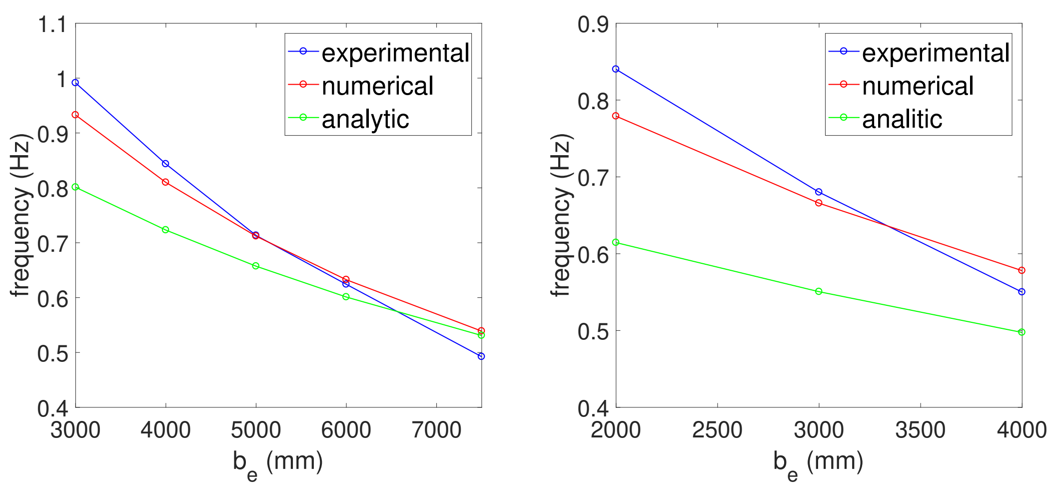

(a) $w_f = 1000\,kg$ (b) $w_f = 2000\,kg$

Figure 8.5: Comparison of the numeric, analytic and experimental results

Final considerations

The current document is the result of a collaboration with Movimatica srl, lasted more than six months, during which it was possible to understand the typical dynamics of an innovative and constantly expanding workplace.
The first part of this document has showed the potentiality that a CAN based telemetry system offers also in non-automotive applications. In particular in the first chapter describes how a CAN network works and how the CAN frames can be easily read and used for applications like a data logger. The *'MERLO VisuaLogger'* GUI is an innovative instrument that can be used in case of accident of the machine. In fact it provides an easy method to visualize the geometric configuration of the machine during the accident. A great advantage of this instrument is its versatility because the database containing the informations about each model of the Merlo machine can be easily updated in case of production of new models. This GUI can also be used to read and convert the ASCII log files directly recorded from the CAN bus. This function could be used, during the final test that each machine undergoes, to easily test the proper functioning of the sensors related to geometric configuration of the machine. In fact if the virtual animation of the machine shows the same operations that the machine has done during the record of the log file, it means that the sensors returns the expected measures.
On the other hand the second part of this activity has demonstrated how an IMU can be used to detect the dynamic behaviour of a telescopic handler. The complementary filter, used to extrapolate the pitch and roll angle from the IMU, was tuned in such a way to use almost exclusively the data of the accelerometer ($c_f = 0.98$). The analysis of some test (not reported in this document) performed making the machine pass over some bumps has required, on the rebound, to take more into account the data of the gyroscope because of the spikes in the accelerometer data. The test at the headquarter of Merlo have showed the poor reliability of the on board inclination sensor on the chassis and have highlighted the possible positions where to install the IMU in

order to minimize the noise produced by the engine and the hydraulic pumps. The comparison between γ and $\delta + \theta$ has confirmed that an IMU can provide a reliable measure of the inclination angle of the boom and, unlike the on-board rotary encoder, it can measure also the oscillations of the boom during the CDC/operator blocks of the boom movement. The Fourier analysis of the boom' s oscillations has shown a certain proportionality between the oscillation frequency of δ and the boom extension. The solution of the eigenproblem of the analytic and numerical model has revealed that the first mode of both the models replicate the behaviour of the machine during the oscillations induced by the block of the boom lowering. Since the stiffness of the front and rear axle (k_1 and k_2) and of the boom (k_b) were unknown, a parametric analysis has been performed to make the resonance frequency of δ match with the first resonance frequency (f_1) of the two models tuning the value of k_1,k_2 and k_b. This analysis has revealed revealed the non-linearity of k_1,k_2 and k_b. The scarcity of data has forced us to consider the boom as a wedged beam with $k_b = k_{0b}/l$ and to charge the non linear effect to the stiffness of the front and rear axle. With some iterative simulation it was possible to find a plausible value to k_{0b} and to k_1 and k_2 for $w_f = 1000$ kg and $w_f = 2000$. Even if those results derive from some strong approximations they can provide important informations for the initial tuning of the new control system. In particular the numeric model has revealed to well emulate the dynamic behaviour of the real machine. The advantage of those two models is that they can predict the behaviour of any model of frontal telescopic handler just modifying the geometric and mass properties. The reliability of those models could be much improved with more precise informations about the stiffness of the wheels and of the boom.

Bibliography

[1] Bs en 15000: Rough-terrain trucks - safety requirements and verification part 8: Variable-reach tractors. Standard, British Standard, 2008.

[2] Gulf Coast Data Concepts. *Human Activity Monitor (HAM) User manual*.

[3] Steve Corrigan HPL. Introduction to the controller area network (can).

[4] ISO 22915-10: Industrial trucks — Verification of stability Part 10: Additional stability test for trucks operating in the special condition of stacking with load laterally displaced by powered devices. Standard, International Standard Organisation, 2008.

[5] ISO 22915-14: Industrial trucks — Verification of stability Part 14: Rough-terrain variable-reach trucks. Standard, International Standard Organisation, 2010.

[6] ISO 22915-20: Industrial trucks — Verification of stability Part 20: Trucks operating with offset load, offset determined by utilisation — Stability tests. Standard, International Standard Organisation, 2008.

[7] Markus Junger. Introduction to j1939. *Vector, version*, 1:1–11, 2010.

[8] PD CEN/TS 1459-8: Rough-terrain trucks - Safety requirements and verification Part 8: Variable-reach tractors. Standard, Comité Européen de Normalisation, 2018.

[9] Singapore Government. Data loggers for mobile cranes, 2015.

[10] W. Voss. *A Comprehensible Guide to Controller Area Network*. Copperhill Technologies Corporation, 2008.

[11] Wilfried Voss. *A comprehensible guide to J1939*. Copperhill Technologies Corporation, 2008.

[12] Wikipedia contributors. High-pass filter — Wikipedia, the free encyclopedia, 2019.

[13] Wikipedia contributors. Inertial measurement unit — Wikipedia, the free encyclopedia, 2019.

[14] Wikipedia contributors. Low-pass filter — Wikipedia, the free encyclopedia, 2019.

[15] Wikipedia contributors. Telescopic handler — Wikipedia, the free encyclopedia, 2019.

Acknowledgements

Finally, I would like to thank Prof. Aurelio Somà to have supported me during the realisation of this document and for the patience that he has always showed to me.
I would also like to thank Ing. Federico Fraccarollo, reference point of Movimatica, that has always helped me both during the intern-ship and the period of realisation of this document. He had a key role in the completion of this work. They steered me in the right direction whenever they thought I needed it.
I can't forget to thank Ing. Stefano Sivo, researcher of Politecnico, who demonstrated an infinite availability to help me during the different phases of this work.
I am also grateful to all the staff of Movimatica, starting from the general manager Ing. Marco Mattioli, who allowed me to do the intern-ship in its company, Giorgio Ponza and Claudio Bertan who have helped me with IT problems.
Last but not the least, I would like to thank my parents Maria Angela and Corrado, my sister Silvia and my grandparents for supporting me with wise advice and for always being by my side.

List of Figures

List of Tables